Structural Fatigue Life Investigation of a Rigidly Mounted Aluminium Fuel Tank

by

Christian Matthys Franken

Thesis presented in partial fulfilment of the requirements for the degree of Master of Science in Engineering (Mechanical) in the Faculty of Engineering at Stellenbosch University

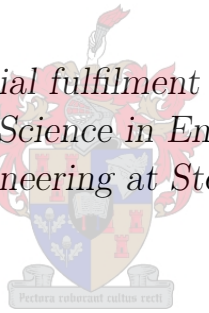

Supervisors:

Prof. G. Venter Dr. E. Terblanche

December 2012

Declaration

By submitting this thesis electronically, I declare that the entirety of the work contained therein is my own, original work, that I am the sole author thereof (save to the extent explicitly otherwise stated), that reproduction and publication thereof by Stellenbosch University will not infringe any third party rights and that I have not previously in its entirety or in part submitted it for obtaining any qualification.

Signature: .....
C.M. Franken

Date: 2012/09/05 .....

Abstract

Structural Fatigue Life Investigation of a Rigidly Mounted Aluminium Fuel Tank

C.M. Franken

Thesis: MScEng (Mechanical)

December 2012

Structural cracks have formed in the sub-structure of a tank that is rigidly mounted onto a truck chassis. These cracks have all formed at welds joining the various components of the aluminium sub-structure. This thesis proposes a solution methodology to address these failures. The first phase of this methodology (failure investigation) relies heavily on determining the life of the structure with fatigue life calculations. These calculations are done using the stress life method supplemented by the hot spot stress method.

Experimental tests were conducted at an operational air force base to compile a composite duty cycle that is representative of the typical operation of the vehicle. This is followed by a finite element analysis which is used to calculate the scaling factor required to determine the hot spot stresses in the structure. These hot spot stresses are determined for three different crack areas and the estimated fatigue life of each of these points are calculated.

The estimated fatigue lives are compared to the actual lives that were reported by the maintenance personnel, to determine a correlation factor. The comparison yields a maximum correlation factor of 9.8 and a minimum of 3.9. It is suggested that the minimum correlation factor of 3.9 is used to assess future solutions. It is also suggested to reduce the stresses by at least 37% to achieve the desired service life. Recommendations regarding the design of a repair are given.

The methodology presented in this thesis provides the groundwork for a typical solution methodology that can be used at GRW Engineering. Recommendations for improvements to the method and its components are given.

Uittreksel

Strukturele vermoeidheidsondersoek van 'n Rigied Gemonteerde Aluminium Brandstof Tenk

("Structural Fatigue Life Investigation of a Rigidly Mounted Aluminium Fuel Tank")

C.M. Franken

Tesis: MScIng (Meganies)

Desember 2012

Strukturele krake het ontstaan in die substruktuur van 'n tenk wat rigied gemonteer is op 'n vragmotor onderstel. Die krake het almal ontstaan op sweislaste wat die verskillende komponente van die aluminium struktuur bind. Hierdie tesis stel 'n oplossingsmetodologie voor om hierdie falings aan te spreek. Die eerste fase van hierdie metodologie (falingsondersoek) maak hewig staat op berekeninge van strukturele vermoeidheid. Hierdie berekeninge word gedoen met behulp van die 'stress-life' metode aangevul deur die 'hot spot stress' metode.

Eksperimentele toetse is uitgevoer op 'n operasionele lugmagbasis om 'n saamgestelde dienssiklus te bepaal wat verteenwoordigend is van die tipiese operationele omstandighede van die voertuig. Dit word gevolg deur 'n eindige element analise wat gebruik word om die skalering faktor te bereken wat nodig is om die 'hot spot' spanning in die struktuur te bepaal. Hierdie 'hot spot' spanning word bepaal vir drie verskillende kraak gebiede ten einde die beraamde vermoeidheidslewe van elk van hierdie punte te bereken.

Die beraamde vermoeidheidslewe word vergelyk met die werklike lewe wat deur die instandhoudingspersoneel berig is, om 'n korrelasie faktor te bepaal. Die vergelyking lewer 'n maksimum korrelasie faktor van 9.8 en 'n minimum van 3.9. Daar word voorgestel dat die minimum korrelasie faktor van 3.9 gebruik word in die bepaling van toekomstige oplossings. Daar word ook voorgestel dat die spanning met ten minste 37% verlaag word om die verwagte lewensduur te bereik. Aanbevelings ten opsigte van 'n verbetering aan die huidige struktuur word ook gegee.

Die metodologie wat in hierdie tesis aangebied word, bied die grondslag vir 'n tipiese oplossingsmetodologie wat by GRW Engineering gebruik kan word. Aanbevelings vir verbeterings aan die metode en die verskeie komponente word ook voorgestel.

Dedication

I dedicate this thesis to my beautiful wife, Anemie, whose love, unwavering support and numerous cups of coffee guided me towards the final goal.
Thank you for standing by me when the nights were long and there was no end in sight.

Acknowledgements

Thank you to GRW Engineering who provided all the equipment, consumables and software. A special thank you to Gerhard and Wentzel van der Merwe, Rossouw van Eeden, Ivan Terblanche, Albert Liebenberg and the rest of the executive committee who provided me with the opportunity to attempt and finish this degree.

I would also like to thank:

Tom Potter of RAF Lossiemouth for the long hours, the patience and all the assistance you provided when it was not expected of you.

Dr Terry Terblanche and Gerhard Venter who 'adopted' me when I was a project orphan and who guided me in the right direction. I owe you a great depth of gratitude.

The friends who provided support and encouragement during these years even though they had to endure months of silence.

My sisters, my new siblings, my mother- and father-in-law and the rest of my family who supported me even though they suffered gross neglect.

Finally a special word of thanks to my parents for their unwavering trust.

Contents

List of figures

List of tables

Nomenclature

Variables

a	Crack length
b	Fatigue stress exponent
C	Material constant associated with crack growth
CF	Correlation factor
$C_{\mathrm{S-N}}$	Constant associated with a particular S-N curve
D	Structural damage fraction caused by cycles at S_i
D_{DC}	The total damage caused by a complete duty cycle
E	Young's Modulus
F_T	Fatigue strength modification factor due to temperature effects
F_C	Scaling factor due to corrosion effects
F_{IT}	Fatigue strength modification factor due to improvement techniques
F_{SE}	Fatigue strength modification factor due to size effects
$f(g)$	A correction factor dependant on the crack and specimen geometry
I	Electrical current
K_c	The critical stress intensity factor at which point rapid, unstable crack growth occurs
K_{hs}	Factor relating the stress at $1.0t$ from the weld to the stress at the hot spot
K_{IF}	Stress intensity factor
K_{th}	The threshold stress intensity factor
$K_{1.0t}$	Factor relating the stress at the gauge to the stress $1.0t$ from the weld
m_{S-N}	The logarithmic slope of the S-N curve
m_1	Material constant associated with crack growth
N	Life to failure
N_i	The life to failure at S_i
n_i	The number of cycles at S_i
R	Stress Ratio
R_e	The yield stress of the material
R_{elec}	Electrical resistance

R_m	The tensile stress of the material
$R_{p0.2}$	The 0.2% proof stress of the material
S_e	Endurance limit
S_u	The ultimate strength of the material
S_{ar}	A fully reversed stress amplitude for a specific life
$S_{f'}$	The fatigue stress coefficient
t	The thickness of the material
X	The direction of travel
Y	The horizontal direction perpendicular to the direction of travel
Z	The vertical direction perpendicular to the direction of travel
$\Delta\sigma$	The stress range
ϵ_G	Strain measured with a strain gauge
$\epsilon_{G_{FEA}}$	Strain at the strain gauge position determined with an FE analysis
ϵ_{hs}	The hot spot strain
$\epsilon_{hs_{FEA}}$	The hot spot strain calculated with an FE analysis
$\epsilon_{0.4t}$	Strain at $0.4t$ from the weld toe, determined either by calculation or experiment
$\epsilon_{1.0t}$	Strain at $1.0t$ from the weld toe, determined either by calculation or experiment
$\epsilon_{1.0t_{FEA}}$	Strain at $1.0t$ from the weld toe determined with an FE analysis
σ_a	The stress amplitude of a cycle
σ_{ben}	The shell bending stress
σ_{hs}	Stress at the hot spot
σ_m	The mean stress of a cycle
σ_{max}	Maximum stress of a cycle
σ_{mem}	Membrane stress
σ_{min}	Minimum stress of a cycle
σ_{nlp}	Non-linear stress peak
σ_r	Remote stress
$\sigma_{2\times10^6}$	A stress value that equates to a fatigue limit of two million cycles
τ_e	The shear stress endurance limit due to torsion

Subscripts

a	Amplitude
C	Corrosion
DC	Duty cycle
e	Endurance
FEA	Finite element analysis

G	Gauge
hs	Hot spot
IT	Improvement techniques
i	Sequential number
m	Mean
min	Minimum
max	Maximum
r	Remote
S-N	Stress-life
T	Temperature
u	Ultimate

Chapter 1

Introduction

An important part of any country's economic growth is the transportation of freight. This includes importing products, exporting the country's produce and moving products from the producer or port to the point of sale or the consumer within the country itself. The importance of transport is evident in South Africa where the country's total logistics costs peaked at an incredible R 339 billion in 2008 (CSIR, 2011). While logistics include air, water and land transport the one most commonly experienced by the average South African is land based transport, specifically road transport. Road transport contributes a massive 88.7% (CSIR, 2011) of the total freight tonnage of land based transport. Effectively this means rail transport carries 11.3%. While there are various projects that try to remove some of the load from the roads, most of them are all still in the planning or construction stages[1]. Even in developed countries, with an established rail system, road transport continues to be one of the key players in the logistics sector and will continue to be in the foreseeable future. This proves that there is a continually growing need that has to be addressed.

While operating their own transport company the Van der Merwe family and their partner R. van Eeden saw this need in the road tanker industry and endeavoured to build their own high quality, competitive tankers. Thus in 1996 GRW Engineering was founded (GRW, 2011).

In the last fifteen years the company has become a market leader in the road tanker industry and has also entered into the feed and powder transport industries. Figures 1.1 to 1.4 show some of the products that GRW produces. Recently the company has expanded its portfolio to include rail tankers and general freight carriers. GRW has also exported and to the UK and various countries in Africa. With such a wide range of products, GRW is involved in most of the land based transport markets.

To remain an industry leader (and to enter and dominate new industries) it is essential for the company to continually improve and develop the products that they present to the market. These improvements are mainly driven

[1]One example is the Durban to Gauteng multi-product fuel pipeline

Figure 1.1: A tanker used to transport fuel

Figure 1.2: An auger bulker that is used to transport animal feed.

Figure 1.3: A pneumatic bulker that is used to transport powdered products.

Figure 1.4: A stainless steel tanker that is used to transport sulphuric acid.

by cost reduction, reduced weight (and hence increased payload) and structural integrity. The first three factors are directly related to each other in terms of vehicle structure, because some of the largest cost and weight savings can be achieved with improved structural design. On the other hand South Africa faces the unfortunate reality that our road conditions are continually deteriorating; especially secondary roads (CSIR, 2011).

To meet these demands the structural geometries tend to become increasingly complex and cannot be assessed with traditional analytical engineering calculations and rules. It also requires that new materials be continually as-

sessed and utilised in unconventional areas.

This produces a new need within the company itself: a department that can produce new structural designs and that can verify these designs with regard to the expected service life of the structures. While the former function has been active in the company for several years the latter has only been touched on recently. The quality of products can be ensured by technical knowledge about the expected service life. This thesis addresses, in part, the growth of this function and department.

As with any rapidly expanding company, growth does not come without growing pains. In 2002 GRW Engineering was contracted to build a tank that was to be mounted onto a truck chassis by the primary contractor and used as an aircraft refueller. The tanks were delivered and the completed vehicles were handed over to the client by the primary contractor. After several years in operation a crack was reported on one of the tanks. This was initially thought to be an isolated incident but was followed by several reports of similar cracks. The number of occurrences proved that there was a general problem that had to be investigated. From initial investigations and finite element (FE) analysis it was not clear what the primary cause of the failures was. This led GRW to launch a full structural fatigue investigation to find the cause of the failures and to assist in providing a solution that will extend the life of the structure to an acceptable service period. This act was the first step in the development of the above mentioned department.

This thesis presents the failures that have occurred and the various steps that are taken to determine the estimated fatigue life of the structure. Chapter 2 presents the theories that are available in literature and their various applications. Chapter 3 presents and discusses the failures that have occurred. At the end of the chapter the solution methodology that will be adhered to throughout this thesis, is presented. The experimental set-up and its results are presented in Chapter 4. This is followed by a brief discussion of the finite element model and the data extracted from it (Chapter 5). Chapter 6 covers the fatigue calculation and its results. In Chapter 7 some recommendations are made for further study and future projects. This chapter also looks critically at the methods that were applied throughout this thesis and suggests future improvements. Finally Chapter 8 presents the conclusions of the author. Throughout the thesis the methods are presented and discussed in a generalised fashion to assist the purpose of proposing a general fatigue investigation methodology.

The primary goal of this thesis is:

To apply the rules of structural life prediction to investigate the failures that have occurred and at the same time to develop and refine a fatigue life prediction methodology that can be used by the company for future designs.

Chapter 2

Literature study

Bannantine *et al.* (1990) defines metal fatigue as "... a process which causes premature failure or damage of a component subjected to repeated loading." It is this metallurgical phenomenon which has caused and continues to cause various failures throughout the field of mechanical engineering. Some of these failures are no more than an inconvenient crack of a household tool while others have disastrous and fatal effects. One such example is the Alexander L. Kielland oil platform capsize which claimed 123 lives in 1980 due to a fatigue crack on a steel brace.

For these reasons fatigue has been widely studied and investigated to determine its causes and to create methods of predicting the service life of a new design. To this day new prediction methods are published while the old ones are continually refined.

The previous chapter mentioned that the subject of this thesis is a tank structure mounted onto a vehicle chassis. At this time it is important to know that all the failures that have occurred in the structure are in welded areas. This chapter will start by presenting the standard fatigue life theories. It will subsequently provide an overview of the unique methods used to assess fatigue life of welded structures. Obstacles like variable amplitude loading (typically associated with a vehicle) are then presented, followed by a discussion about how a fatigue life estimation method can be used to practically predict the life of a structure or repair. Finally it will conclude by presenting the choice of methods that will be used in this thesis and the reason for selecting each.

2.1 Fatigue life methods

Currently three primary fatigue analysis methods exist. These are the stress-life (S-N) approach, the strain-life approach and the fracture mechanics approach. Each method has its own region of application although there are cases where combinations of the methods can be applied. This chapter will briefly discuss the stress-life and fracture mechanics methodologies and the scope of their application. The strain-life method will not be discussed since

it is not commonly used to assess welding fatigue (derived from the methods presented by MacDonald (2011*a*), Hobbacher (1996), CEN/TC250 (2005) and CEN/TC250 (2007)) which is the basis of this thesis. This section will present a brief explanation of the stress-life method and the fracture mechanics method as derived from the chapters of Bannantine *et al.* (1990).

2.1.1 Stress-life method

The stress-life method was the first method used to try and quantify metal fatigue and has been used for more than a 100 years. The basis for the stress-life method is the S-N diagram.

2.1.1.1 The S-N diagram

The S-N diagram is also known as the Wöhler diagram in honour of August Wöhler's contributions to the study of fatigue. It is a plot of stress range (S) versus cycles to failure (N) and is determined by physically testing a material specimen by subjecting it to a constant stress amplitude, with a specific mean stress, until failure occurs. The mean stress can deviate from zero if it is required that the effects of compressive or tensile mean stresses are incorporated in the S-N curve. Common mean stresses chosen for S-N curves are $R = 1$ or $R = 0$ (see Appendix A for the definition of R). These are known as classical Wöhler tests (Lee *et al.*, 2005). Using statistical averaging, an S-N diagram is created and can be used to predict the fatigue life of a given component at a given stress amplitude. An example of such a diagram is shown in Figure 2.1. These tests provide a quantified representation of the material's resistance to fatigue fracture. For this reason the S-N diagram is sometimes referred to as a fatigue resistance curve.

2.1.1.2 The Endurance limit

When plotting the S-N data of various steels on a log-log curve it can be seen that the graph has a 'knee'. This is the stress level below which the material is considered to have infinite life. This stress level is known as the endurance limit, S_e, of the particular material. Non-ferrous alloys tend not to have an endurance limit which suggests that, given enough cycles, the component will eventually fail at any stress level. For these alloys a pseudo-endurance limit is taken as the stress level corresponding to a life of $1\text{x}10^7$ cycles (Hobbacher, 1996). In these cases it is very important for the design engineer to have a clearly defined design life for the component.

2.1.1.3 Mean stress effects

This section will present the basic concept of mean stress effects but will not go into the micro structural detail or how it is compensated for in fatigue analysis.

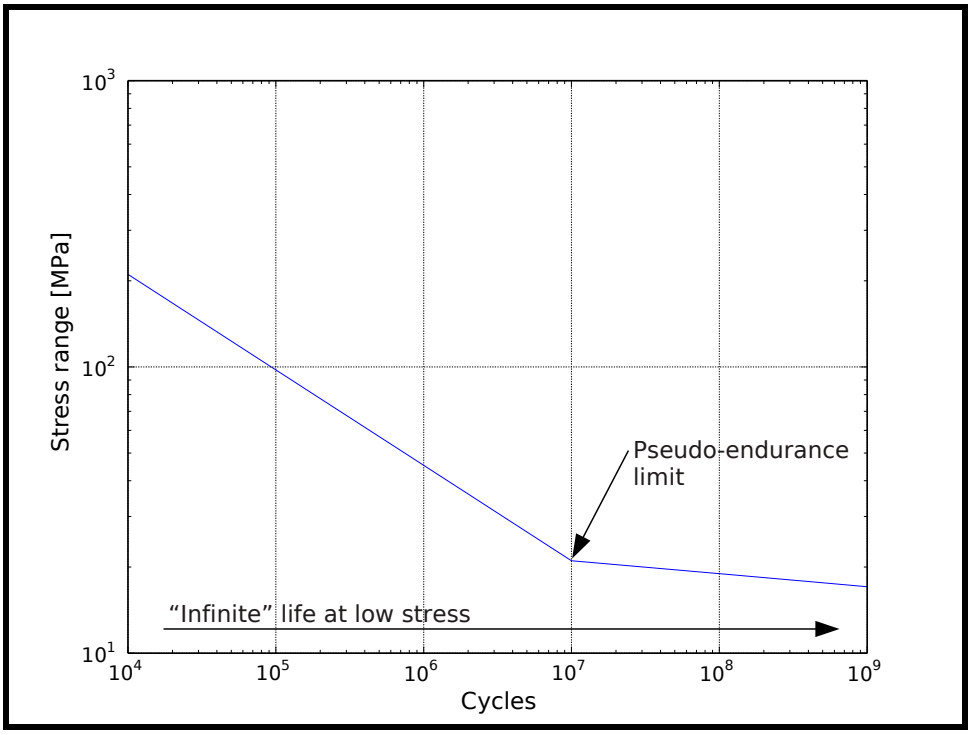

Figure 2.1: A characteristic S-N curve plotted according to the instructions of Hobbacher (1996)

Further information regarding this subject can be obtained from Bannantine *et al.* (1990) and Lee *et al.* (2005). Fatigue damage due to cyclic stresses is influenced by the mean stresses[1] at which the cycles occur. Mean stress is defined as:

$$\sigma_m = \frac{\sigma_{min} + \sigma_{max}}{2} \tag{2.1}$$

Where:

σ_m	=	The mean stress of a cycle	[MPa]
σ_{max}	=	The maximum stress of a cycle	[MPa]
σ_{min}	=	The minimum stress of a cycle	[MPa]

Normal mean stress influences the opening and closing of micro-cracks and hence influences the endurance limit of a structure subjected to it. It is important to note that tensile mean stresses negatively affect the fatigue life of a component while compressive mean stresses are beneficial in terms of fatigue life. Below are two of the earlier and commonly accepted empirical equations that relate the effect of mean stresses to the endurance limit.

$$\text{The Goodman equation: } \frac{\sigma_a}{S_e} + \frac{\sigma_m}{S_u} = 1 \tag{2.2}$$

[1]See Appendix A for definitions of the variables associated with alternating stress

$$\text{The Gerber equation: } \frac{\sigma_a}{S_e} + (\frac{\sigma_m}{S_u})^2 = 1 \tag{2.3}$$

Where:

σ_a	=	The stress amplitude of a cycle	[MPa]
S_e	=	The endurance limit of the material	[MPa]
S_u	=	The ultimate strength of the material	[MPa]

For small mean stress loading and in the case of aluminium alloys, the Smith, Watson and Topper (SWT) method is quite popular (Lee *et al.*, 2005).

$$\text{The SWT equation: } S_{ar} = \sqrt{\sigma_{max}\sigma_a} = S'_f(2N)^b \tag{2.4}$$

Where:

S_{ar}	=	A fully reversed stress amplitude for a specific life	[MPa]
S'_f	=	The fatigue stress coefficient	[MPa]
N	=	Fatigue life to failure	[cycles]

2.1.1.4 Other Factors

Various other factors can influence the fatigue life of a component and it is necessary to compensate for these factors. Some of these factors are:

Material size

Fatigue cracks always start at a flaw in the material. If a larger section of material is subjected to fatigue loading there is a greater probability that such a flaw will fall within the stressed area of the material. Even in bending a larger volume of material is subjected to the critical stress. This increase in failure probability means that larger material sections tend to have a lower fatigue limit.

Empirical data from various sources (Bannantine *et al.* (1990), Hobbacher (1996)) provides modification factors to compensate for these size effects. Usually it only needs to be considered for cylindrical sections larger than 50 mm and plate sections larger than 25 mm.

The type of loading

Whether the specimen is subjected to bending, axial or torsional loading also influences the probability of fatigue failure. The volume concept of the previous section is once again applicable. A specimen which is subjected to an axial load has a much higher volume of stressed material than if it was subjected to a bending load. The same holds true for a torsional load. Bannantine *et al.* (1990) suggests the following equations to compensate for loading variations:

$$S_e(\text{axial}) = 0.70S_e(\text{bending}) \tag{2.5}$$

$$\tau_e(\text{torsion}) = 0.577 S_e(\text{bending}) \tag{2.6}$$

Where:

τ_e = The shear stress endurance limit due to torsion [MPa]

Component surface finish

Any surface imperfection can adversely affect the fatigue life of a component. This includes pits, scratches, grinding marks, indentations, machining marks, etc. All of these cause stress concentrations at which a crack can initialise and propagate. It should also be noted that certain mechanical processes such as machining can induce tensile residual stresses which reduces fatigue life.

Surface finish is especially important when assessing high cycle fatigue. It also tends to be of greater importance in high strength steels (Bannantine *et al.*, 1990).

Surface treatments

Fatigue cracks commonly initiate at the free surface of a material. This implies that any surface treatment will have a great effect on fatigue life and any treatment that affects the surface properties of the component must be noted and assessed. What typically happens during processes such as plating, machining, hot and cold rolling, etc. is that a residual stress is induced on the surface of the material. A tensile residual stress will adversely affect the fatigue life of the structure while a compressive residual stress is beneficial. Table 2.1 lists various component treatment methods and their effect on residual stresses.

Table 2.1: Material treatment methods and their effect on residual surface stresses. Derived from the text of Bannantine *et al.* (1990)

Method	**Residual stress**
Prestressing	Compressive
Nickel plating	Tensile
Decarburization due to hot rolling or forging	Tensile
Cold rolling	Compressive
Shot peening	Compressive

Operating temperatures

Most materials experience a significantly reduced fatigue life at high temperatures (Hobbacher, 1996) while some exhibit an improved fatigue life at low temperatures (Bannantine *et al.*, 1990). If the component will be operating

in high temperatures it is important to take this effect into account when designing. Temperatures above half of the melting point of the material tend to induce creep effects. At this point the stress-life method is no longer applicable.

Corrosive environments

Corrosive environments are related to the surface treatment section above since the effect of corrosion is to 'damage' the surface of the material. This damage can be in the form of pitting or flaking. While the oxide layer would normally protect the material from further degeneration (Bannantine *et al.*, 1990), the cyclic loads causes cracks in this layer and exposes more parent material to the corrosive environment. This fatigue-corrosion interaction is detrimental to the fatigue life of any component.

2.1.1.5 Scope of use

The stress-life method is mainly used in high-cycle applications where the stress ranges are in the elastic region of the material. It is not suited for applications where the applied strains have a significant plastic component. In the case of the endurance limit it is important to note that this limit can be altered or eliminated by periodic overloads, corrosive environments and high temperatures.

2.1.2 Fracture mechanics

The fatigue life of structures consists of two stages: The crack initiation stage and the crack propagation stage. Fracture mechanics is a fatigue theory that focuses purely on the latter of these two stages. This means that to use fracture mechanics approaches, the crack size must be known or assumed.

The point of transition from crack initiation to crack propagation is an entirely subjective point since it all depends on the method of assessment used by the analyst. If the occurrence of a crack is investigated microscopically the point of transition will be different from that of a visual inspection or a dye penetrant inspection. It is however possible to assume a microscopic crack length based on statistical data of flaws in the material or structure.

Most off the current fracture mechanics theories use the Linear Elastic Fracture Mechanics (LEFM) methods. These methods require knowledge of the mode of loading, the remote stress, the stress intensity factor (K_{IF}) and various material constants.

2.1.2.1 Loading modes

There are three loading modes associated with LEFM. These are the tensile (opening) mode, the in-plane shear (sliding) mode and the anti-plane shear (tearing) mode. These modes are known as mode I, mode II and mode III

respectively and are depicted graphically in Figure 2.2. The most commonly found mode in engineering application is mode I (MacDonald, 2011*b*), thus it will be the focus of the following discussions.

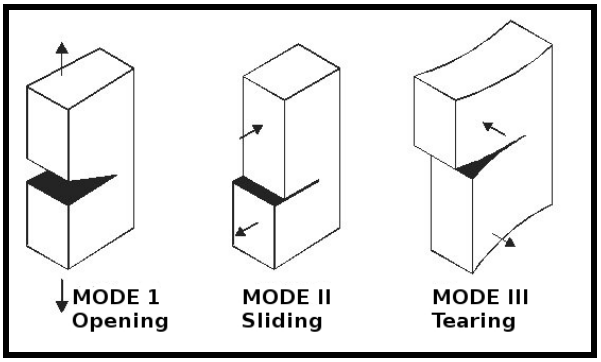

Figure 2.2: The three loading modes associated with fracture mechanics (Adapted from UL FGG (2011*b*))

2.1.2.2 Stress intensity factor

The stress intensity factor, K_{IF}, defines the magnitude of the local stress state near the crack tip. It is dependant on remote loading, crack size and shape and sample geometry. It is defined by equation 2.7.

$$K_{IF} = f(g)\sigma_r\sqrt{\pi a} \tag{2.7}$$

Where:

$f(g)$	=	A correction factor dependant on the crack and specimen geometry. Several analytical solutions are available in literature (Lee *et al.*, 2005).	[-]
σ_r	=	The remote stress	[MPa]
a	=	Crack length	[mm]

A wide range of stress intensity factors have already been determined for various problems. Some of these are published in Sih (1973) and Rooke *et al.* (1976).

2.1.2.3 Fatigue crack growth

To predict fatigue life with fracture mechanics it is necessary to calculate the fatigue crack growth rate, da/dN. When this rate is plotted versus ΔK_{IF} on a log scale a typical sigmoidal curve is obtained. Crack growth is then divided into three regions as illustrated in Figure 2.3. Region one is associated with threshold effects. This region ends when K_{IF} reaches K_{th} which is the value at which crack growth should start. Region two is known as the Paris region due

to the popular use of the Paris equation to predict life in this region. Region three is associated with rapid, unstable crack growth that leads to fracture.

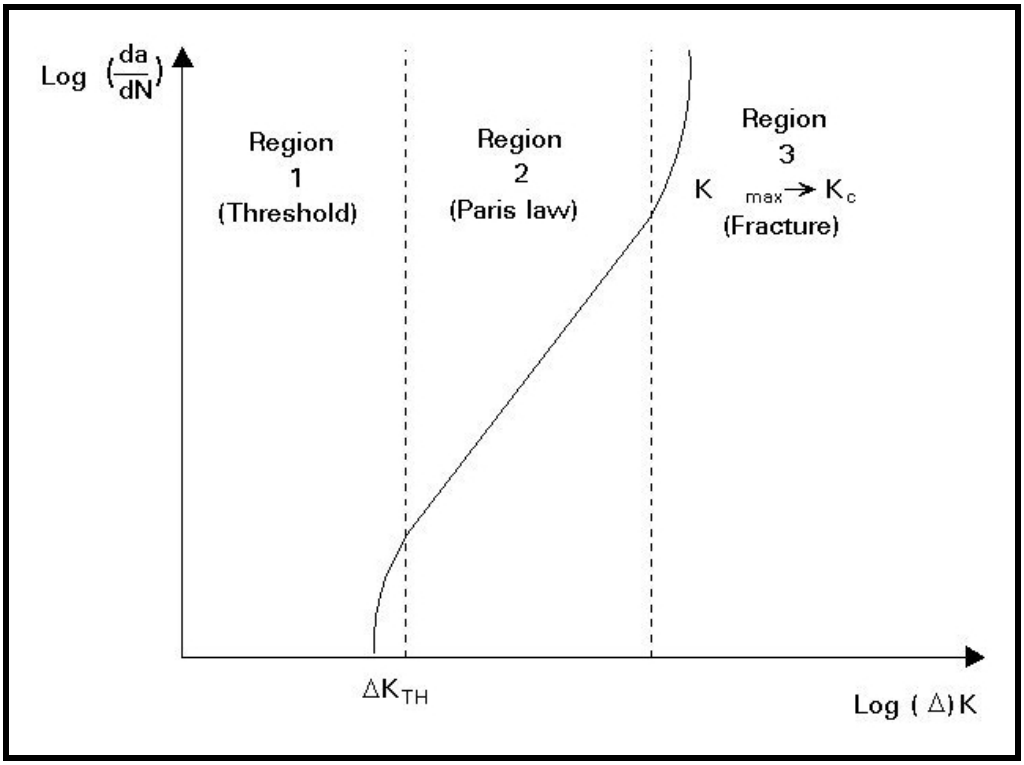

Figure 2.3: The crack propagation regions associated with fracture mechanics (UL FGG, 2011*a*). In this figure K is equal to K_{IF}.

The bulk of fatigue life defined by crack growth is associated with region two. Although many LEFM theories have been suggested to define the fatigue life in this region the most widely accepted theory is the Paris equation (Bannantine *et al.*, 1990):

$$\frac{da}{dN} = C\ (\Delta K_{IF})^{m_1} \tag{2.8}$$

Where:

C	=	Material constant associated with crack growth	[-]
K_{IF}	=	Stress intensity factor	[-]
m_1	=	Material constant associated with crack growth	[-]

Material constants C and m_1 can be found in literature and codes. The constants as well as the threshold values for steel and aluminium are shown in Table 2.2. It is shown in the table that ΔK_{th} is dependant on R[2].

[2] R is the stress ratio of the stress range and provides an indication of the mean stress range. A definition of R is available in Appendix A

Table 2.2: Material parameters for the Paris power law (dimensions in mm and N) from Hobbacher (1996) and BS7910:2005 (2005)

Material	**Constants**	**Threshold values ΔK_{th} [Nmm$^{-3/2}$]**			
		$R \geq 0.5$	$0 \leq R \leq 0.5$	$R < 0$	Surface crack depth < 1 mm
Steel	$C = 5.21 \times 10^{-13}$ $m_1 = 3.00$	63	$170 - 214R$	170	≤ 63
Alu	$C = 1.41 \times 10^{-11}$ $m_1 = 3.00$	21	$56.7 - 72.3R$	56.7	≤ 21

2.2 Fatigue of welded components

The fatigue data and theories presented in the previous section are based on parent material and only take into account the statistical variations related to the manufacturing of sheet metal or cast components. These manufactured products are stringently controlled by the applicable material specifications in terms of size, tolerances, defects, thinning process, chemical composition, etc. However, this is not the case for a welded component. While there are specifications that determine acceptable weld quality, the variations are greater and present their own challenges.

On the fatigue resistance side the standard material data (S-N curves) cannot be used since the weld itself has negatively affected the material and reduced its fatigue resistance (Maddox, 2011). This is illustrated in Figure 2.4. The welding process has introduced impurities, porosity, residual stresses, welding imperfections and, in some cases, it has changed the molecular structure of the material (Fricke, 2003). For these reasons it is necessary to create a fatigue resistance curve for each specific welding detail.

On the loading side it is necessary to determine the governing stress, in terms of fatigue, in the structure. Since welding is primarily a metal joining method a multitude of different geometries exist and need to be assessed. This is due to the fact that the structural detail as well as the weld itself creates stress concentrations due to secondary bending and geometrical discontinuities. The various methods to determine these stresses are discussed in the next section.

Due to the unique problems that are associated with welding fatigue (and since most metal structures incorporate some welding) various guides and codes have been written to assist with the design of welded structures. This section will present some of these guides and codes and will discuss their use and the methods they propose.

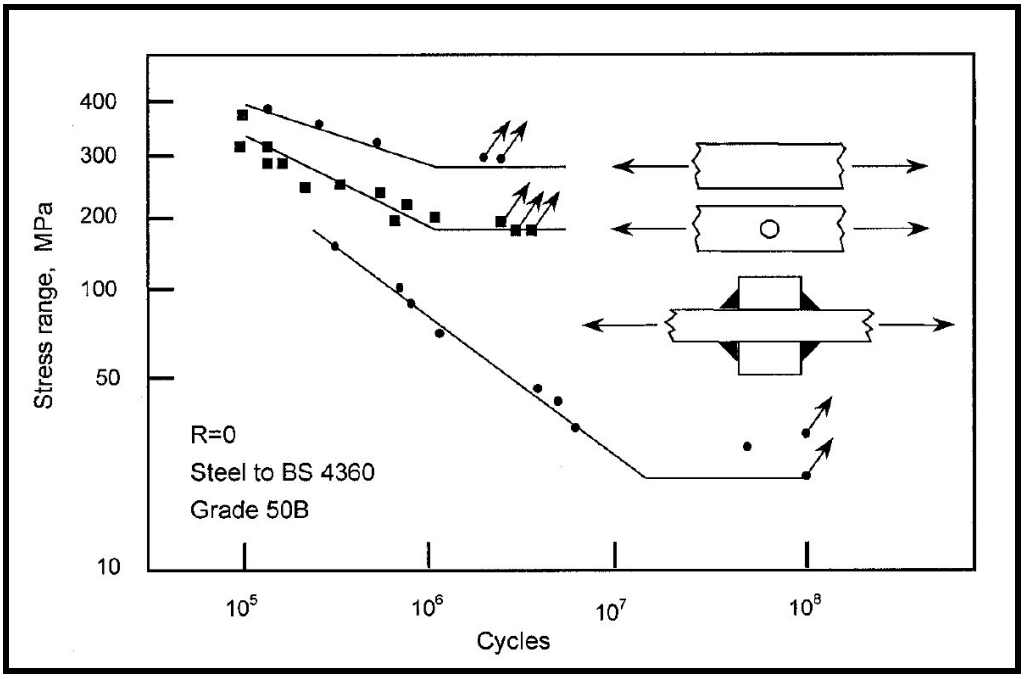

Figure 2.4: The effect of welding on fatigue strength (Maddox, 2000)

2.2.1 The International Institute of Welding recommendations

In 2008 the International Institute of Welding (IIW) published a revised edition of their popular 'Recommendations for Fatigue Design of Welded Joints and Components' (Hobbacher, 1996). This document is applicable to the fatigue design of ferritic or bainitic structural steels (with a yield stress not exceeding 960 MPa), austenitic stainless steels and aluminium alloys. It is not applicable to low cycle fatigue where the maximum nominal stress exceeds yield or where the nominal stress range exceeds 1.5 times yield. By definition this means that the recommendations do not present the use of the strain-life method.

The document gives recommendations regarding fatigue actions, determining stresses, stress history and fatigue improvement methods and provides fatigue resistance data. These will be discussed in the sections below where applicable.

2.2.2 Eurocode

In May 2005 the European Committee for Standardisation (CEN) published a revised edition of Eurocode 3 (CEN/TC250, 2005). This code provides methods for the assessment of fatigue with a specific focus on steel structures. In May 2007 the CEN published a revised edition of Eurocode 9 (CEN/TC250, 2007). This code is similar to Eurocode 3 but focuses specifically on aluminium structures. The latter of the two codes will apply to this thesis, since

the structure under investigation is an aluminium structure.

2.2.3 Stress determination methods

In the previous section it was mentioned that one of the challenges of determining the fatigue life of welded components is to determine the governing stress. This section presents three methods to determine these stresses.

2.2.3.1 General

Due to the geometric shape of a weld its root and toes can be classified as notches (MacDonald, 2011*c*) as shown in Figure 2.5. This means that each weld toe and root produces a notch effect and thus a non-linear stress peak. The structural geometry and even the geometry of the weld itself also causes secondary bending stresses that needs to be taken into account when assessing the fatigue life of the weld.

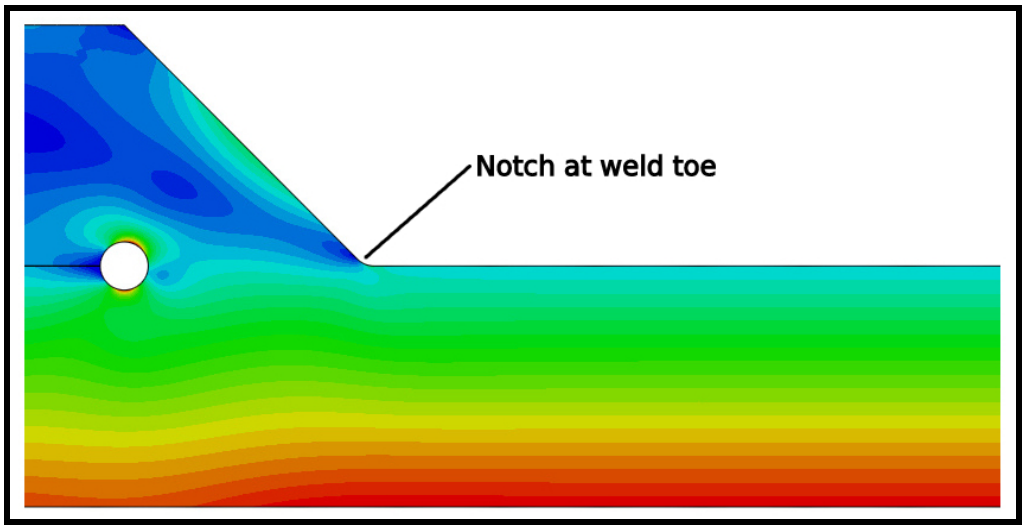

Figure 2.5: A FE analysis contour plot of the notch effect caused by the weld toe. In this case the geometry is subjected to pure bending.

Figure 2.6 is a plot of the stress on the surface of the structure as a function of distance from the weld toe. It also presents the different stress components that combine to produce the notch stress. These components are:

- Nominal stress: The stress calculated in the sectional area of the material under consideration. This stress excludes any secondary bending stresses caused by the joint or the weld geometry.
- Structural stress: This stress includes all secondary bending stressed caused by the joint geometry but excludes the influence of the local weld geometry.

- Notch stress: This is the non-linear stress peak which includes the effects of the joint geometry and the local weld geometry.

These stress components will be discussed in more detail in the following subsections along with the various methods that can be used to determine the stress. This includes choosing the applicable fatigue resistance curve that is required to calculate fatigue life.

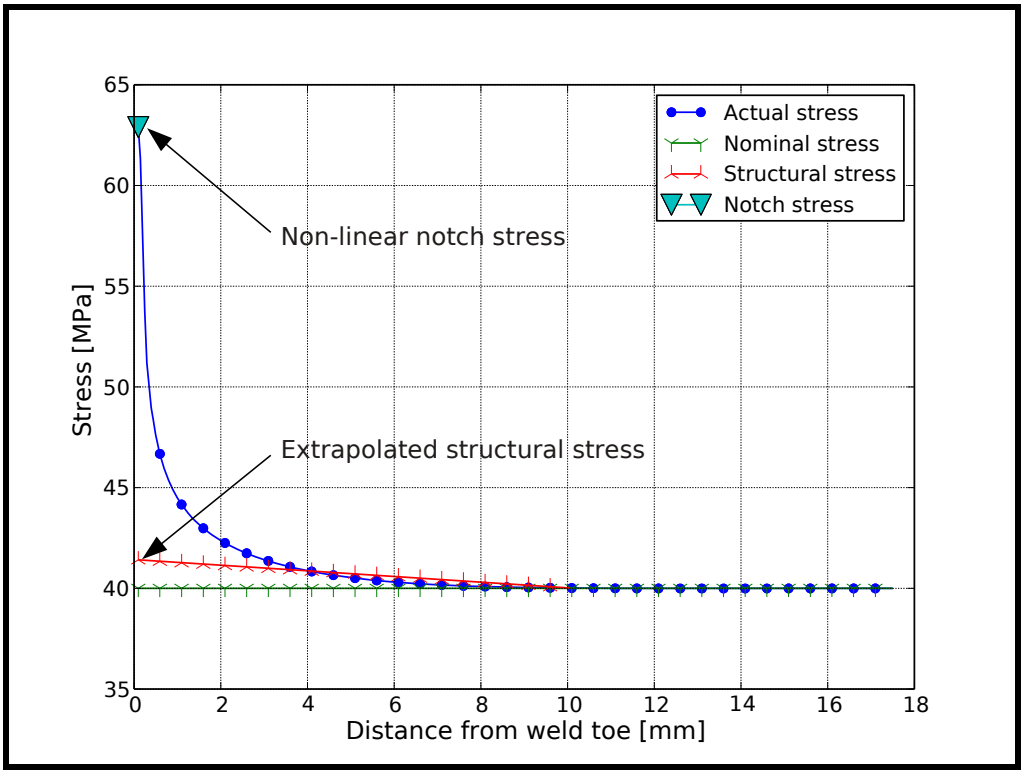

Figure 2.6: A plot of stress versus distance from the weld toe as well as the various stress components

2.2.3.2 Nominal stress method

This method assumes the nominal stresses have been determined, either by calculation or strain measurement, and can be used to calculate the fatigue life of the component. In this case the fatigue resistance data incorporates the non-linear stress peak of the notch as well as any secondary stresses that have been caused by the structural- and weld geometry. This is illustrated in Figure 2.7.

Where:

σ_{mem}	=	Membrane stress	[MPa]
σ_{ben}	=	Shell bending stress	[MPa]
σ_{nlp}	=	Non-linear stress peak	[MPa]

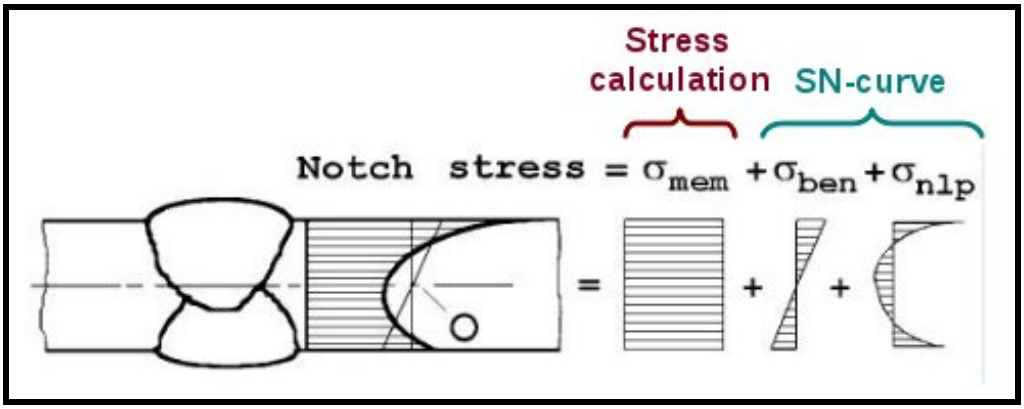

Figure 2.7: A graphical representation of the stress components associated with a welded geometry. It illustrates how each stress component is incorporated in the nominal stress method. Adapted from Hobbacher (1996).

This method relies on the fact that the geometry in question has been tested and a S-N diagram has been constructed based on the nominal stress range. The IIW (Hobbacher, 1996) and the Eurocodes (CEN/TC250, 2005, 2007) provide various geometries and allocate a FAT (fatigue) class to each of them. These FAT classes can then be used to create the fatigue resistance curves applicable to that geometry. An example of such geometries and their classifications are shown in Figure 2.8.

No.	Structural Detail	Description (St.= steel; Al.= aluminium)	FAT St.	FAT Al.
600	**Lap joints**			
611		Transverse loaded lap joint with fillet welds Fatigue of parent metal Fatigue of weld throat	 63 45	 22 16
612	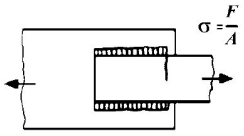	Longitudinally loaded lap joint with side fillet welds Fatigue of parent metal Fatigue of weld (calc. on max. weld length of 40 times the throat of the weld)	 50 50	 18 18

Figure 2.8: A sample of S-N curves and their FAT classification to be used in the nominal stress method (Hobbacher, 1996)

The advantage of this method is that it is very simple to use and requires very little effort in terms of calculating stresses. The disadvantage of the method is that it only applies to the listed geometries. If the geometry or the loading deviates from the tabled structural details, and the deviation cannot

be accounted for by means of calculation or a scaling factor, the data is no longer valid. It can also be the case that the complexity of the structure makes it difficult to distinguish the nominal stress from other stress components.

2.2.3.3 Hot spot stress method

Frequently it is not possible to determine the nominal stress in a structure or the specific joint geometry is not available in the tables. In this case the hot spot stress method can be used. This method requires the designer to determine the structural stress near the weld toe or root. When the structural stress has been determined, it is used in conjunction with the applicable S-N curve to determine fatigue life. In this case the structural stress influence has been excluded from the fatigue resistance information while the non-linear stress peak of the toe is still included (see Figure 2.9).

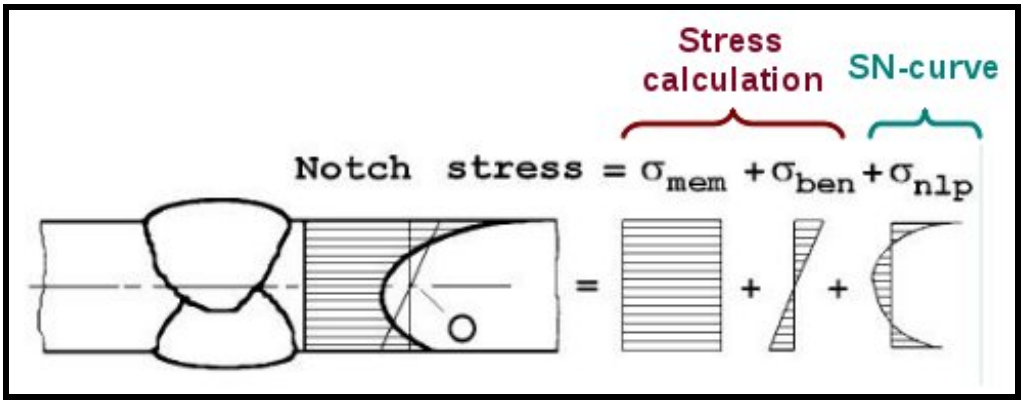

Figure 2.9: A graphical representation of the stress components associated with a welded geometry. It illustrates how each stress component is incorporated in the hot spot stress method. Adapted from Hobbacher (1996).

The advantage of the hot spot stress method (also known as the structural stress method) is that any type of geometry can be assessed. It also has the advantage that the stresses can be determined by both calculation and measurement (or a combination of both). The disadvantage of the method is that each weld still needs to be classified according to the given geometries. The stress determination methods also require interpolation to the weld toe. Because of these two reasons the method cannot readily be used for a full software analysis of the fatigue life.

2.2.3.4 Notch stress method

This method requires the designer to determine the non-linear stress in the notch. The method to determine these stresses is given in the IIW recommendations (Hobbacher, 1996). In this case there is only one S-N curve and it

does not include the influence of structural stress or the non-linear stress peak. This fact is illustrated in Figure 2.10.

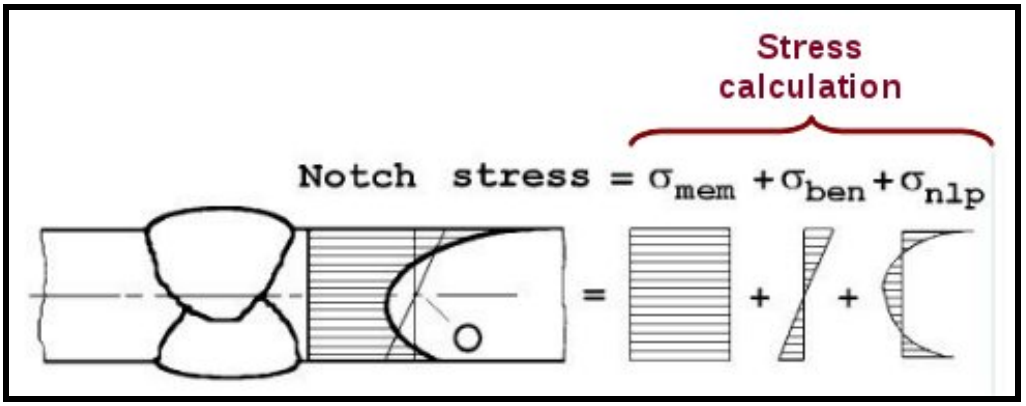

Figure 2.10: A graphical representation of the stress components associated with a welded geometry. It illustrates how each stress component is incorporated in the notch stress method. Adapted from Hobbacher (1996).

The advantage of this method is that it allows full software analysis due to the fact that no weld detail classification needs to be done. The disadvantage is that it requires detailed FE analysis which is not always practical on large structures. This type of FE analysis is necessary due to the fact that there are numerous cases where it is not practical to measure this stress.

2.3 Variable amplitude loading

While almost all published S-N curves are based on constant amplitude loading, various structures exist that are subjected to variable amplitude loading. These include the automotive, rail, aircraft, offshore and military industries. The challenge is to utilise the constant amplitude S-N curve to predict an accurate fatigue life with a known variable amplitude loading sequence.

This section presents a damage summation method that relates variable stresses to constant amplitude S-N data. It also discusses the cycle counting method which is used to condense the variable amplitude stress data into a usable format.

2.3.1 Fatigue damage

Fatigue damage can be defined as a fraction of the total life of a structure that is depleted by each cycle or group of cycles. The most popular damage summation theory is the linear damage rule proposed by Palmgren in 1924 and developed further by Miner in 1945. This is commonly called the Palmgren-Miner rule. This rule uses a basic assessment where the damage caused by each

stress range is expressed as a fraction of the number of times it occurs versus the total life of the component at the given stress range (see equation 2.9). The total damage of a given load sequence is the sum of all these fractions as stated in equation 2.10. According to the rule this means failure occurs when the total damage is equal to 1.

$$D_i = \frac{n_i}{N_i} \tag{2.9}$$

$$D_{total} = \sum \frac{n_i}{N_i} \leq 1 \tag{2.10}$$

Where:

D_i	=	The damage fraction caused by cycles at S_i	[-]
n_i	=	The number of cycles at S_i	[cycles]
N_i	=	The life to failure at S_i	[cycles]
D_{total}	=	The total damage	[-]

Several studies have been conducted in an attempt to verify the Palmgren-Miner rule and mixed results have been obtained. Recent research has shown that a damage failure criterion of one can be non-conservative. For this reason the IIW (Hobbacher, 1996) recommends a failure criteria of damage equal to 0.5.

The unreliability of the Palmgren-Miner rule has prompted several researchers to propose non-linear damage summation rules (Hashin (1980), Subramanyan (1976)). However, these rules are complex and require material constants that can only be determined by time-consuming and expensive tests. Because of this reason, and the simplicity of the Palmgren-Miner rule, it is still widely accepted and used.

2.3.2 Cycle counting methods

To be able to assess the fatigue damage of a complex load history, the history needs to be reduced into a number of events that can be compared to the available constant amplitude data. This compression of data is called cycle counting. Various methods have been developed over the years. These methods include level crossing counting, peak counting, range pair counting and the rainflow counting method (Downing and Socie, 1982). The most commonly used and accepted method today is the rainflow counting method (Marquis, 2011).

Since this name was established by the analogy[3] presented by Matsuishi and Endo (1968) it has become a generic term to describe a cycle counting method that attempts to produce cycles which corresponds to a closed hysteresis loop. Figure 2.11 illustrates this concept by 'producing' the loops A-D-A, B-C-B, E-F-E and G-H-G. This example shows cycles in the plastic range of the material

[3]The analogy is that cycles are defined by how rain drips off Japanese pagoda roofs.

(A-D-A and E-F-E). If high cycle metal fatigue is considered, the loops will all be linear lines corresponding to the modulus of elasticity of the material.

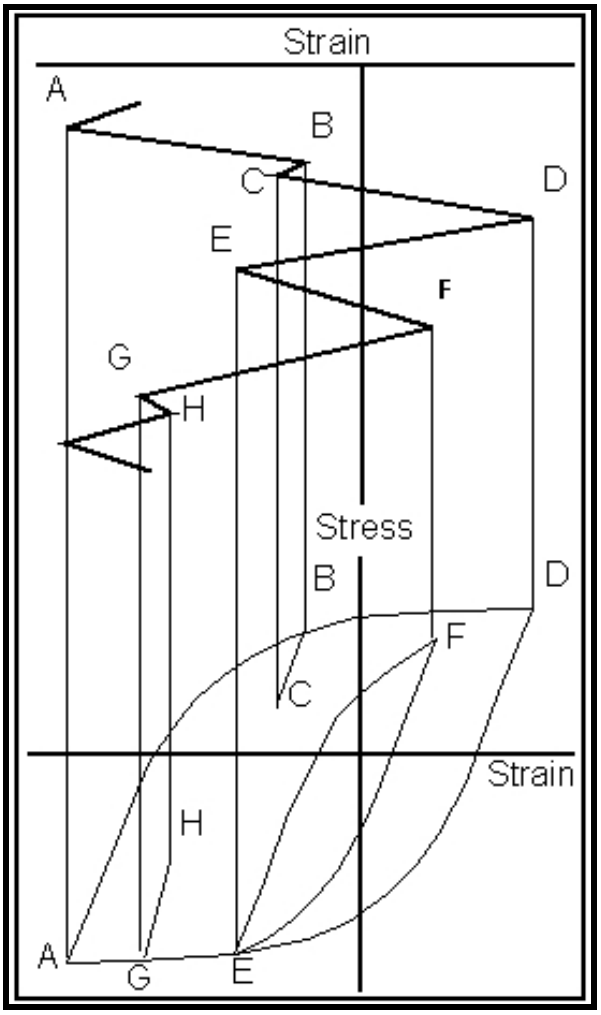

Figure 2.11: A graphical representation of the 'Rainflow' analogy and how it relates to a closed hysteresis loop (MSC Software Corporation, 2012).

Several variations of the original method have been published (Lee *et al.*, 2005). One of these variations is the three-point cycle counting technique as presented by the Society of Automotive Engineers (SAE) and American Society for Testing and Materials (ASTM) standards. This technique requires that the stress time history data be reduced to peaks and valleys and rearranged to start with either the highest peak or the lowest valley. When this is done, three consecutive stress points (S_1, S_2, S_3) are used to define two stress ranges:

$$\Delta S_1 = |S_1 - S_2| \tag{2.11}$$

$$\Delta S_2 = |S_2 - S_3| \tag{2.12}$$

If $\Delta S_1 \leq \Delta S_2$ a single cycle spanning S_1 to S_2 is counted (the range and its mean stress value are recorded) and the two points are removed from the time history data (essentially creating a new data set). No cycle is counted if $\Delta S_1 > \Delta S_2$. These rules are illustrated in Figure 2.12. These rules are repeatedly applied to the data until all cycles are counted. Additional information and examples of algorithm programming is provided by Downing and Socie (1982), Bannantine *et al.* (1990) and Lee *et al.* (2005).

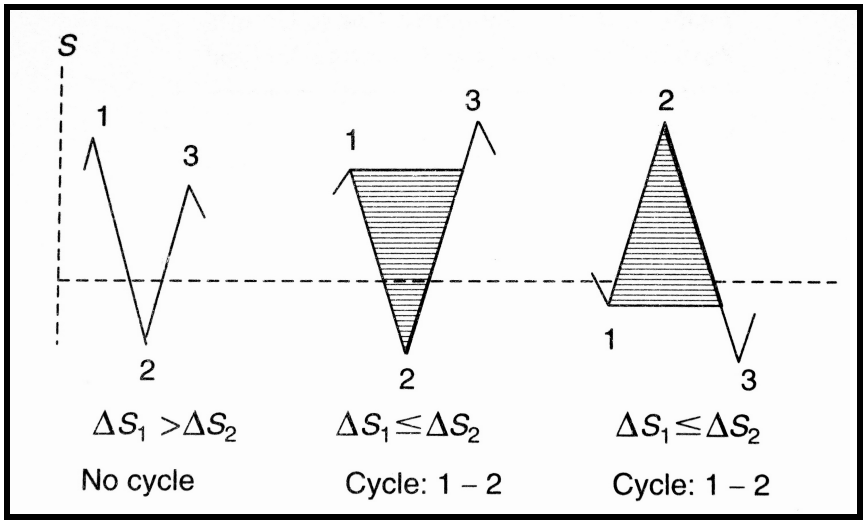

Figure 2.12: Rules of three point cycle counting (Lee *et al.*, 2005)

2.4 Correlation factor

All the methods and theories mentioned in this chapter can be combined and used to predict the life of a structure. However this calculated value will always be an **estimation** of the actual life of the structure. No current fatigue theory can predict the exact time and date that a component will fail. This inaccuracy is compounded by unknowns such as welding variations, loading variations and material property variations.

The best way to assess the accuracy of a fatigue life calculation is via testing. Laboratory testing is expensive and is also subject to the load cases used in the tests, thus it is only used by companies whose revenue (and risk) can justify the expenditure[4]. The most accurate test specimens are units that have already operated in the field. If a company has a large enough population of vehicles in the field it can use the failure (or lack of failure) data of those vehicles to determine a correlation between the actual life of the structure and

[4]Most (if not all) of the large automobile suppliers do extensive laboratory and track tests before releasing a product into the market.

the estimated life. This correlation factor (CF) can then be used in future designs to predict a more accurate life expectancy for the design[5].

It must be noted that the calculated correlation factor is specific to the type of vehicle, its operating environment and the materials that were used to manufacture the vehicle. For example, data for a steel vehicle travelling on highway roads can not be extrapolated to an aluminium vehicle that traverses dirt roads. Even on the same structure the consistency of load cases has to be taken into account. A correlation factor determined due to a varying gravity load cannot be extrapolated to an area that is damaged due to localised resonance.

2.5 Selection of method

GRW's products are primarily part of the automotive industry. This implies that the loads that the various structures are subjected to are variable in amplitude and frequency. Their design is also governed by various laws and regulations that are derived from, or reference, the European (EN) codes and regulations. Due to this reason it makes sense to use European codes as a guide to fatigue. The methods used in this thesis are based on Eurocode 9 and the IIW recommendations.

The expected high cycle fatigue loads warrant the use of the stress-life method. The structure, that is the subject of this thesis, contains various complex geometries that cannot easily be related to a documented geometry. To determine the stresses in these areas the hot spot stress method will be used. This method will be applicable to most of the structures that are manufactured by GRW.

As stated earlier the fatigue loads are variable. To relate this to the constant amplitude fatigue resistance data, the rainflow counting and the Palmgren-Miner damage summation methods will be used.

[5]This method is used by several internationally acclaimed automotive companies, but since the data and methods are not published these companies can not be mentioned or cited in this document.

Chapter 3

Problem statement

In the introduction it was mentioned that this document discusses the structural failures of the rigid[1] shown in Figure 3.1. This chapter presents the structural geometry of the tank in question as well as the applicable material information. It then presents each failure region and finally it discusses the general solution methodology that will be used for the investigation.

Figure 3.1: The tank mounted onto a freight carrier chassis

[1]In the tanker industry the term 'rigid' refers to a vehicle where a tank is mounted onto a purpose built truck chassis known as a freight carrier.

3.1 Tank geometry

Figure 3.2 shows a three dimensional model of the tank and its different sections. The tank shell itself is manufactured from 5 mm 5182 aluminium alloy (5182 H111) sheet metal joined to each other via rolled extruded sections. The base structure consists of two extruded angles running down the length of the shell. These, in turn, are supplemented by three cradles constructed from two 5 mm aluminium alloy (5182 H111) bent up 'outriggers', two 5 mm aluminium alloy (5182 H111) central sections, two mild steel cross braces and two 20 mm thick aluminium alloy (6061 T6) 'mounting feet'.

A cross section of the second cradle is shown in Figure 3.3. This picture shows how the various cradle components are attached to each other. The tank is mounted to the chassis by bolting each mounting foot to the structure with two M16 grade 10.9 steel bolts.

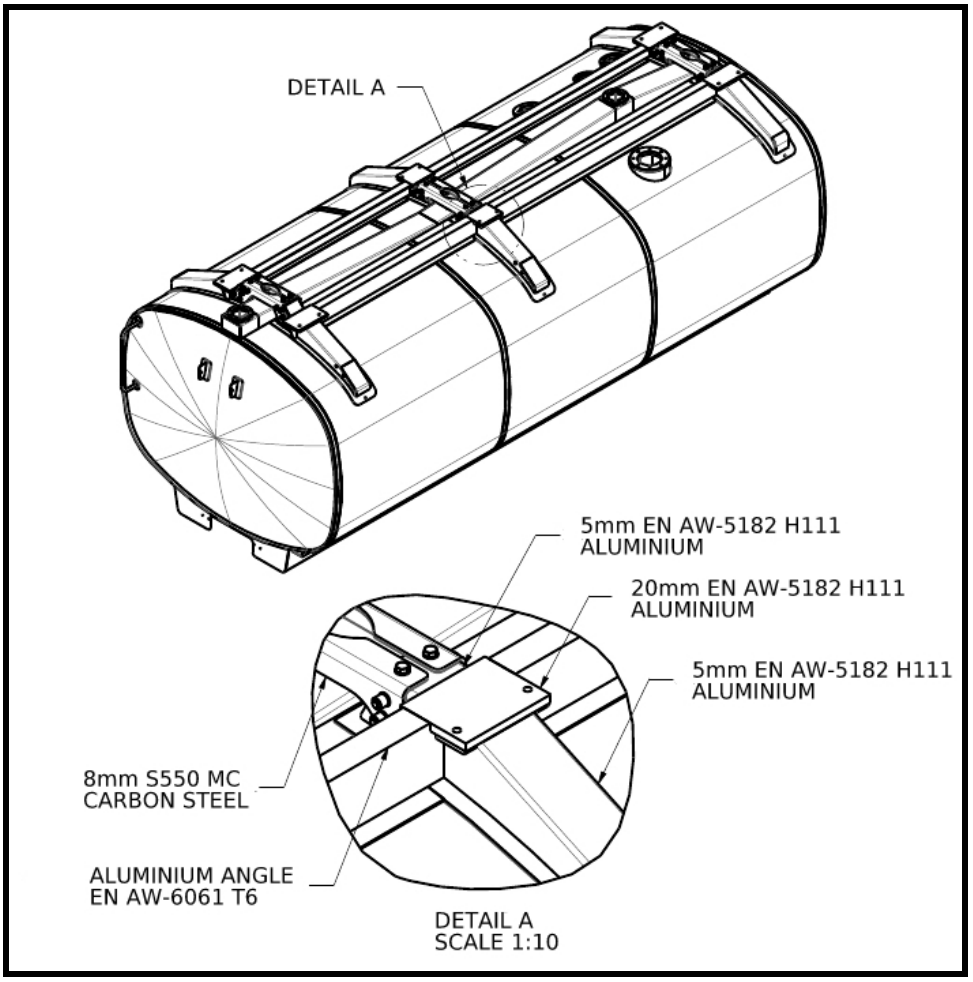

Figure 3.2: A 3D model of the tank structure

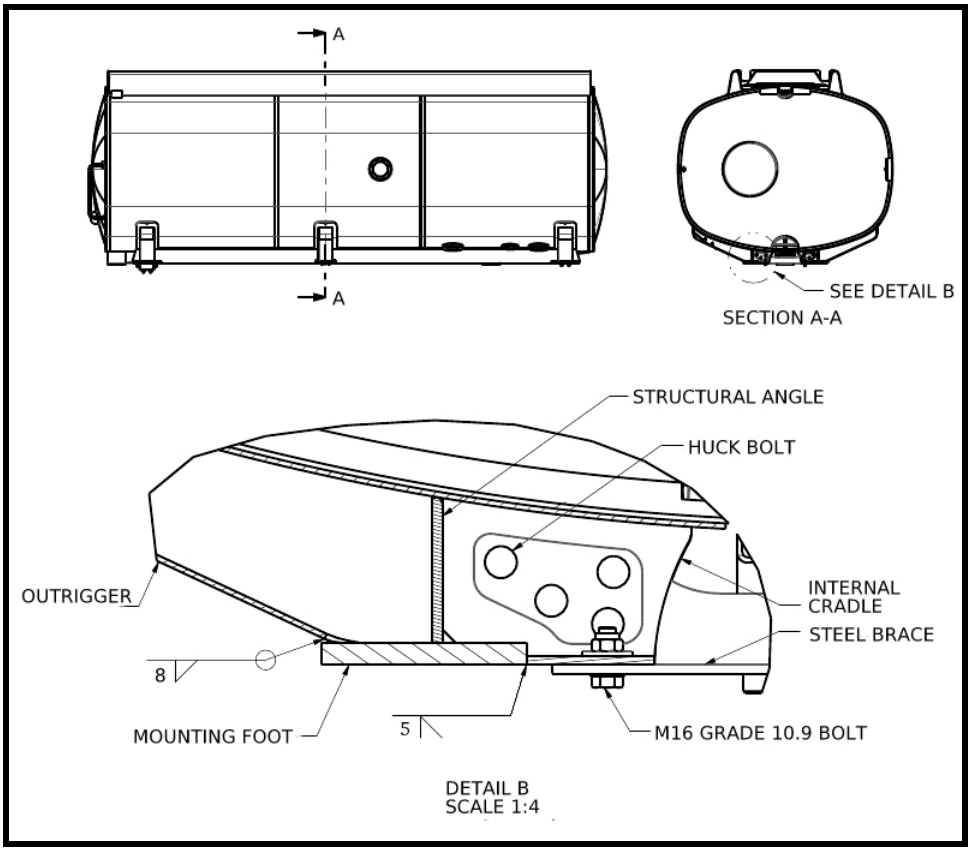

Figure 3.3: A cross section showing the cradle geometry

3.2 Crack areas

All cracks that will be investigated in this thesis occur on the second cradle in the mounting foot area (shown in Figure 3.3). It is important to note that all the crack initiation sites occur at a weld toe. Due to the fact that all the vehicles are still in operation it was not possible to remove a sample containing the crack to do a microscopic investigation. From visual inspection it is clear that the cracks are not caused due to ductile fracture, but have the characteristics of brittle fracture even though the affected metal is a ductile material. It is also clear that all cracks start in notched areas. This and the fact that the cracks have occurred on several vehicles in the population indicate that the cracks are typical fatigue failures.

This section will present each crack area and briefly discuss the relevant field data.

3.2.1 Crack one

The first crack position that is presented occurs where the aluminium alloy central sections are welded to the mounting feet. Figure 3.4 shows the crack initiation site as well as the propagation directions. This is the failure that has

occurred most often in the field. Figure 3.5 shows a close-up view of a crack that has propagated extensively.

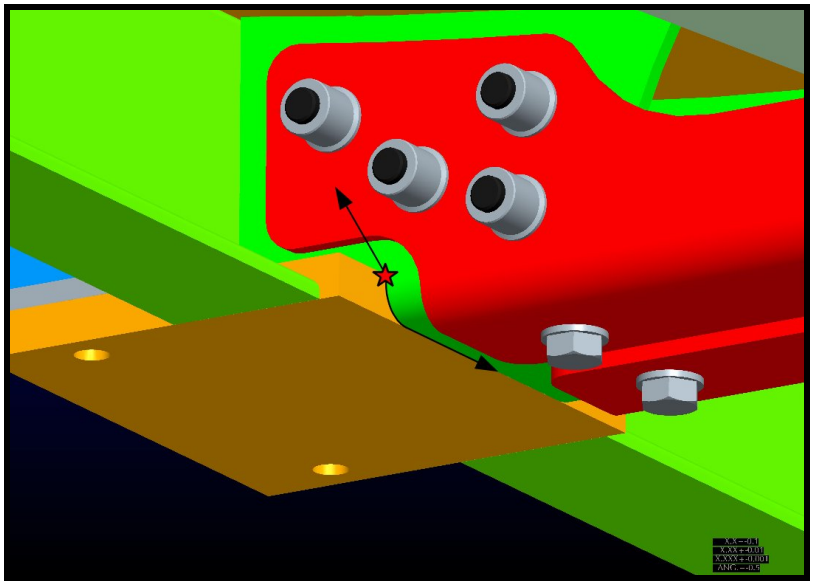

Figure 3.4: Crack one initiation position and propagation directions. Tank mountings not shown

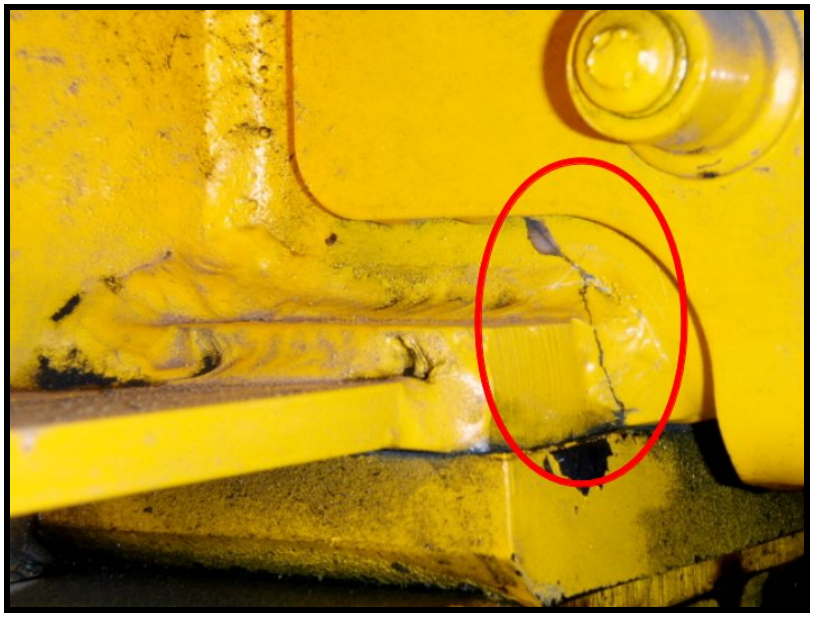

Figure 3.5: Close-up of crack one with the tank in the mounted position

3.2.2 Crack two

The second crack position occurs where the aluminium outriggers are welded to the mounting feet. Figure 3.6 shows the initiation site and the crack propagation directions. This failure has the second most occurrences in the field. Figure 3.7 shows a close-up view of such a crack.

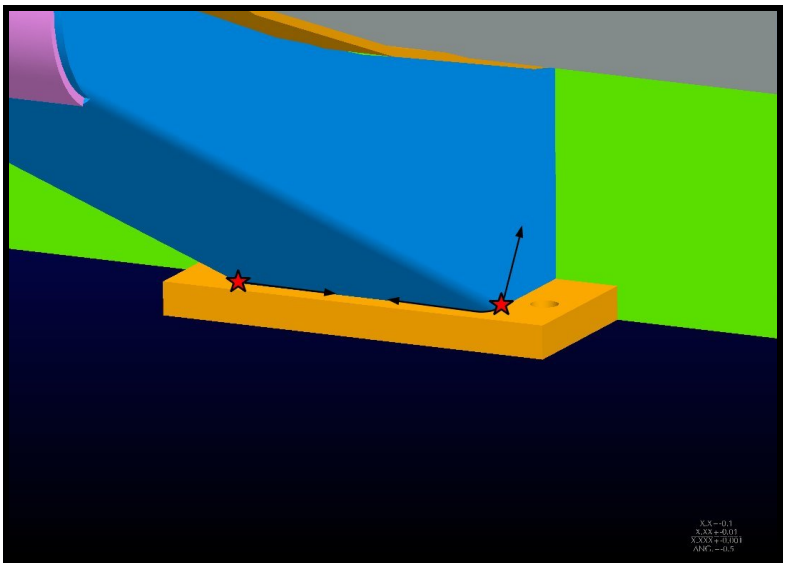

Figure 3.6: Crack two initiation position and propagation directions. Tank mountings not shown

Figure 3.7: Close-up of crack two. The extents of the cracks have been marked after a dye-penetrant test.

3.2.3 Crack three

The third crack occurs where the longitudinal angles are welded to the mounting foot. This area is presented in Figure 3.8. Figure 3.9 shows a close-up view of such a crack.

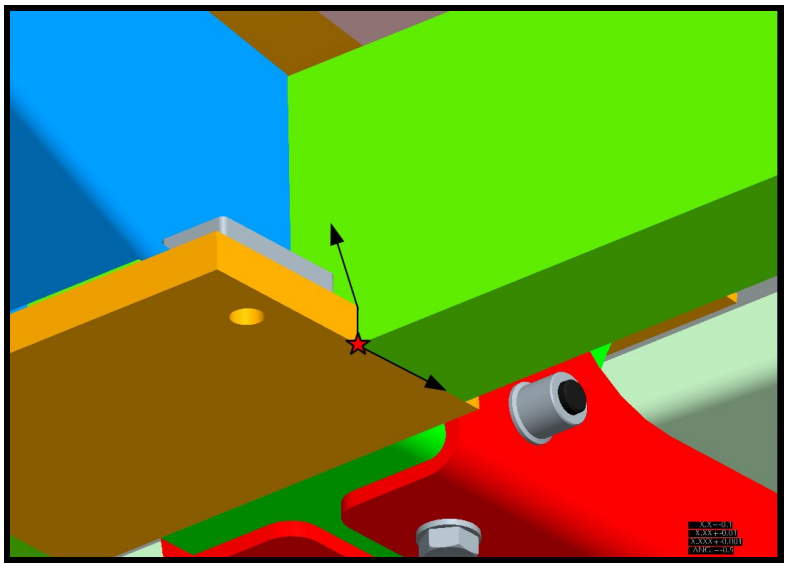

Figure 3.8: Crack three initiation position and propagation directions. Tank mountings not shown

Figure 3.9: Close-up of crack three with the tank in the mounted position

3.3 Solution methodology

Figure 3.10 shows a typical failure investigation and solution methodology. In phase one the failures are investigated and analysed to determine the reason for failure and to determine if calculations could predict this failure. This is important to know before solutions are proposed. In phase two solutions are proposed and refined to narrow the concepts down to a structurally and practically acceptable field fix. In phase three this concept is applied and tested to verify it's suitability.

The investigation to date has covered phase one and a part of phase two. However, this thesis only presents the first phase of the solution methodology and will discuss the various factors needed to complete that phase.

Phase one consists of five discrete steps. Firstly the failure data has to be collected from the field. This includes any data regarding the failure frequency in the population. Typical information is:

- How frequently was the structure operated before the cracks started (km, cycles, hours, etc)?
- How many vehicles in the population have shown these symptoms?
- What is the extent of the failures? Is it catastrophic failure or visible cracking?
- What are the implications?
- What is the current crack propagation rate?
- Is a crack sample available?

The difficulty associated with this step is getting accurate data from the operating personnel. The information tends to be based on emotion rather than fact and can be distorted by company politics. For this reason a site visit, arranged as soon as possible, becomes crucial in order for the validity of the claims to be assessed. As soon as the occurrences of failure have been established, the information listed above must be compiled to assess the implications and scope of the failures.

The next step is to acquire field measurements of the actual strain in the structure. This includes calculating the operational duty cycle for use in subsequent steps. The process is discussed in Chapter 4.

In step three a finite element model is created and verified with the strain results. In most cases this model would already have been created to assist with defining the measurement positions of step two. The model is then used to calculate the required scaling factors. Step three is the subject of Chapter 5

Finally Chapter 6 covers steps four and five which encompass the structural fatigue life calculations and the determination of the correlation factor. The correlation factor is the ratio of actual life versus calculated life. This factor

is a means of relating the damage caused by the composite duty cycle to the damage of the actual operational loads. If all variables stay the same this factor can be used to predict the **actual** life of any improvements that are done to the vehicle.

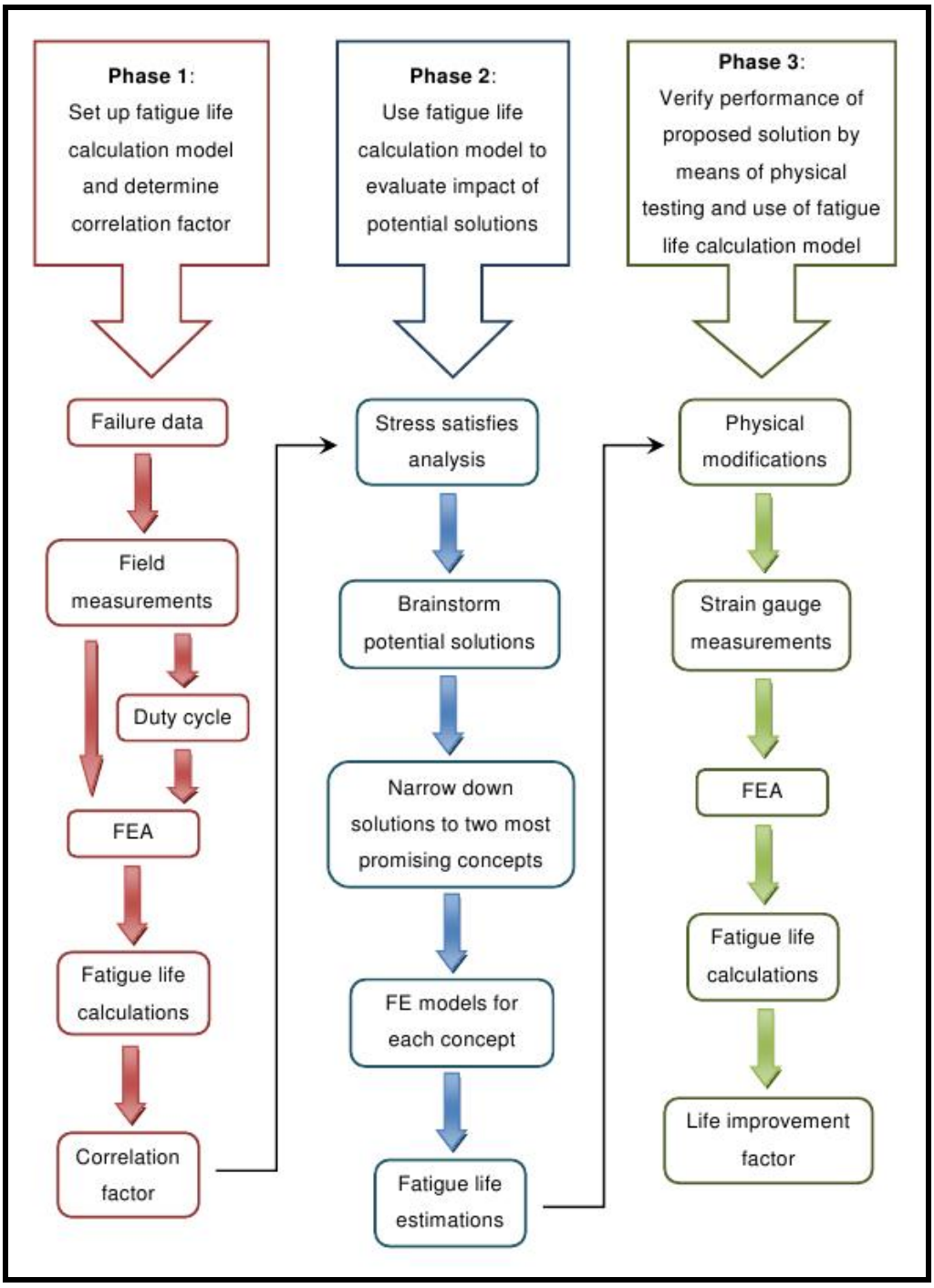

Figure 3.10: A graphical representation of a typical failure investigation and solution methodology (Franken, 2010)

Chapter 4

Acquiring operational strain data

To accurately determine the estimated fatigue life of the different crack areas, it is necessary to measure the actual strain in the structure. This experimental approach produces the strain data, for various sections of a duty cycle, that is then used to calculate the fatigue life.

The test itself has three major goals. Firstly it provides strain data that is used to correlate the FE model to ensure its accuracy. Secondly it provides the necessary data for the fatigue life calculations that will subsequently be used to determine the correlation factor between the actual life and the calculated life of the structure. The final goal is to assist in understanding the mechanisms that are causing the cracks so that an adequate solution can be found.

Tests had to be done on a tank that is in service so several restrictions were imposed on the experimental set-up. This chapter presents and explains the tests that were conducted and briefly discusses the resulting data.

4.1 Test equipment

Several transducers are used to acquire the data for the investigation. Strain gauges are used to measure the strains in the structure. This data is supplemented by acceleration data acquired with accelerometers. To assist in understanding the details of an event, speed and positional data are also recorded via CAN bus[1] and GPS. Details of the transducers are presented below.

Strain gauges

The gauges that are used are manufactured by HBM. A typical data sheet of these gauges is given in Appendix B. These are 350 Ω gauges with a 6 mm grid size and are selected to have the correct thermal expansion coefficient for the applicable material. All the gauges have a gauge factor that varies between 2.1 and 2.09. Mostly uniaxial gauges are used although some triaxial (three

[1] A vehicle bus that uses the controller area network (CAN) protocol for internal vehicle communications.

element rosette) gauges are used where deemed necessary. The selection of each of these gauges will be explained in the relevant sections below.

Accelerometers

The accelerometers are ±4 g and ±10 g three-axis capacitive accelerometers from MEMSIC (previously Crossbow) with a DC to 100 Hz range. These are extensively used in the automotive and aircraft industry. Specification sheets of the accelerometers are presented in Appendix C.

Data acquisition

The data acquisition system that is used is an e-DAQ lite manufactured by SOMAT. The system has been set up to provide seventeen bridge channels (with built-in 350 Ω completion resistors) and three analogue channels. The analogue channels are used with the accelerometers mentioned above, to measure the accelerations that the tank is subjected to.

The e-DAQ is also fitted with a CAN bus channel and a GPS channel. These provide operational information from the truck itself and GPS coordinates respectively.

Additional equipment

The e-DAQ was housed within an IP65 rated box (Figure 4.1) along with a 24-12 V DC-DC transformer, a back-up battery and a Wi-Fi router with a 3G modem. The router and modem are used to access the e-DAQ remotely without opening the box and to check on it via the Internet. The back-up battery is added to protect the integrity of the data by ensuring that the e-DAQ powers down properly each time.

4.2 Test set-up

24V Power is provided via the vehicle's electrical system. The power connections to the vehicle were made in accordance with MAN's bodybuilder bulletin 103. The truck is protected from a short circuit via a 10 A in-line fuse. This power source is then converted to 12 V with the 24-12 V DC-DC transformer. The 12 V feed supplies power to the e-DAQ and the router and it charges the battery. The router served as a wireless method to access the e-DAQ during testing.

The gauges are applied according to the recommendations of Hoffman (1989). Since long term measurements are required, it was necessary to compensate for any change in temperature. Temperature compensation was accomplished by connecting a 'dummy gauge' in a half bridge configuration to

Figure 4.1: Box in which all the equipment was housed.

each of the gauges. The 'dummy gauge' must be exposed to the same temperature fluctuations as the active gauge but must not be subjected to structural strain. The 'dummy gauge' consisted of a strain gauge from the same batch as the active gauge or a batch with a similar gauge factor. This gauge was applied to a small aluminium or steel plate and the plate was then applied as closely as possible to the active gauge with double sided tape. The double-sided tape provided sufficient isolation from the structural strains in the structure.

Figure 4.2 shows a typical application and use of the temperature compensating 'dummy gauge'. This particular configuration of a Wheatstone bridge requires a bridge factor of one since only one gauge is actively measuring strain (Hoffman, 2001).

Figure 4.2: Typical dummy gauge application

In total twenty-two strain positions and four acceleration measurement

points were recorded during several test situations. Only the data that is relevant to phase one of the solution methodology will be discussed in this thesis. Information about the remaining strain gauge and accelerometer positions can be found in Appendix D.

Due to the fact that the vehicle in question transports a flammable liquid (aviation fuel), restrictions were imposed on the project due to health and safety law constraints. The most significant restriction was that no 'hot work' could be done on the tank. This includes grinding, drilling and using unauthorised electrical equipment. Risk assessments were done to obtain permits to use the soldering iron and the laptop in the vicinity of the vehicle. All cleaning and sanding was done either manually or with pneumatic equipment.

4.3 The failure positions

This section presents the strain gauge set-up at each of the various failure positions and explains the reasoning behind each gauge choice, position and application method. At this time a preliminary FE model was created and used to determine the exact strain gauge positions and principal strain directions. Even though these directions were predicted, three element rosette gauges were used in selected positions due to uncertainty regarding the dynamics of the vehicle.

4.3.1 Crack one

Due to the hot work restrictions that were mentioned in the previous section, it was not possible to remove the steel brace that is huck bolted to the two internal cradles. This made it impossible to measure strain at the crack initiation site. To navigate around this problem three uniaxial gauges were applied at strategic positions that will be used to calculate the strain at the crack position. These gauges are shown in Figure 4.3.

The first of these gauges is gauge number thirteen and is shown, along with its 'dummy gauge', in Figure 4.3a. This gauge measures all strains that impact on the cradle combination since this area is very sensitive to tank movement. This gauge provides the data from which strain at crack position one will be calculated. Gauge twenty and twenty-one (Figure 4.3b) are used to determine the loading mechanism that produces the strain in gauge thirteen along with the accelerometer data. The two positions enable the author to determine if the load was due to vertical, sideward or forward motion. This provides good correlation data for the FE analysis that is used to determine the relationship between gauge thirteen and crack position one. The calculations to determine this relationship will be discussed in more detail in the next chapter.

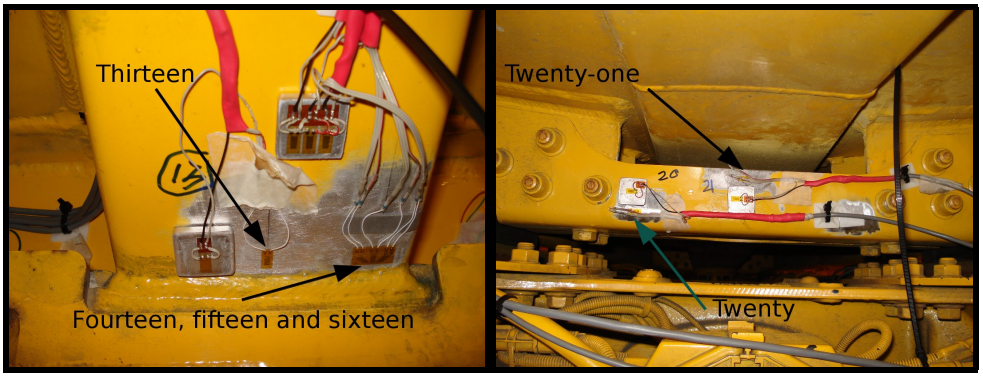

(a) Gauges on centre outrigger - far side (b) Gauges on steel brace

Figure 4.3: Gauge positions to determine strain at crack position one

4.3.2 Crack two

To investigate this crack, a three element rosette was positioned at the corner of the outrigger near the weld to determine the strain at the crack initiation point. Gauges fourteen, fifteen and sixteen (the 135°, 90° and 45° gauges respectively; where the angle is measured anti-clockwise from the horizontal) are shown in Figure 4.4. Preliminary FE analyses suggest that the principal stress direction at this point does not deviate greatly with varying loads. This implies that a uniaxial gauge should be sufficient. Due to the unusual geometry in this area, a three element rosette is used to verify this assumption and to ensure that any damaging stresses that disprove this assumption, are not overlooked.

The geometry and the size of the gauge does not make it practical to bond it exactly at the initiation point. The gauge is bonded as closely as possible (10 mm from the weld and 20 mm from the bend line) to the initiation point and the strain values are then scaled by factors determined from the FE analysis. This will be discussed in the next chapter.

4.3.3 Crack three

In this case strain is measured at the corner of the angle to mounting foot interface. Uniaxial strain is measured on one side of the cradle (gauge twelve) while a three element rosette (gauges seventeen, eighteen and nineteen) is used on the other side to verify the assumption of uni-directional strain. Gauges seventeen, eighteen and nineteen are the 90°, 45° and 0° gauges respectively. Figures 4.5 and 4.6 show the strain gauge applications. Both gauges are positioned 10 mm from the bottom of the angle and 20 mm from the weld toe.

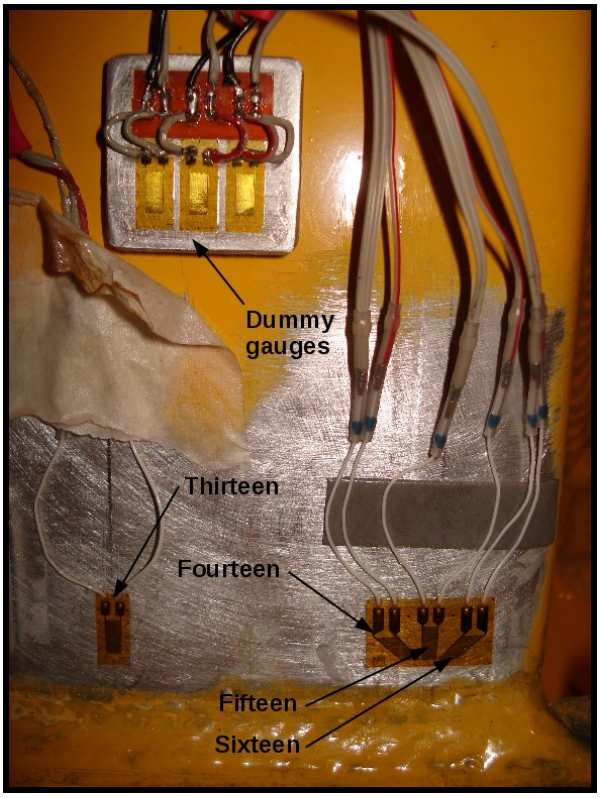

Figure 4.4: Gauges at crack position two

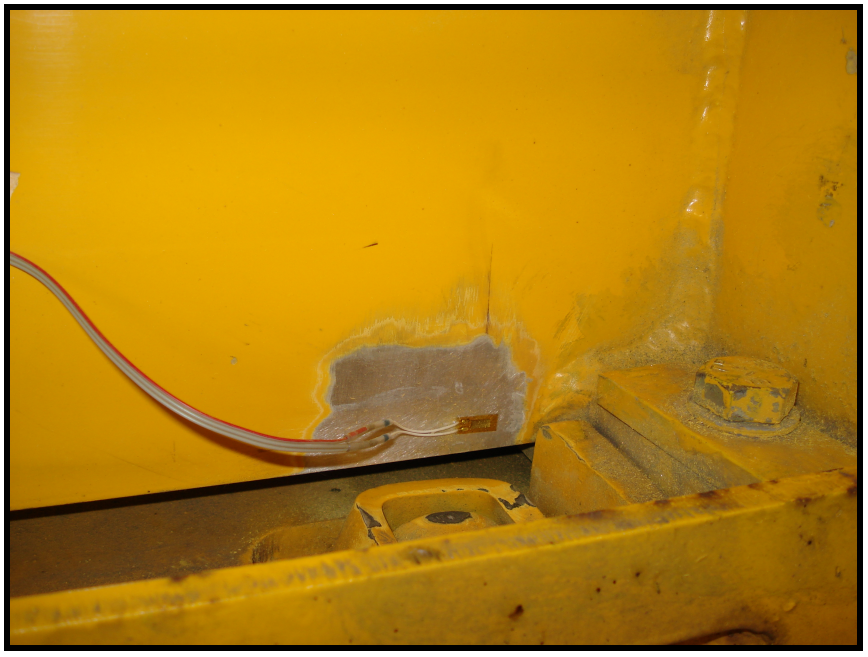

Figure 4.5: Uniaxial gauge (gauge twelve) at crack position three

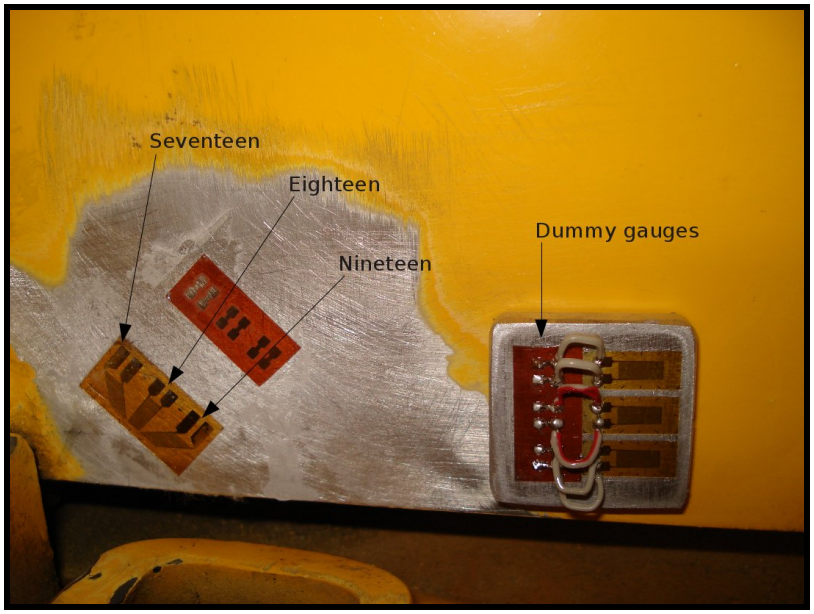

Figure 4.6: A three element rosette (gauges seventeen, eighteen and nineteen) at crack position three

4.4 Acceleration measurements

To relate the measured strains to vehicle dynamics it is necessary to measure time dependant vehicle accelerations. This is achieved by mounting a ±4 g and a ±10 g accelerometer on the left and right side of the vehicle respectively. Both are mounted with x in the driving direction, y to the right and z downwards. It was not expected that accelerations higher than 4 g would occur in the fore and aft and sidewards directions. For this reason the ±4 g accelerometer is set up to measure in the y and x directions to achieve the appropriate sensitivity in those measurement directions. The ±10 g accelerometer, in turn, is set up to measure in the z direction since higher forces can be generated in this direction.

Each accelerometer is placed on a central mounting above a gusset to ensure it is attached to the chassis as rigidly as possible. This prevents measuring a damped signal. The device is mounted by bonding a tapped aluminium plate onto the mounting with Pratley epoxy and then bolting the device to the plate. This ensures an integrated attachment while providing a means to remove the accelerometer without damaging it. This set-up is shown in Figure 4.7.

4.5 Additional measurements

Along with the previously discussed measurements, GPS data and CAN bus data are also recorded. The GPS data is of significance because it is used to pinpoint the coordinates of a particularly damaging event and it provides

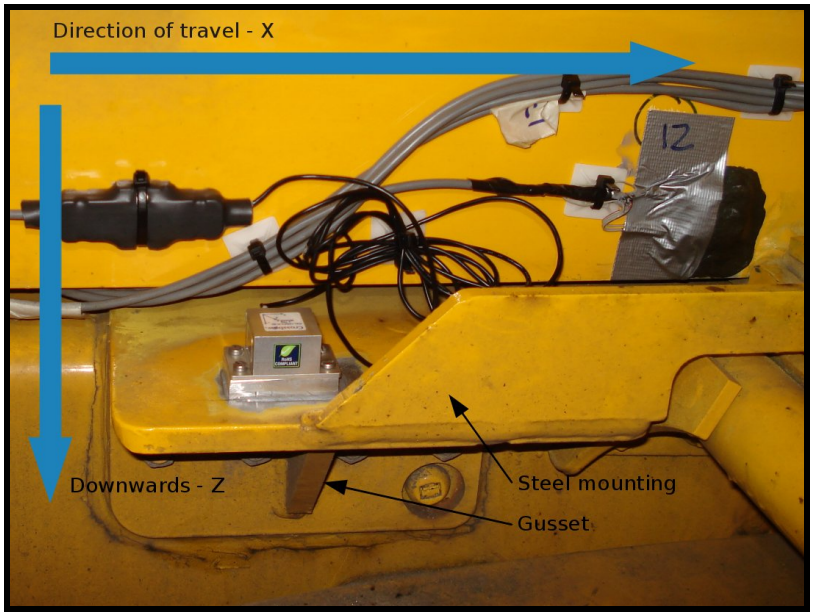

Figure 4.7: ±10 g Accelerometer fitted on the far side, centre mounting

speed and duty cycle data.

The CAN bus data was collected using the customer specific control module (KSM) provided on the truck. This is an interface that MAN has provided to enable the customer to have access to specific engine controls. The connection was made according to the MAN's bodybuilder bulletin 100. The CAN bus protocol is J1939 and provides speed, ambient temperature, braking and various other data. This data assists the analyst in understanding the circumstances surrounding a particular event.

4.6 Test procedure

The tests were conducted on a Royal Air Force (RAF) base in the north of Scotland. The base is situated on the outskirts of the town Lossiemouth, roughly 100 km east of Inverness. This base was chosen because it has a 100% failure rate and for this reason it can safely be assumed to be the worst case. An aerial view of the base is shown in Figure 4.8.

The tests were conducted on an operational site to ensure that the composite duty cycle closely represented the actual operational cycles.

The tests consisted of two parts. The initial tests recorded time-series data of the gauges and accelerometers during a typical operational cycle. Ideally it would have been best to have these tests done by several different drivers, but the operation at that time did not allow for this. Since all the tanks at the specific site had failed, it is safe to assume that driver influence is negligible and is not the root cause of the problem.

Figure 4.8: A satellite photo of RAF Lossiemouth

The second part of the tests concentrated on isolated load cases. These tests were used to determine the structural damage effect of each load case. The results of these tests can also be combined to create the composite duty cycle. This is discussed in more detail in Chapter 6. Each load case is discussed briefly in the sections below.

Cornering

In this load case the vehicle was driven in tight circles on a concrete surface (part of the service road). These circles represent the manoeuvring that the vehicles need do in their daily tasks. Figure 4.9 shows a typical manoeuvring surface with the tyre marks left on it. The maintenance managers stated that it is not unusual for a set of tyres to last for as little as 6000 km. This test was done with an empty tank and repeated with a fully loaded tank.

Braking

This load case simulated typical braking loads that would happen during operation. Figure 4.10 shows the results of a typical braking simulation. The top graph shows acceleration in the x direction while the second graph illustrates vehicle speed. Four braking tests were conducted: three 'sharp braking' events at 15 km/h, 25 km/h and 34 km/h while the fourth test was a gradual stop.

Figure 4.9: Tyre marks on a manoeuvring surface

This information is evident when looking at the x-acceleration results. These tests were conducted with a full and an empty tank.

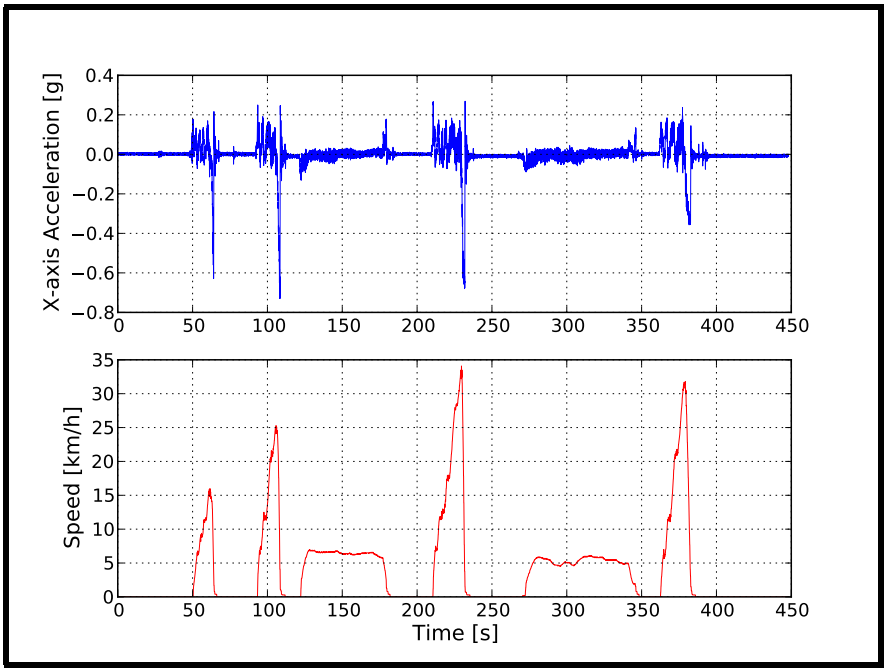

Figure 4.10: X-acceleration and speed data recorded during a braking simulation

Driving over a stone grid

One major concern for the RAF is Foreign Object Debris/Damage (FOD). This includes any object on the runway that can get sucked into an aircraft's engine and cause engine damage. Due to the impact that such an object can have on an aircraft, the RAF is vigilant about ensuring that no such objects are carried onto the runway and taxi roads by the service vehicles. All roads leading to the aircraft manoeuvring areas have a stone grid (similar to a cattle grid) to remove any stones that are stuck in the tyres of the service vehicles. After the vehicle has crossed the stone grid, the driver stops and visually inspects the tyres. This is an operational load case that occurs in each cycle.

Figure 4.11 presents the z-axis acceleration results from such an event. These tests were conducted with a full and an empty tank.

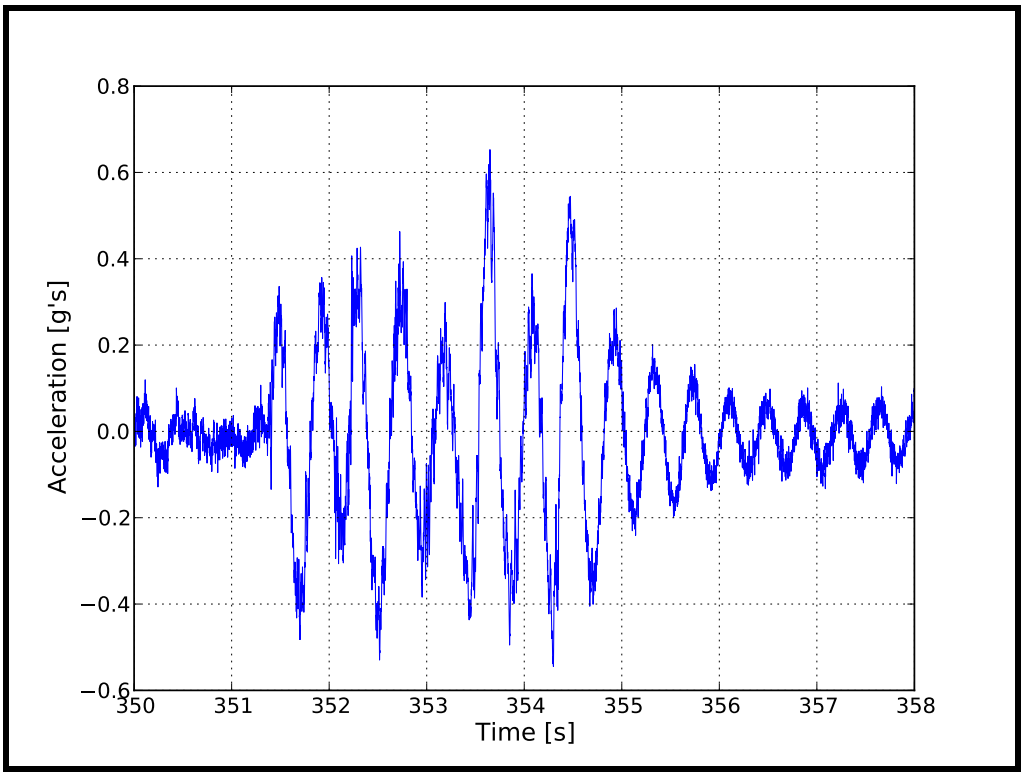

Figure 4.11: Z-acceleration data recorded while driving over a stone grid at 6.5 km/h

Driving over containment humps

One of the typical events in an operational cycle is refilling the tanker after it has refuelled an aircraft. To be 'battle ready' this is done as soon as possible after the tank has been emptied.

These refuelling stations have a U-shaped access road with dedicated entrance and exit gates. Each road has a containment hump (shown in Figure 4.12) that helps to contain fuel in the event of a spillage. This means that the empty vehicle has to enter the area by driving over one such a hump and exit the area driving over the second one while full.

Although the humps are not particularly high they are quite aggressive which is why the drivers always approach them at a 45° angle. This produces severe rocking and twist loads on the chassis and the mounted tanker.

Figure 4.12: A typical containment hump at RAF Lossiemouth

Filling the tank

This is the event where the stationary tanker is filled with product. A full load of 19 864 L was loaded into the tank while strain values were recorded. Figure 4.13 shows the strain values measured on gauge thirteen during this event. A compressive strain gradually increases as is expected.

Due to the fact that the vehicle is stationary in this case, it can be assumed to be a quasi static event. This makes this data ideal to correlate with a static FE analysis.

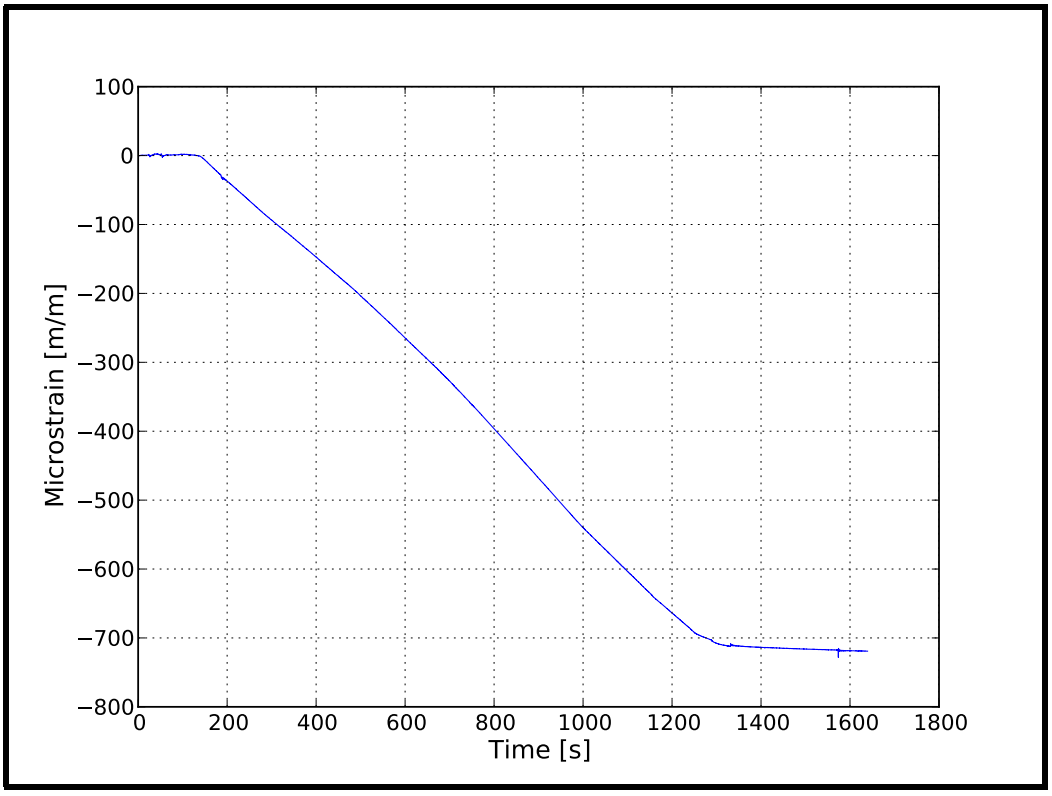

Figure 4.13: Strain values measured on the right side, centre outrigger during filling

4.7 Results

A vast amount of data was recorded during the tests mentioned above. All the data was checked for common errors and statistical validity, but these checks are numerous and will not be presented in this document. This section will present a sample of the data to illustrate, in a general sense, what results were obtained. It will also investigate and discuss some of the assumptions stated earlier in the chapter.

4.7.1 Sample data

This section will present some data that was measured while driving from the drivers' station to the refuelling bunker. Figure 4.14 shows the GPS data from this trip superimposed on a Google Earth satellite photo.

Figure 4.15 presents an acceleration spectral density (ASD) plot of the accelerations measured during this trip. Note the 'spike' in the z-axis acceleration data at 2.5 Hz. This indicates that there is a lot of energy at this frequency compared to the rest of the frequency range. This could indicate that a resonance exists at this frequency. It is clear from Figure 4.16 that the same frequency exists in the strain data, which indicates that it is not damped

Figure 4.14: GPS data super-imposed on a Google Earth satellite photo

by the rubber mountings or the inertia of the tank. While this will have to be investigated to ensure that a suitable solution is found, this falls outside of the scope of this thesis.

Figure 4.17 presents an amplitude distribution plot of the accelerations measured during the trip. The z-acceleration produces a well-shaped curve (a good statistical sample) with no events as is expected from driving on a flat road. The x- and y-acceleration data produces data with evident event spikes. These can be attributed to the turns and the stop-starts made during the trip.

4.7.2 Assumptions

In Section 4.3.2 and 4.3.3 it was stated that a uniaxial gauge should be sufficient to determine the governing strains in the area but that a three element rosette is used to verify this assumption. This section will investigate the validity of these assumptions.

Mohr's circle calculations are used to determine the principal strains and the direction of these strains with regards to the measured directions. These calculations are presented in Appendix E.

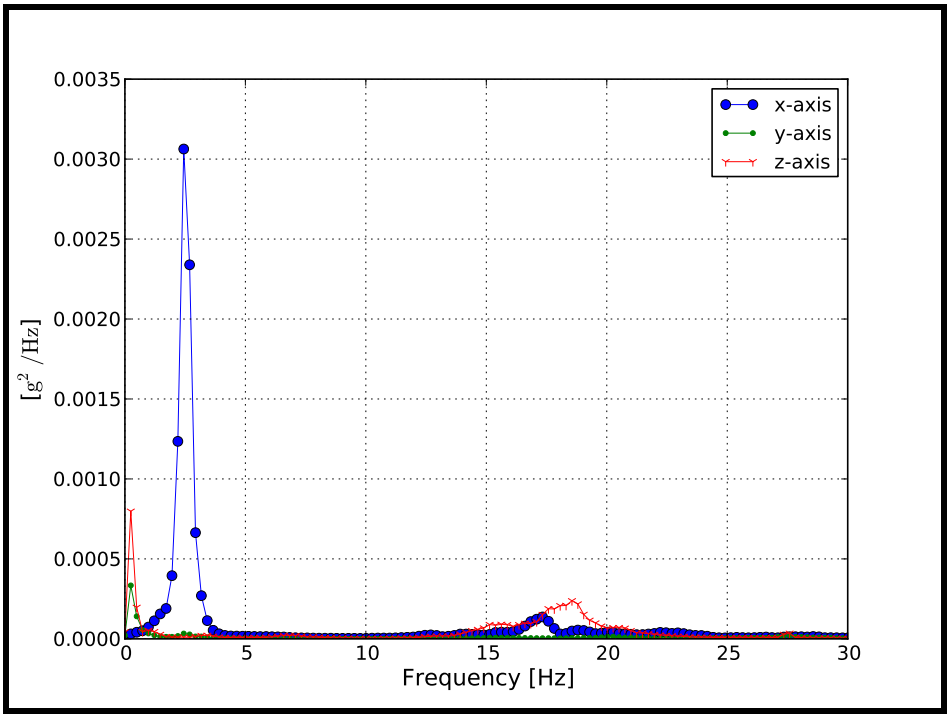

Figure 4.15: An acceleration spectral density plot of x, y and z acceleration data

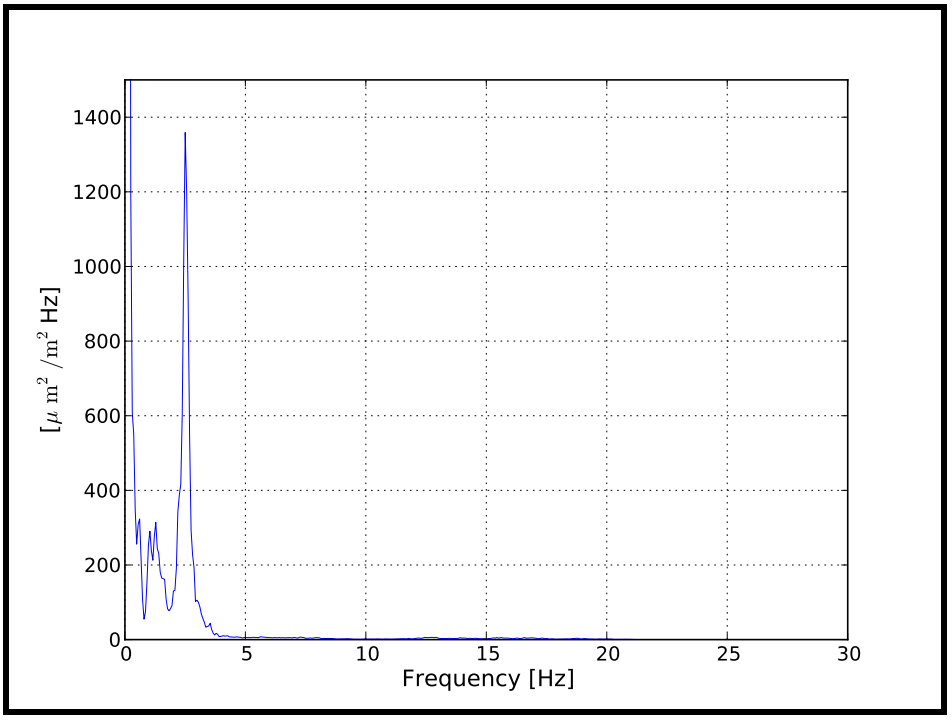

Figure 4.16: A strain spectral density plot of gauge thirteen strain data

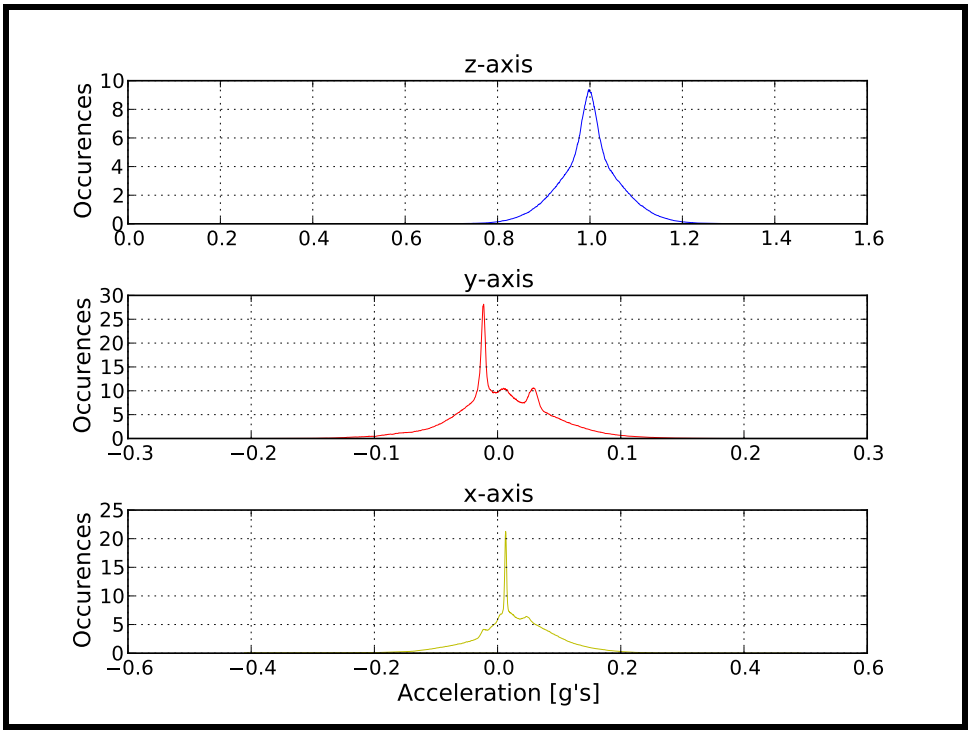

Figure 4.17: An amplitude distribution plot of x, y and z acceleration data

4.7.2.1 Gauges fourteen, fifteen and sixteen

Figure 4.18 shows the minimum principal strain, the maximum principal strain and the angle of maximum principal strain for a section of the trip discussed in the previous section. The averages of each of these components are summarised in Table 4.1. From the graphs and the tabular data it is clear that the minimum principal strain is the dominant one and that the maximum principal stress angle remains relatively constant. This proves that the assumption of uniaxial strain is valid. However gauge 15 does not seem to be perfectly aligned with the minimum principal stress direction. For this to have been true, the principal strain angle had to be 45°.

Table 4.1: Average principal stress values calculated from gauges fourteen, fifteen and sixteen

Description	**Value**	**Units**
Maximum Principal strain	-39	μm/m
Maximum Principal stress	-2.7	MPa
Minimum Principal strain	-710	μm/m
Minimum Principal stress	49.7	MPa
Maximum Principal strain angle	38	°

This data is for a full tank. For an empty tank it is not clear from the

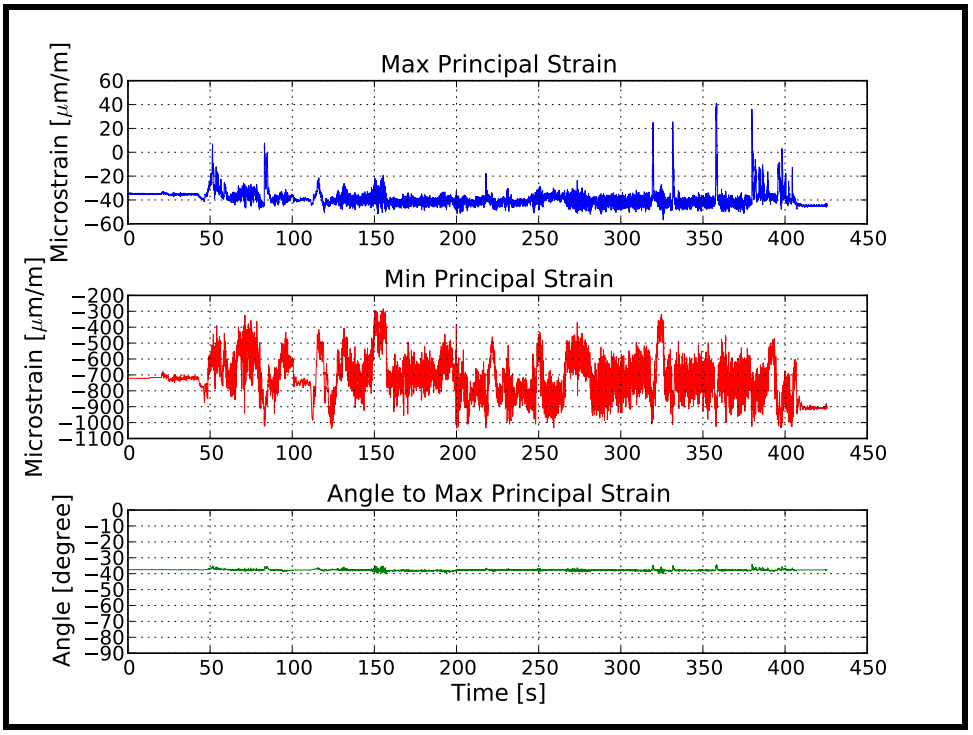

Figure 4.18: A sample of the principal strain data calculated from gauges fourteen, fifteen and sixteen

maximum principal stress angle that the perpendicular stress is the dominant one. This is due to the fact that the stress continually varies from tensile to compressive. Further inspection still proves that the maximum stress range is perpendicular to the weld. For detail of this proof see Appendix F.

4.7.2.2 Gauges seventeen, eighteen and nineteen

The assumption regarding these gauges are validated in the same way as in the previous section (see Figure 4.19). In this case, however, the maximum principal stress has a much larger component (see Table 4.2). Since this stress is parallel to the weld toe and still relatively small, it can be disregarded.

Table 4.2: Average principal stress values calculated from gauges seventeen, eighteen and nineteen

Description	Value	Units
Maximum Principal strain	173	μm/m
Maximum Principal stress	12	MPa
Minimum Principal strain	-746	μm/m
Minimum Principal stress	52.2	MPa
Maximum Principal strain angle	-3.4	$^\circ$

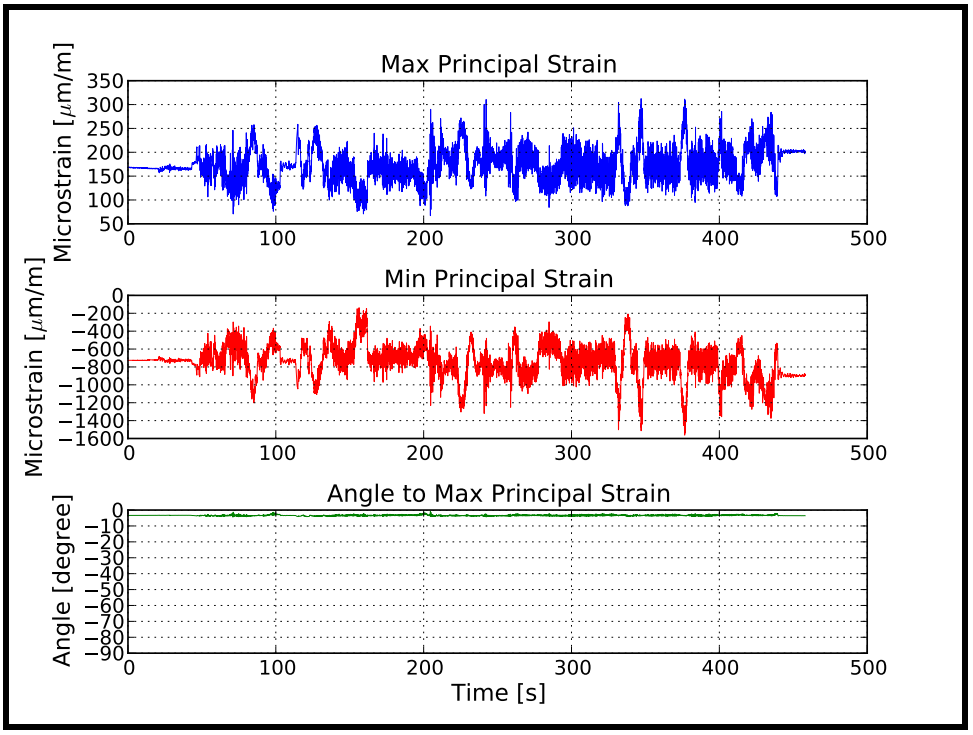

Figure 4.19: A sample of the principal strain data calculated from gauges seventeen, eighteen and nineteen

4.8 Chapter summary

This chapter has covered the experimental testing that is required for the fatigue analysis. Strain measurement was done with 6 mm grid, 350 Ω strain gauges and accelerations were measured with accelerometers. The strain gauge positions for each crack position are shown. It also presents the various load cases that will be used to compile the duty cycle. These are:

- Cornering
- Braking
- Driving over a stone grid
- Driving over containment humps
- Filling the tank

Finally, the uniaxial strain assumptions for crack positions two and three were verified.

Chapter 5

Structural calculations

To conduct the investigation several structural calculations need to be done to determine the stresses and strains in the tank structure. This includes calculating the principal strain directions to determine the strain gauge orientations, calculating the strain magnitudes to verify the experimental tests and to determine the strain gradient near the weld toe.

Due to the complex geometry of the structure, a FE calculation will be used to numerically determine the required strain vectors. This chapter will present and discuss the FE model and its construction. It will also present the various investigative steps, where they are used and any additional models or modelling techniques that are used in these steps.

5.1 The FE model

The FE software that is used to construct the model is Abaqus CAE v6.10 while Abaqus standard v6.10 is used to solve the equations.

The model itself consists of a shell element model of the tank, a solid element model of the rubber mountings, and a shell element model of the freight carrier chassis. These components were combined in an assembly and connected, using various techniques provided by the Abaqus software. Figure 5.1 shows a screen shot of the model and its various components.

The mounting rubbers are attached to the chassis model using Abaqus' 'tie' constraint. This constraint type constrains two surfaces to each other by setting the degrees of freedom of the slave surface's nodes equal to the degrees of freedom of an adjacent node on the master surface (Abaqus Analysis user Manual).

The tanker is connected to the chassis using bolt definitions and a surface contact interaction. This allows the mounting foot to separate from the rubber mount instead of being constrained by it. The bolt itself is also defined with a non-linear axial stiffness. In the compression direction it has an almost zero stiffness, to prevent it from constraining the mounting foot, and in the tension direction, it has the stiffness of a 16 mm bolt.

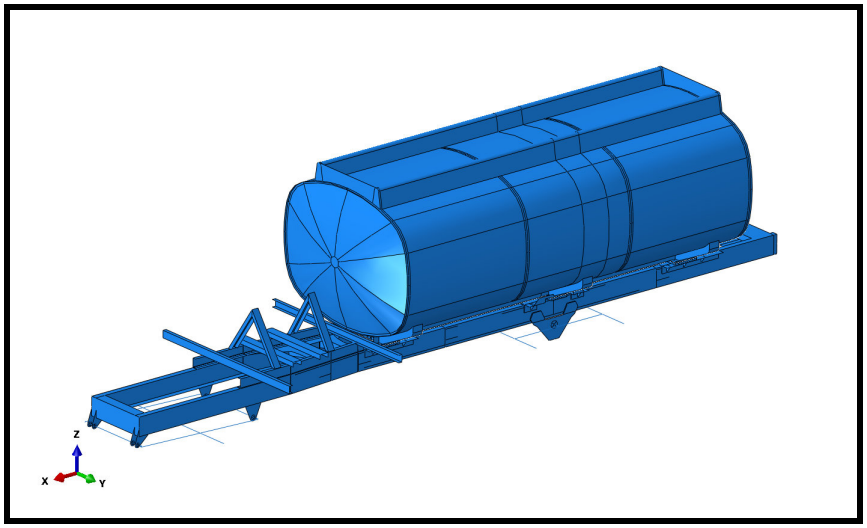

Figure 5.1: The FE model assembly

Figure 3.2 shows that the tank was constructed of several materials. These materials and their mechanical properties are listed in Table 5.1.

Table 5.1: A list of the materials that were used in the construction of the tank along with their mechanical properties

Material description	R_e **or** $R_{p0.2}$ [MPa]	R_m [MPa]	**E** [N/mm^2]	ν
EN AW-5182 H111	140	280	70×10^3	0.33
EN AW-6061 T6	240	290	70×10^3	0.33
S550 MC	550	600	193×10^3	0.3

5.1.1 The freight carrier chassis

It became apparent early on in the investigation that the FE model could not achieve the required accuracy without the freight carrier chassis being incorporated in the model. This is due to the fact that the chassis contributes greatly to the stiffness of the system as a whole and influences the force distribution on the mountings. This section presents the FE model of the chassis and explains the reasoning behind the modelling methods.

The chassis frame model shown in Figure 5.2 was created using drawings obtained from the chassis manufacturer. It is modelled entirely with shell elements (Abaqus' S4R elements) except for the axles and suspension which are modelled using beam elements. Particular attention was given to detail that contributes to the overall bending and torsional stiffness of the vehicle while less attention was paid to the attachment detail of the various sections

of the chassis since the chassis stresses are not of particular interest in this analysis.

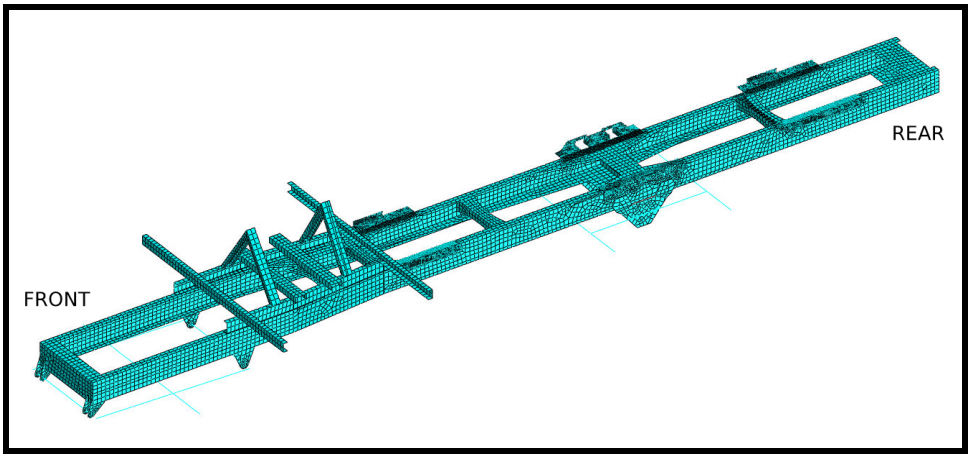

Figure 5.2: A meshed FE model of the freight carrier chassis

This particular vehicle was fitted with mechanical (spring) suspension. The force-deflection curve, presented in Appendix G, for this suspension is linear. This means that the axles and suspension can be accurately modelled using linear beam elements.

It is important to note that the rear suspension on this truck is a bogie suspension[1]. This means that the rear axles are connected to a central shaft which allows the combination to rotate with respect to the chassis itself. The section of the chassis where this shaft is located is extremely stiff since it must be capable of transferring the entire load carried by the rear axle combination. In this application the load is twenty-three tonnes (static load). This fact is significant since the cradle which exhibits the failures is mounted directly above this attachment point.

Also note the frame that is attached towards the front of the chassis. This is a frame that is manufactured and mounted to the chassis by the primary contractor. It was added to the model to incorporate the additional weight in the analysis and to take into account any stiffness that it adds to the chassis itself.

The chassis model consists of 17 547 elements and 18 535 nodes.

5.1.2 The mounting rubber

The tank is mounted on rubber pads manufactured from nitrile rubber with a 65 IRHD hardness. A photo of a such a pad is shown in Figure 5.3. A compression test was performed on these rubbers to determine its stress-strain

[1]Mechanical suspension that allows the axle combination (bogie) to rotate freely around a central axis

characteristics and to attempt to calculate an apparent elastic modulus that can be associated with the rubber. Figure 5.4 shows the stress strain results of the compression test where a load of 25 tons was slowly applied and released several times. For the sake of this analysis the area of interest is the load application side of the curve between 0 and 13 tons. The curve in this area is basically linear which supports the use of a linear elastic approach. An apparent modulus of elasticity of 40 N/m^2 was calculated from the data. This correlates well with shape factor dependant calculations suggested in literature.

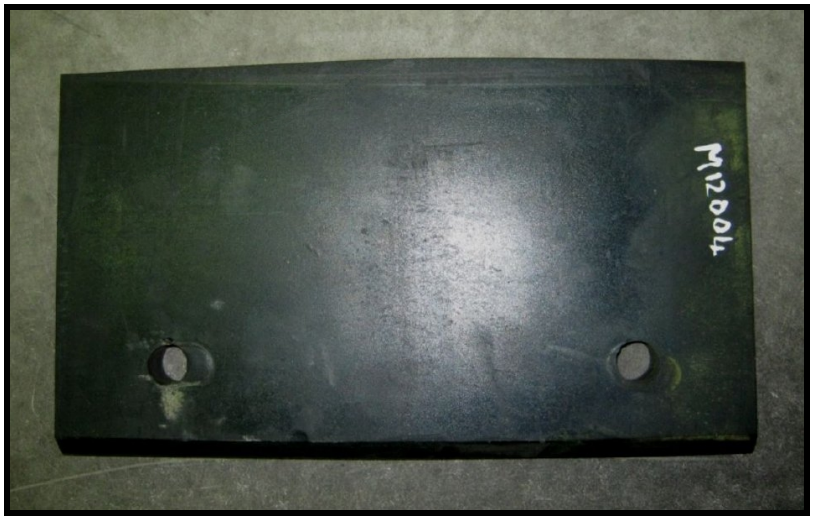

Figure 5.3: A photograph of a typical rubber pad on which the tank is mounted (Hansen, 2010).

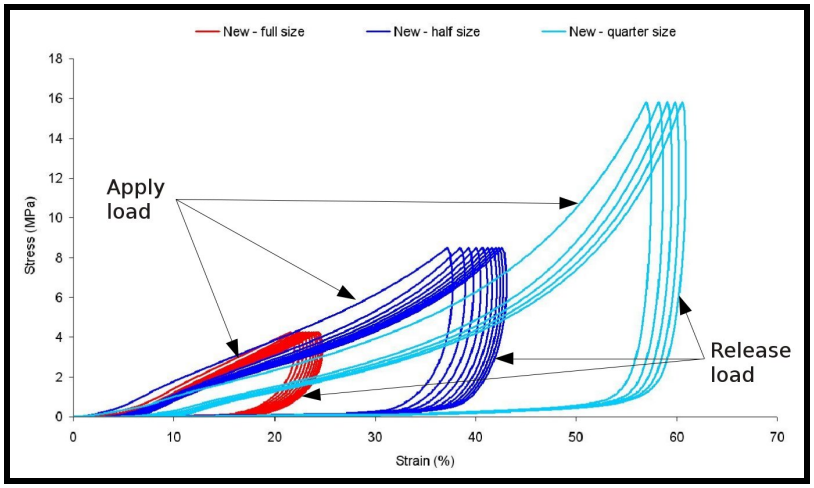

Figure 5.4: Compression test results done on three sections of a rubber pad. A 25 ton load was slowly applied and released several times to produce these results. Adapted from Hansen (2010)

The elements that are used to model these mounting rubbers are continuum shell elements (Abaqus' SC8R elements). These elements were used to allow the rubber to deform in the thickness direction which would not be possible with standard shell elements. Initially quadratic hexahedron elements with reduced integration (Abaqus' C3D20R elements) were used but were rejected due to computational time consumption.

The model consists of 482 elements and 831 nodes.

5.1.3 The tank

The tank and its mountings are modelled with shell elements throughout (S4R elements). The meshed geometry is shown in Figure 5.5. To accurately determine the scaling factors for each crack position it is necessary to create solid sub-models of the detail. These models will be discussed in more detail in section 5.4.

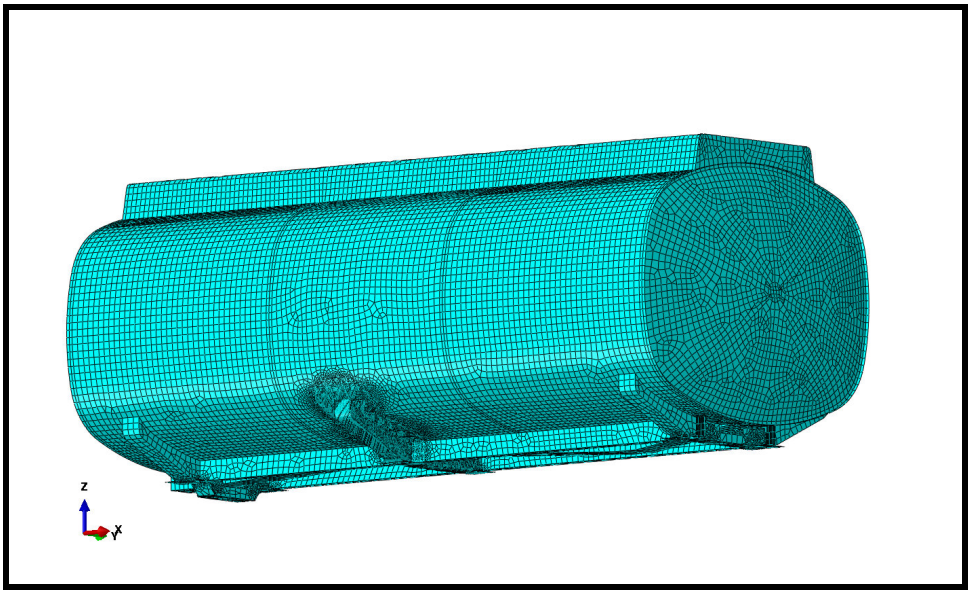

Figure 5.5: The shell element mesh of the tank model

The model consists of 616 497 elements and 612 008 nodes.

5.1.4 Constraints

In reality the only 'constraint' that is placed on the vehicle is between the road surface and the tyres. Since only a static analysis is done, it is necessary to constrain the vehicle in a way that does not allow free body movement, but does not add additional stresses by over constraining the model.

To achieve this, the axles are all constrained at the wheel positions. All the 'wheels' are constrained in the Z direction; the left side wheels are constrained

in the Y direction and the two front wheels in the X direction. This allows a realistic relative movement between the wheels. A graphical representation of the constraints is shown in Figure 5.6.

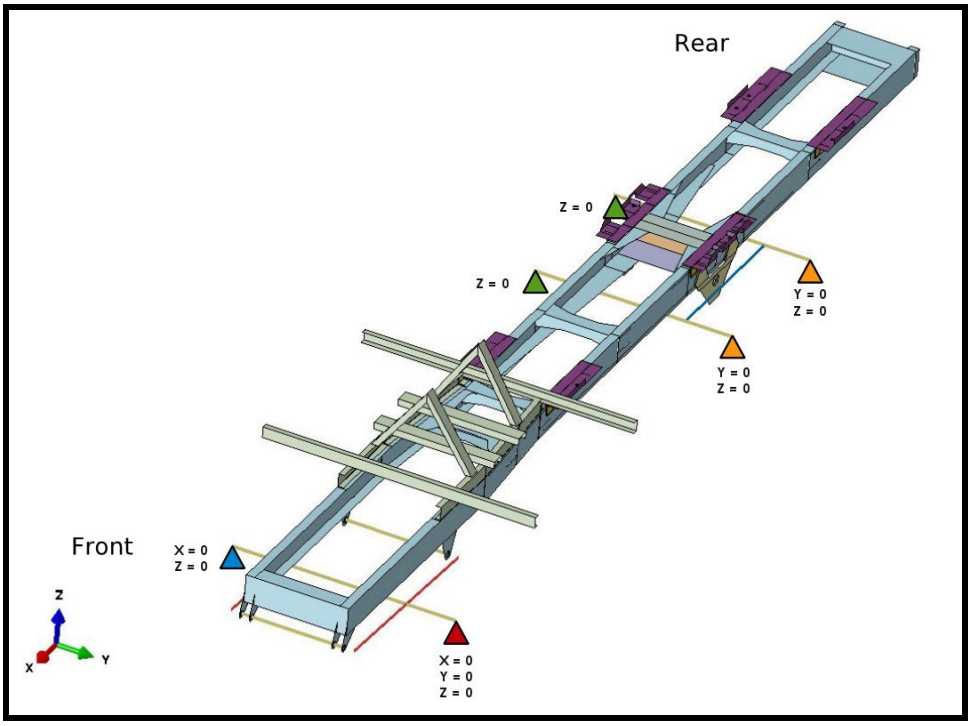

Figure 5.6: A graphical illustration of the constraints imposed on the FE model

5.2 Determining stress directions

The initial purpose of the FE model was to assist in determining strain gauge positions and directions for the experimental part of the investigation. A linear analysis was done with the standard ADR[2] load cases (WP.15, 2008) presented in Table 5.2. These load cases provide a basis on which stress directions and relative magnitudes can be assessed. This information helped to determine the exact position and direction in which the strain gauges had to be applied. The stress magnitude also served as a check to determine the validity of the strain gauge application.

At this point it should be noted that the primary indicator of the damaging stress position and direction is naturally the crack itself. The initiation site is the position and a crack usually propagates perpendicular to the primary

[2]ADR is 'The European Agreement concerning the International Carriage of Dangerous Goods by Road'. It is a document that provides recommendations to regulate the design and construction of vehicles and containers for the international carriage of dangerous goods by road (WP.15, 2008).

Table 5.2: The design load cases mandated by ADR 2009, section 6.8

Load direction	**Magnitude [g's]**
Direction of travel, +X	2
At right angles to the direction of travel, ±Y	1
Vertically upwards +Z	1
Vertically downwards -Z	2

stress direction. However, in the field of welding fatigue a principal stress that deviates as much as 60° (Hobbacher, 1996) from a line perpendicular to the weld, can cause a crack that propagates along the weld toe. Thus, to ensure that the highest strains are measured, it is important to ascertain the principal stress direction.

5.3 Correlating the model

The established FE model is used to determine the scaling factors that are needed in the fatigue analysis discussed in Chapter 6. It will also be used to assess future designs to find a solution to the failures. As stated before, this will not be discussed in this document.

To ensure the accuracy of these calculations it is important to correlate the model with the measured data. If good correlation is achieved, it proves that the model is an accurate representation of reality and can be used to make accurate predictions.

The load used for correlation in this case is the filling load that was presented in Section 4.6, because it is a quasi-static load case. Table 5.3 presents the stresses calculated from the measured strains as well as the stresses calculated using the FE model. The stresses determined from the FE analysis were taken at the centre of the gauge position. This is acceptable since the stress gradients in this area are linear over the 6 mm grid area. It is important to note that the listed gauges were applied in high stress-gradient areas and averaged the strain over a 6 mm grid area. With this taken into account the 20-27% deviation is acceptable and is considered to be good correlation. In phase two and three of the solution methodology the same model will be used to conduct comparative improvements, which means the deviation from actual data is not important as long as the general model remains unchanged.

5.4 Determining the scaling factors

In Chapter 2 it was concluded that the hot spot stress method will be used in this thesis to determine the estimated fatigue life of each failure position. A crucial element of this method is to determine the hot spot strains and stresses.

Table 5.3: Correlation of the FE model and the measured data

Gauge number	Stress from FEA [MPa]	Measured stress [MPa]	Difference [%]
20	-19	-18	5.6
13	-60	-50	20.0
15	-67	-53	26.4
19	-33	-26	26.9

This section discusses how the strains for this method are determined and its application in the various crack regions. The results and scaling factors for each region are also presented. The strains in this section are determined using the filling load case (the same load case that was used in the previous section) since it is a quasi-static load and is representative of the most damaging load cases.

5.4.1 Method to determine the hot spot strain

To determine the hot spot strain Niemi *et al.* (2006) suggests that the stress or strain should be extrapolated from points measured at finite distances from the weld. The standard approach is a linear extrapolation of two points measured $0.4t$ and $1.0t$ from the weld toe, where t is the plate thickness. These values are then substituted into equation 5.1 to determine the hot spot strain at the weld toe.

$$\varepsilon_{hs} = 1.67\varepsilon_{0.4t} - 0.67\varepsilon_{1.0t} \tag{5.1}$$

Where:

ε_{hs}	=	Actual strain at the hot spot	[m/m]
$\varepsilon_{0.4t}$	=	Actual strain at 0.4t from the hot spot	[m/m]
$\varepsilon_{1.0t}$	=	Actual strain at 1.0t from the hot spot	[m/m]

This method is applicable to experimental methods as well as FE methods, which provides a welcome flexibility with regards to its application. Due to geometric and economic reasons it is not always practical to apply two gauges at each point of interest. Thus it makes sense to only apply one gauge at $1.0t$ during testing and then to determine the stress gradient with a FE analysis. Since it is a linear approach and all strains are assumed to fall within the elastic region of the material properties, it is possible to determine a linear scaling factor using this method. Equation 5.2 provides a mathematical representation of this concept.

$$\varepsilon_{hs} = \frac{\varepsilon_{hs_{FEA}}}{\varepsilon_{1.0t_{FEA}}}\varepsilon_{1.0t} = K_{hs}\varepsilon_{1.0t} \tag{5.2}$$

Where:

$\varepsilon_{hs_{FEA}}$	=	The hot spot strain calculated with a FE analysis	[m/m]
$\varepsilon_{1.0t_{FEA}}$	=	Strain at $1.0t$ from the weld toe determined with a FE analysis	[m/m]
$\varepsilon_{1.0t}$	=	Strain at $1.0t$ from the weld toe	[m/m]
K_{hs}	=	Factor relating the stress at $1.0t$ from the weld to the stress at the hot spot	[mm]

As mentioned earlier the gauges that were used for this experiment have a 6 mm grid size. This is in part due to the unavailability of smaller gauges at the time. The physical size of the gauge makes it impractical to apply it at the suggested distances. To overcome this hurdle all gauges were applied at a distance of $2.0t$ from the weld toe. The measured strain is then related to the strain at $1.0t$ before scaling to the weld toe. Equation 5.3 shows how this is achieved while equation 5.4 presents the method to determine the hot spot strain from the measured strains. The same method is used in the case of crack position one where the weld was inaccessible.

$$K_{1.0t} = \frac{\varepsilon_{1.0t_{FEA}}}{\varepsilon_{G_{FEA}}} \tag{5.3}$$

$$\varepsilon_{hs} = K_{1.0t} K_{hs} \varepsilon_G \tag{5.4}$$

Where:

$\varepsilon_{G_{FEA}}$	=	Strain at the strain gauge position determined with a FE analysis	[m/m]
ε_G	=	Strain measured with a strain gauge	[m/m]
$K_{1.0t}$	=	Factor relating the stress at the gauge to the stress $1.0t$ from the weld	[mm]

5.4.2 Finite element sub-models

Due to the large geometrical discontinuities in the cradle area it is necessary to model the cradle section using solid elements to ensure that an accurate assessment of the initiation sites can be made. The major part of the detail in question consists of 5 mm sheet metal sections. This means that to achieve a mesh of acceptable quality, a mesh size of 5 mm or less must be used. Because this is still not small enough to justify the use of linear elements, quadratic elements are used instead. This model is built as a 'sub-model' and is driven by the shell model discussed above, using Abaqus' 'node based sub-modelling' constraint. Figure 5.7 shows the meshed geometry of the sub-model.

The model consists of 287 358 quadratic elements with 433 453 nodes. This produces 1 300 359 degrees of freedom.

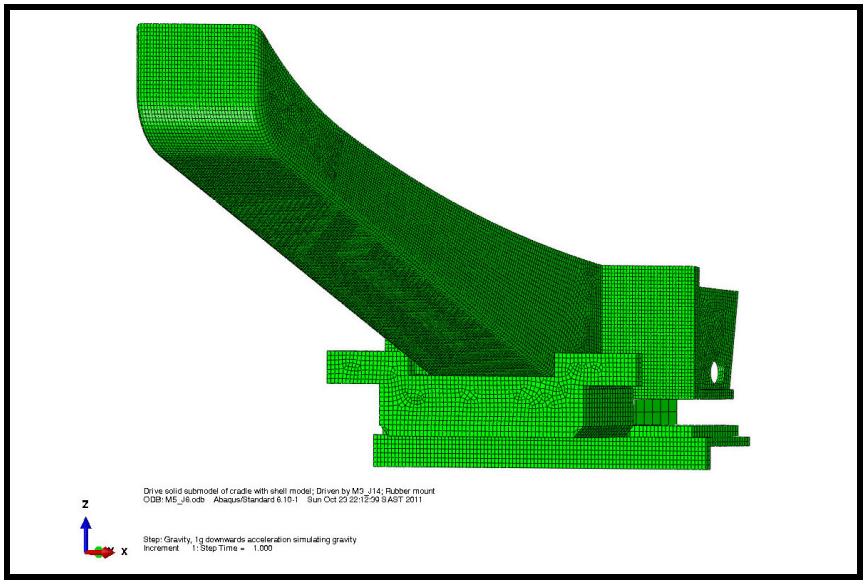

Figure 5.7: The meshed geometry of the submodel

5.4.3 Crack area one

Figure 5.8 shows a contour plot of the sub-model focused on the area where crack one originates. These results are used to determine the scaling factor for the hot spot strains at crack position one. The governing strains in this area are compressive (negative) strains. Due to this fact attention is paid to the minimum principal strains.

Strains are determined at the $0.4t$ and $1.0t$ positions from the weld toe. It was established in section 4.3.1 that gauge thirteen will be used to extrapolate the measured stresses in this region, so strain is also determined from the FE analysis at the position of gauge thirteen ($\varepsilon_{G_{FEA}}$). These values and the resulting scaling factors are presented in Table 5.4. The scaling factors are determined using equation 5.2 and equation 5.3 respectively.

Table 5.4: Strain values and scaling factors at crack one

Description	**Symbol**	**Value**	**Unit**
Strain at 3.2 mm from the weld	$\varepsilon_{0.4t_{FEA}}$	-1762	μm/m
Strain at 8 mm from the weld	$\varepsilon_{1.0t_{FEA}}$	-1124	μm/m
Hot spot strain at the weld toe	$\varepsilon_{hs_{FEA}}$	-2191	μm/m
Averaged strain at the gauge position	$\varepsilon_{G_{FEA}}$	-931	μm/m
Scaling factor to the hot spot	K_{hs}	1.95	-
Scaling factor from the gauge position	$K_{1.0t}$	1.21	-

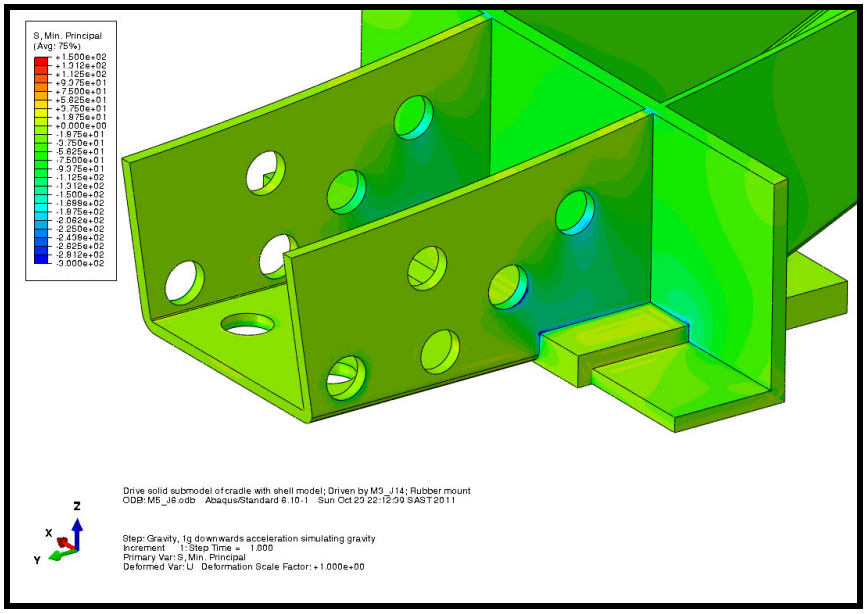

Figure 5.8: A sub-model of crack position one using 20 node quadratic hexahedron elements

5.4.4 Crack area two

Figure 5.9 shows the meshed model used to determine the scaling factor for the hot spot strains at crack position two. The model consists of a section of the outrigger and the 20 mm base plate. It was driven by the model described in section 5.4.2 using the 'node based sub-modelling' technique. The mesh consists of 10 node quadratic tetrahderon elements (Abaqus element C3D10). These elements were chosen due to the complexity of the weld geometry that was added to the model. This made it impossible to achieve an acceptable mesh using hexahedron elements. The model has 71 686 elements with 399 021 nodes which relate to 1 353 204 variables that need to be solved. The strains in this area are all compressive (negative) strains, thus the values of interest are the minimum principal strains.

The applicable strains are measured and summarised in Table 5.5. The table also presents the calculated scaling factors.

Table 5.5: Strain values and scaling factors at crack two

Description	Symbol	Value	Unit
Strain at 2 mm from the weld	$\varepsilon_{0.4t_{FEA}}$	-2104	μm/m
Strain at 5 mm from the weld	$\varepsilon_{1.0t_{FEA}}$	-1342	μm/m
Hot spot strain at the weld toe	$\varepsilon_{hs_{FEA}}$	-2615	μm/m
Averaged strain at the gauge position	$\varepsilon_{G_{FEA}}$	-975	μm/m
Scaling factor to the hot spot	K_{hs}	1.95	-
Scaling factor from the gauge position	$K_{1.0t}$	1.38	-

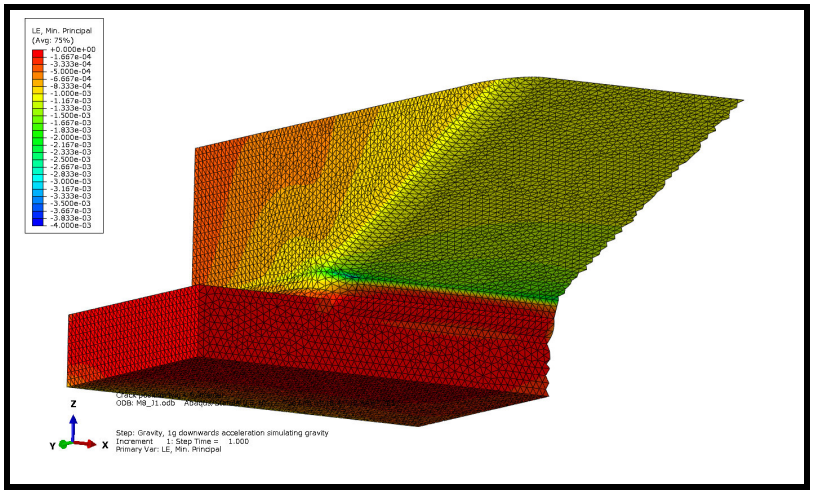

Figure 5.9: A sub-model of crack position three using 10 node quadratic tetrahedron elements

5.4.5 Crack area three

Figure 5.10 shows a contour plot of the sub-model focused on the area where crack three originates. These results are used to determine the scaling factor for the hot spot strains at crack position three. The governing strains in this area are compressive (negative) strains. Due to this fact attention is paid to the minimum principal strains.

Strains are determined at the $0.4t$ and $1.0t$ positions from the weld toe. Strain is also determined from the FE analysis at the position of gauge nineteen ($\varepsilon_{G_{FEA}}$). These values and the resulting scaling factors are presented in Table 5.6. The scaling factors are determined using equation 5.2 and equation 5.3 respectively.

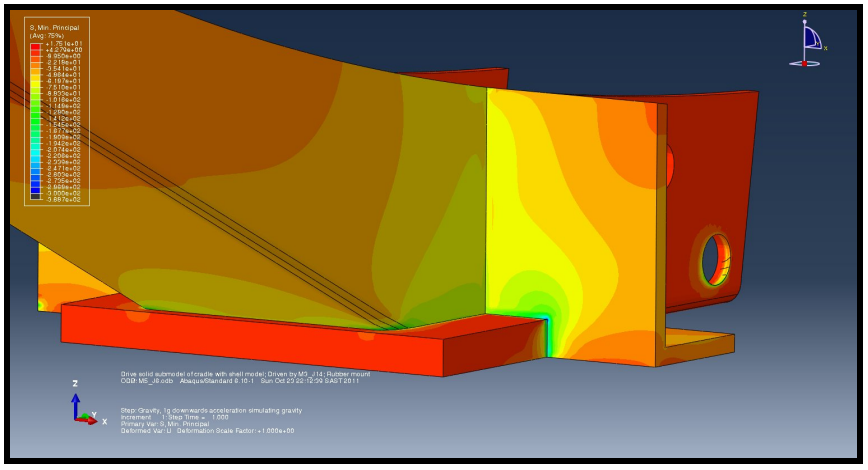

Figure 5.10: A close-up view of the sub-model at crack position three

Table 5.6: Strain values and scaling factors at crack three

Description	Symbol	Value	Unit
Strain at 3.68 mm from the weld	$\varepsilon_{0.4t_{FEA}}$	-1554	μm/m
Strain at 9.2 mm from the weld	$\varepsilon_{1.0t_{FEA}}$	-1214	μm/m
Hot spot strain at the weld toe	$\varepsilon_{hs_{FEA}}$	-1782	μm/m
Averaged strain at the gauge position	$\varepsilon_{G_{FEA}}$	-564	μm/m
Scaling factor to the hot spot	K_{hs}	1.47	-
Scaling factor from the gauge position	$K_{1.0t}$	2.15	-

5.5 Chapter summary

This chapter has presented the FE model that was used to do the structural calculations for this project. The experimental results were utilised to assess the accuracy of the model. Good correlation was achieved.

The model was then used to determine the scaling factor from the gauge position to $1.0t$ and from $1.0t$ to the hot spot. These factors will be used in the next chapter to determined the hot spot stress history of the duty cycle.

Chapter 6

Fatigue calculations

This chapter discusses the method that is used to determine the fatigue life of each crack site. The methods and calculations are based on the recommendations of the IIW and Eurocode 9.

6.1 Method

Due to the complexity of the geometry, and the fact that it is extremely difficult to accurately determine the nominal stresses at the failure positions, the nominal stress method cannot be used for this investigation. For the purposes of fatigue calculation the hot spot stress method will be used.

The stress values determined in this way include the nominal (membrane) stresses as well as any secondary bending stresses. It does not include the non-linear stress peak found at the weld toe; these are accounted for in the fatigue resistance curve. The determined stress values, along with the applicable S-N curve, are then used to determine the structural fatigue life of the welded structure.

6.2 Composite duty cycle

To be able to calculate the fatigue life of a structure it is necessary to determine the various load cases that the structure will endure in its daily operations and the number of occurrences of these loads. A routine load cycle which includes all of these load cases (in their appropriate quantities) is called a duty cycle.

To have a truly accurate load cycle it would be necessary to measure and record data of a structure throughout its life. This data would then constitute one cycle where the cycle is equal to total life. This is rarely[1] practical and has the disadvantage that it will be applicable to that structure and its specific

[1]Certain structures like bridges and large buildings are continually monitored for possible signs of failure.

service load cycle. This is not of much use when a population of vehicles needs to be assessed.

To overcome this a composite duty cycle is compiled that represents a general service load cycle for the vehicle. This duty cycle should represent the loads that produce the highest failure probability. For this reason the most aggressive site was chosen to compile the duty cycle.

After inspecting several typical service routes a duty cycle is compiled that represents an average of the load cases seen during these service cycles. The various load cases in the routes are isolated, counted and then recompiled to produce a composite duty cycle. The various components of the duty cycle and their quantities are shown in Table 6.1.

Table 6.1: The various events used to compile the composite duty cycle

Event	**Number of occurrences per cycle**	**Total event distance [m]**
Straight line driving (empty)	1	350
Left hand turn (empty)	2	65
Right hand turn (empty)	2	65
Gradual start-stop (empty)	1	80
Stone grid (empty)	0	-
BFI - Enter empty and leave fully laden	1	130
Straight line driving (full)	1	5 470
Left hand turn (full)	14	330
Right hand turn (full)	14	330
Gradual start-stop (full)	4	375
Stone grid (full)	1	15
Total distance		**7 210**

The composite duty cycle that is compiled from Table 6.1 is based on the service cycle shown in Figure 6.1. The route shown in the satellite picture is divided into two phases. Phase 1 is the vehicle travelling to the aircraft and refuelling station from its base. Phase 2 is the route it takes as it returns to its base.

6.3 Determining the stresses used in the calculation

As discussed in Section 5.4 several scaling factors have been determined to relate the measured strain to the hot spot strain at the weld toe. This strain is then multiplied with Young's modulus (equation 6.1) to provide the stresses

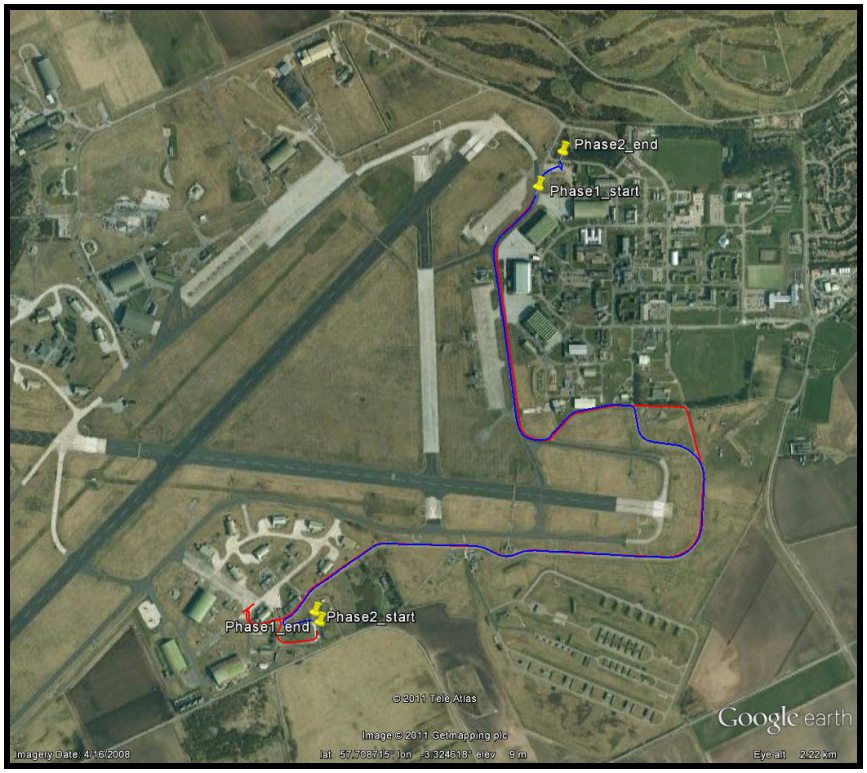

Figure 6.1: A GPS plot of the service cycle that forms the basis of the composite duty cycle.

that are used in the life calculation. This assumption will only remain valid while the stresses are still within the linear range of the material's properties (see Table 5.1).

$$\sigma_{hs} = EK_{1.0t}K_{hs}\varepsilon_G \tag{6.1}$$

Where:

σ_{hs}	=	Stress at the hot spot	[MPa]
E	=	Young's modulus	[N/m^2]

6.4 Modifying factors

Chapter 2 mentions that several factors needed to be taken into account when calculating the fatigue life of a component. This section will discuss these factors and their effect on the fatigue class. The fatigue class and its use will be discussed further in the next chapter.

6.4.1 Mean stress effects

The IIW as well as Eurocode 9 allows a fatigue enhancement ratio $f(R)$ to be used to increase the FAT class if the stress ratio (equation 6.2) is compressive. This is due to the beneficial effect that compressive mean stresses can have on fatigue life. Since most of the stress ranges that are measured, have compressive mean stresses it seems obvious that this factor would have to be incorporated in the calculations.

$$R = \frac{\sigma_{min}}{\sigma_{max}} \tag{6.2}$$

Where:

R	=	Stress Ratio	[-]
σ_{min}	=	Minimum stress	[MPa]
σ_{max}	=	Maximum stress	[MPa]

However, welding tends to induce large tensile residual stresses in the welded region. These residual stresses could be large enough that $R > -1$. In other words, the effective mean stress is tensile (MacDonald, 2011*a*). Due to this fact the enhancement ratio is only applicable if the component has been stress relieved or if the residual stresses are known. Hobbacher (1996) also states that high tensile residual stresses are included in the given S-N curves, which means that these stresses are already accounted for in the calculations since it is bad practice to stress relieve aluminium components (PVE/1, 2009). The residual stresses in the component have never been tested, so the conservative approach of $f(R) = 1$ is taken.

6.4.2 Material size effects

Thicker material has a negative effect on fatigue due to three size effects (Issler, 2011):

- Technological size effect
- Statistical size effect
- Gradient size effect

The mechanics behind these effects will not be discussed in this document. However, but it is important to note that increased plate thickness could adversely influence the fatigue life of the structure. The IIW fatigue resistance curves are applicable to steel and aluminium structures with a wall thickness of up to 25 mm. Since none of the materials in the structure has a thickness larger than 20 mm, the size effect factor (F_{SE}) is equal to one.

6.4.3 Corrosion and elevated temperature effects

It is intuitive that corrosion and elevated temperatures could have a detrimental effect on the fatigue life of a structure. Since the tank is a painted aluminium structure operating in UK atmospheric conditions, it is safe to assume that both these effects are negligible. Thus $F_T = 1$ and $F_C = 1$.

6.4.4 Improvement techniques

Various improvement techniques have been developed to improve the weld toe profile and the residual stress conditions. These include:

- Machining or grinding of the weld toe
- TIG-dressing
- Peening[2] (hammer-, needle-, shot-, etc)
- Tensile over-stressing to produce a compressive residual stress
- Stress relief

None of these techniques were employed during the manufacturing process, thus $F_{IT} = 1$.

6.5 S-N curve

To do a life calculation the applicable S-N curve must be chosen. In this case this means a S-N curve based on hot spot stress ranges.

For the purpose of these calculations the IIW's (Hobbacher, 1996) fatigue resistance curves based on the structural hot spot stress will be used. All three failure positions are load-carrying fillet welds. For these types of welds a FAT class[3] of 36 MPa is recommended. This value is the characteristic stress range that equates to two million cycles (in MPa). The FAT class must be modified to incorporate all the factors mentioned in the previous section. Equation 6.3 shows how this is done.

$$\begin{aligned} \sigma_{2\times10^6} &= FAT \times f(R) \times F_{SE} \times F_T \times F_C \times F_{IT} \\ &= 36 \times 1 \times 1 \times 1 \times 1 \times 1 \\ &= 36 \text{ MPa} \end{aligned} \tag{6.3}$$

[2]Peening is a mechanical method of plastically deforming the material at the weld toe to induce compressive residual stresses on the surface (Hobbacher, 1996; MacDonald, 2011*d*).

[3]A FAT (an abbreviation for 'fatigue') class is the characteristic S-N curve that is assigned to a specified geometry

The curve has a knee point at $N = 10^7$. Historically this knee point has been known to be the constant amplitude fatigue limit, or endurance limit, of the material. New experimental data has proved that this limit does not truly exist (Hobbacher, 1996). For high cycle fatigue a curve exists after the knee point where the stress range has a 10% decay per decade.

The S-N curve is defined by:

$$N = \frac{C_{\text{S-N}}}{\Delta\sigma_{S-N}^{m}} \tag{6.4}$$

Where:

$C_{\text{S-N}}$	=	Constant associated with a particular S-N curve	[-]
$\Delta\sigma$	=	Stress range	[MPa]
m_{S-N}	=	The slope of the curve	[-]

The equation for the FAT 36 curve is:

$$N = \begin{cases} \frac{9.331\times10^{10}}{\Delta\sigma^3} & \text{where } 10^4 \leq N \leq 10^7 \\ \frac{3.465\times10^{40}}{\Delta\sigma^{22}} & \text{where } 10^7 < N \end{cases} \tag{6.5}$$

The curve defined by equation 6.5 is presented in Figure 6.2.

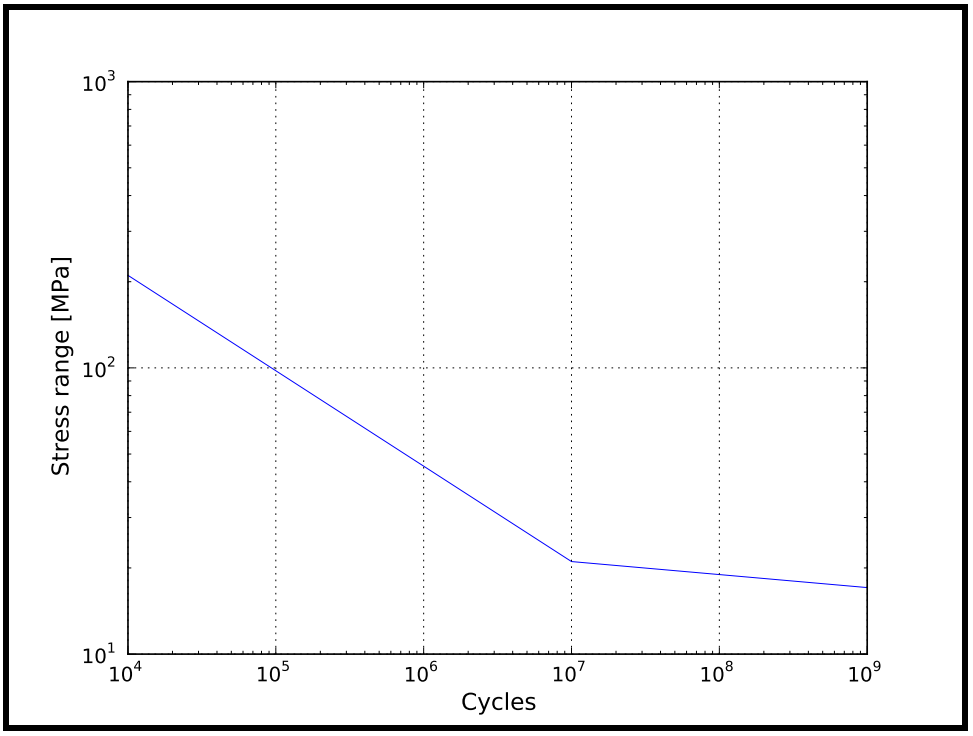

Figure 6.2: The S-N curve for the FAT 36 fatigue class

6.6 The fatigue calculation

The fatigue calculation itself is based on the linear damage summation rule of Palmgren-Miner. To do this calculation the stresses of the composite duty cycle is processed using the rainflow counting method. This produces the histogram shown in Figure 6.3. Since mean stress correction is not taken into account the matrix is essentially two dimensional. These stress ranges are then used to calculate the total damage of the duty cycle.

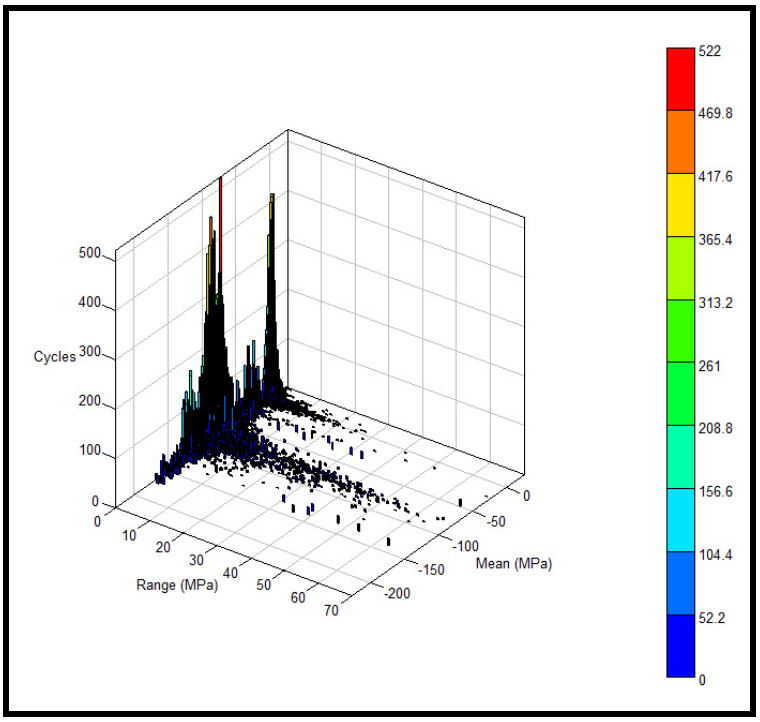

Figure 6.3: A histogram of the range-counting results of the rainflow method

For the purpose of this calculation the failure criterion is a damage sum of 1.0[4]. This implies that the total number of cycles that can be achieved is the failure criterion divided by the damage of a single duty cycle (equation 6.6). It is important to note this value since the results of these calculations will be compared to future calculations. For the sake of consistency the same failure criteria must be used throughout the rest of the methodology. The results of the calculations for each failure position are presented in Table 6.2.

$$\text{Number of cycles} = \frac{1.0}{D_{DC}} \tag{6.6}$$

[4]It is important to note that this failure criterion should be used throughout the study, since it is a comparative study. A value of 0.5 (as suggested by the IIW) could also have been used as long as it is consistently used throughout the solution methodology.

Where:

D_{DC}	=	The total damage caused by a complete duty cycle	[-]

Table 6.2: The results of the fatigue calculation for each failure position

Failure position	**Damage**	**Cycles**	**Distance [km]**
One	0.00178	561	4047
Two	0.00306	327	2355
Three	0.00112	890	6419

6.7 Correlation factor

A correlation factor can now be determined. The correlation factor is defined as the actual life divided by the estimated life:

$$CF = \frac{N_{actual}}{N_{estimated}} \tag{6.7}$$

Where:

CF	=	The correlation factor	[-]
N_{actual}	=	The actual life of the structure	[cycles]
$N_{estimated}$	=	The calculated life of the structure	[cycles]

Table 6.3 summarises the results for each failure position and presents the calculated correlation factor.

Table 6.3: The calculated correlation factor for each crack

Estimated life [km]	**Averaged actual life [km]**	**Correlation factor [-]**
4047	19 000	4.7
2355	23 000	9.8
6419	25 000	3.9

6.8 Verifying the results

The strain results presented in Chapter 5 seem to be very high for a statically loaded structure. To ensure that the life calculations presented in this chapter are valid, it is necessary to look critically at the source data. Table 6.4 presents results for the nominal stress, the hot spot stress and the stress range. For the sake of this verification exercise the nominal stress values are approximated by the calculated stress at $1.0t$.

Table 6.4: Maximum, mean and minimum stress components for each crack position

Stress component	**Maximum stress [MPa]**	**Mean stress [MPa]**	**Minimum stress [MPa]**
Nominal stress at crack one	9	-52	-119
Nominal stress at crack two	25	-63	-139
Nominal stress at crack three	18	-49	-154
Hot spot stress at crack one	18	-102	-233
Hot spot stress at crack two	49	-124	-270
Hot spot stress at crack three	26	-72	-226
Stress range at crack one	254	-	0
Stress range at crack two	323	-	0
Stress range at crack three	255	-	0

From Table 5.1 it is known that $R_{p_{0.2}}$ of the parent material at crack position one and two is equal to 140 MPa. At crack position three $R_{p_{0.2}}$ is equal to 240 MPa. The IIW states that all **nominal** stress values should fall within the elastic properties of the material while the **hot spot stress range** should not exceed two times the proof strength. All these conditions are met for crack position one and three. However, for crack position two the second condition is not met because the maximum stress range of 323 MPa exceeds 280 MPa.

This implies that the application of the stress life method to crack one and three is valid, but that a different method[5] should be applied to crack two. This could explain the large variation in the correlation factor of crack two versus that of crack one and three.

Since the hot spot method was used with a single S-N curve and the damaging load cases are consistent, one would expect that the correlation factor for the various areas should be very similar. This is true for crack one and three. It would also be beneficial to choose a single factor since any high stress area present in the design of the repair has to be assessed using this factor. Even though the method is validated for crack one the very high hot spot stress (which exceeds $R_{p_{0.2}}$) in this area is still a matter of concern. For this reason the correlation factor of crack three should be used in the other two phases of the failure investigation process. As it is also the lowest of the three factors, one would expect to err on the conservative side.

6.9 Chapter summary

This chapter dealt with the components and the calculations of the estimated fatigue life. The definition and compilation of the composite duty cycle was

[5]Fracture mechanics could be considered as an option

presented. This duty cycle was used along with the FAT36 diagram to calculate the estimated fatigue life of the various crack positions. These values were then used to determine a correlation factor of 3.9.

Chapter 7

Recommendations for future improvements

With the advantage of hindsight it is possible to suggest some improvements that can be made to the investigation procedure as well as to provide recommendations for future designs and rectification procedures. This chapter will present and discuss some suggestions regarding the testing procedure, the fatigue calculations, the structural design and a repair design.

This chapter is an essential part of establishing the second thesis goal: refining the life prediction procedure.

7.1 Experimental strain measurements

To ensure accurate measurements, especially regarding the chosen fatigue methods, it is essential to measure as closely to the problem area as possible. As stated before, for the material thicknesses in question, a practical distance is $1.0t$. This requires a gauge with a measurement grid of roughly 1-2 mm[1]. The 6 mm grid gauge used in this analysis is not ideal.

It is also important to be sure of the strains at the position of interest. Due to the critical importance of crack one, the interpolation method used to determine the strains at this position is not adequate for accurate life prediction. Although the theory is sound, there are too many possible variations due to manufacturing and dynamic loading to confidently extrapolate the strains to this area. It is suggested that the steel brace (mentioned in Section 4.3.1) be removed for gauge application and replaced for the tests. The reasons why this was initially not done, are still valid but can be overcome with adequate time and planning.

For the sake of this investigation the data is still valid since it will be used to assess the validity of an improvement. As long as the future measurements

[1]Naturally self-heating effects (IR^2_{elec}) should be taken into account, but in the case of a 350 Ω gauge bonded to aluminium this should not be a concern.

and methods are consistent with the ones used for this leg of the investigations, the conclusions will still be accurate.

7.2 The fatigue calculations

For truly accurate life assessments it is necessary to obtain S-N curve data for the particular welded material, using GRW's manufacturing techniques and welding personnel. This requires various samples and tests. For complex geometry (as for the severe discontinuity at the mounting foot) it might be required to test the actual geometry to failure. However, this is very costly and can only be done if the size or risk of the project justifies the expenditure. Since the IIW and EN curves have been obtained from various tests and published data it is a good starting point for a conservative life prediction.

The statement at the end of Chapter 6 suggests that the stress life method is not applicable to all the cracks that were investigated in this thesis. For academic interest it would be of value to investigate these cracks using the strain life and fracture mechanic methods. However, the material data that is required for this investigation, (especially for the strain life method) is extremely expensive to obtain and does not provide any advantage to the company since one would always design for high cycle fatigue where the stresses fall within the elastic limits of the material.

7.3 The structural design of the tank

The fact that the tank structure has several failures suggests that the design has an inherent flaw. In this section some of these 'flaws' will be pointed out and recommendations will be made for future designs.

The 20 mm mounting foot is a severe thickness deviation from the adjoining materials. This causes stiffness discontinuities which in turn cause very high localised stresses. The method with which the mounting foot was introduced is not ideal either since the structural angle had to be cut (reducing its strength) and it did not provide the geometry for an adequate weld detail. To navigate around this problem it is suggested that large thickness variations be avoided as much as possible.

The positional placement of the cradles also had a profound effect on the stresses in the structure. The central cradle is positioned above the attachment point of the bogie pivot which is an extremely stiff section of the chassis while the front and rear cradles are mounted on flexible parts of the chassis. From the FE analysis it was determined that the central cradle carries $\pm 75\%$ of the weight of the structure when loaded. Several strain measurements (not discussed in this document) confirmed this ratio. It is recommended that the cradles be spaced in such a way that the load is more evenly distributed.

The mounting method is not ideal either. The tank is mounted onto rubber mounts with only twelve bolts and has no positive means of preventing it from moving forward or rearward. This places a lot of strain on the bolts themselves and could cause them to loosen if the rubber properties change over time. Although not detrimental to the strength of the structure, it includes an unpredictability into the design and the analysis that makes accurate stress and life prediction very complex. A mounting method with at least one (symmetrical) fixed point should be used. If flexibility is required, it has to be controlled and allow movement only in specified directions.

7.4 The repair

Only a small percentage of the population has had failures, but the entire fleet has been subjected to fatigue damage. Due to this fact it is extremely difficult to predict the estimated fatigue life of a repaired tank without having extensive knowledge of its service history. For this reason it is suggested that the load from the central cradle be alleviated entirely with additional supports, one on either side of the bogie attachment. If practical, the discontinuity should also be removed and replaced with an appropriate structure.

Excessively damaging loads must also be investigated to see if they can be reduced or eliminated. The resonance noted in section 4.7.1 is damaging to the tank structure and should also be resolved or reduced. This entails a dynamic investigation that falls beyond the scope of this document.

Another damaging load is twisting that is induced in the tank structure due to bending of the chassis. To reduce the effect of this load case the mounts at the front of the tank should be modified to isolate the tank structure from the relevant movement of the chassis.

Chapter 8

Conclusion

This thesis presents the investigation of the fatigue failures that occurred on a rigidly mounted tank with the aim of calculating a correlation factor that can be used for future improvement assessments. This is the first phase of the solution method presented in Chapter 3, that needs to be followed to produce a viable structural improvement. The investigation is also meant to serve as a basis for the fatigue life calculations that GRW Engineering needs to do on current and future designs to verify the life expectancy of their products. These goals were motivated by the search for a suitable solution to the failures and a corporate commitment to validating the integrity of GRW's structural designs.

Strain gauge testing was done at RAF Lossiemouth. The tests revealed load cases that were previously unknown to GRW and which significantly impacted on the life of the structure. These include the harsh containment humps in the BFI areas, the stone grids and the numerous, sharp turns that the vehicles have to make. It also revealed the operational condition that requires the vehicles to be fully loaded at all times. The tests provided adequate data of all the various load cases and was used to compile the composite duty cycle.

A FE model was constructed and analysed. Constructing the model provided several challenges since the method of mounting the tanker is unreliable and unpredictable. This is due to the fact that the steel mounts are not rigid, the dynamic effect of the rubber mount is difficult to predict and the small number of bolts used in the mounting connection causes the system to be reliant on friction and prone to separation. It is suggested that future solutions and designs should rely on a more predictable method of mounting since it will improve the accuracy of the initial life prediction and it will be less prone to operational and manufacturing deviations.

The results of the analyses were compared to measured data to assess the correlation between the model and reality. A maximum strain deviation of 26% was calculated and was judged to be acceptable considering the circumstances. The model was then deemed to be accurate enough to determine the required scale factor for each crack position.

The calculated scale factors and the measured strains provided the neces-

sary data to calculate the estimated fatigue life of the structure and consequently the required correlation factor. Even though the validity of the calculations have been brought into question for crack one and two, the calculations for crack three are considered to be accurate. The calculated fatigue life is low which is to be expected considering that failures have occurred rather early in the life of the tank. This early failure implies that either the design was inadequate, the load cases were unknown (or not fully understood at the time of initial design), or a combination of both.

Even though the calculated fatigue life does predict the failure it still estimates a much lower and more conservative service life than experienced in reality. This could be due to a conservative S-N curve or a deviation from the failure criteria of the Palmgren-Miner sum. It could also mean that the duty cycle is not representative, but this is unlikely in this case since the measurements were taken at the site itself during a routine operation. To account for these deviations in future improvement concepts, a correlation factor of 3.9 was calculated. Using a safety factor of two means that a correlation factor of ≈ 2 should be used.

Ultimately what is the service life one should aim at achieving? For these types of tankers a 15 year uninterrupted service life is acceptable. Based on the available data this equates to roughly 71 000 km which is 3.75 times more than what was achieved. To achieve ≈ 4 times the life, a stress range reduction of at least 37% is required (based on equation 6.4). This must be used as a starting point when designing and assessing solution concepts.

This provides sufficient data to conduct the next two phases of the solution methodology which was the first goal of the thesis. The fatigue life prediction method itself was applied successfully and refined to produce a practical method that can be applied to various structures and designs, thus the second goal has also been achieved.

Admittedly there is an immense depth of further study and investigation that can be done in the field of welding fatigue, but this thesis has paved the way for future development in this field in GRW Engineering. The author also suggests that fracture mechanics should be investigated as a means of predicting fatigue life in the future since it seems to provide flexibility and increased accuracy. Literature also indicates that fracture mechanics is used increasingly as this field matures in the industry.

Appendix A

Variables associated with alternating stress

This appendix provides common variables that are associated with alternating stress as presented by Bannantine *et al.* (1990). The equation for each variable will be provided and an illustration of its meaning is shown in Figures A.1 and A.2.

Stress range

$$\Delta\sigma = \sigma_{max} - \sigma_{min} \tag{A.1}$$

Stress amplitude

$$\sigma_a = \frac{(\sigma_{max} - \sigma_{min})}{a} \tag{A.2}$$

Mean stress

$$\sigma_m = \frac{(\sigma_{max} + \sigma_{min})}{a} \tag{A.3}$$

Stress ratio

$$R = \frac{\sigma_{min}}{\sigma_{max}} \tag{A.4}$$

Amplitude ratio

$$A = \frac{\sigma_a}{\sigma_m} \tag{A.5}$$

Common loading situations are:
Fully reversed loading

$$R = -1 \tag{A.6}$$

Zero to maximum

$$R = 0 \tag{A.7}$$

Zero to minimum

$$R = \infty \tag{A.8}$$

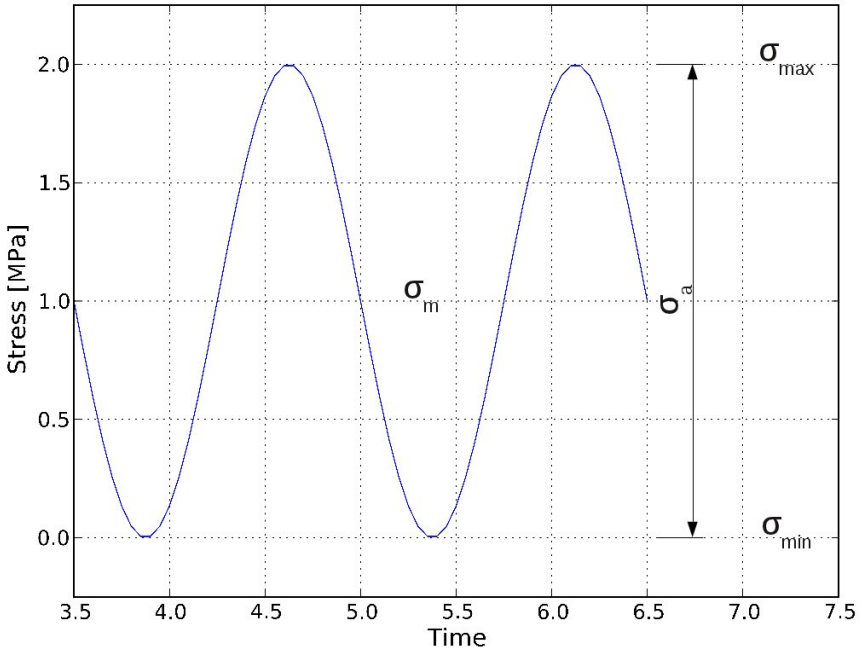

Figure A.1: A graphical representation of alternating stress terminology

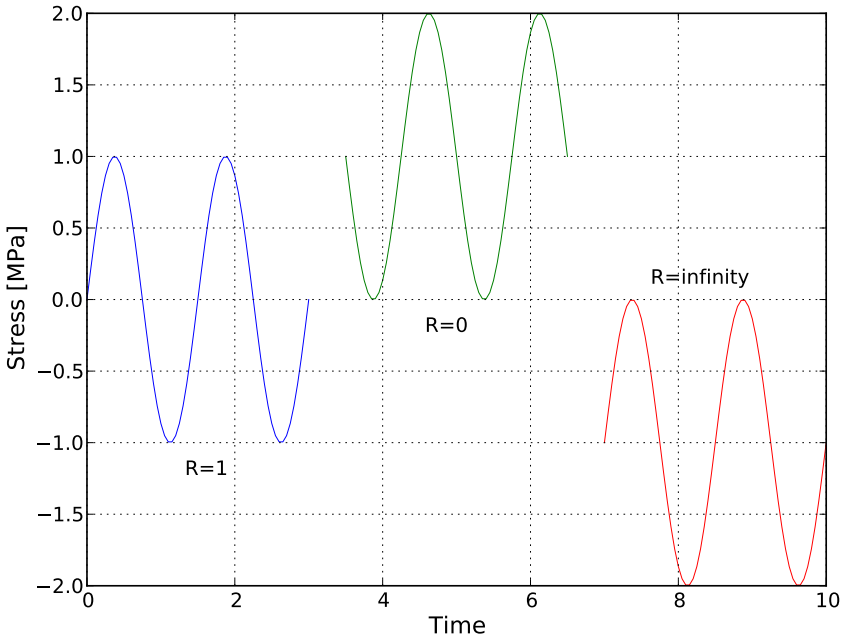

Figure A.2: A graphical representation of the effect of the loading offset on the stress ratio (R)

Appendix B

Strain gauge data sheet

HBM

Dehnungsmeßstreifen
Strain Gauges
Jauges d'extensométrie

Bestellnummer
Order No.
No. de réference
K-LY43-6/350-3-0.5M

Typ
Type
Type
6/350LY43-3-0.5M

Widerstand Resistance Résistance	350 Ω ± 0.35 %
Stückzahl Contents Quantité	10
k-Faktor Gauge factor Facteur k	2.09 ± 1 %
Temperaturkoeffizient des k-Faktors Temperature coefficient of gauge factor Coefficient de température du facteur k	101 ±10 [10^{-6} / °C] (-10...+45°C)
Querempfindlichkeit Transverse Sensitivity Sensibilité transverse	-0.4 %
Folienlos Lot Lot de la feuille	A381/10
Herstellungslos Batch Lot de fabrication	812046327

Temperaturkompensation: Angepaßt für
Temperature Compensation: Compensated for
Compensation de température: Compensation pour

Aluminium mit
Aluminium with
Aluminium avec

α = 23 [10^{-6} / °C]

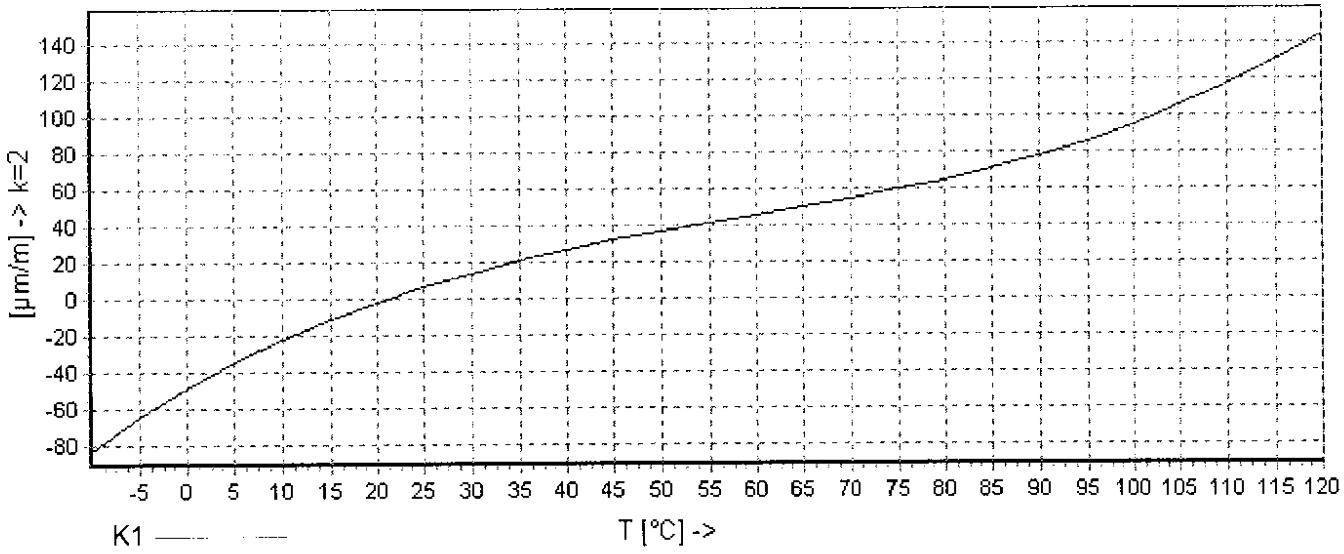

$$\varepsilon_S(T) = -45.4 + 2.82 * T - 3.58 * 10^{-2} * T^2 + 2.03 * 10^{-4} * T^3 + 0.172 * (T-20)\ \mu m/m \pm 0.3\ (\mu m/m)\ °C^{-1}$$

Alle technischen Daten nach OIML IR 62, bei Beachtung der abweichenden Toleranzangaben auch nach VDI/VDE 2635. Geben Sie bei Rückfragen bitte DMS-Typ und Herstellungs-Los an.

All technical data in accordance with OIML IR 62, also compliant with C˙VDI/VDE 2635 if deviating tolerances are observed. In case of further inquiries please indicate gauge type and batch number.

Toutes caractéristiques techniques selon OIML IR 62 et VDI/VDE 2635 pour les indications différentes de tolérance. Pour toutes questions, indiquer le type de la jauge ainsi que le lot de fabrication.

Temperaturgang der Dehnungsmeßstreifen bei Applikationen mit umseitig angegebenen Wärmeausdehnungskoeffizienten α. Gemessen bei kontinuierlicher Temperaturänderung.

Kennlinie 1: DMS mit nicht kürzbaren Teflonanschlußbändchen.
T = Temperatur in °C

Comportement en température des jauges d'extensométrie appliquées sur des matériaux dont les coefficients de dilatation termique α sont indiqués au verso. Mesuré au d'une variation continue de la température.

Courbe 1: Jauges avec fils de sortie de Teflon.
T = température en °C

The **Thermal output** refers to strain gauges when bonded to materials with coefficient of thermal expansion α given overleaf. Values are measured at a continous temperature progression.

Curve 1: Gauges with Teflon connecting leads.
T = temperature in °C

Appendix C

Accelerometer data sheet

Crossbow

CXL-GP Series

GENERAL PURPOSE ACCELEROMETER

RoHS COMPLIANT

- High Performance, 1-Axis and 3-Axis Accelerometers
- Small, Low-Cost
- Reliable Packaging with Screw-Down Mounting
- Factory Calibrated

Applications

- Automotive Testing
- Instrumentation
- Equipment Monitoring

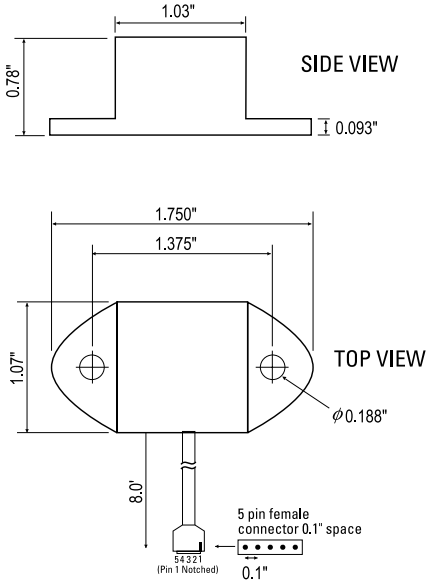

Standard Package Dimensions

GP Series

The GP Series accelerometers are low cost, general purpose, linear acceleration and/or vibration sensors available in ranges of ±4g, ±10g, and ±25g.

Common applications are automotive testing, instrumentation, and equipment monitoring. The GP Series sensing element is a silicon micro-machined capacitive beam. The capacitive beam is held in force balance for full scale non-linearity of less than 0.2%.

The GP Series offers wide dynamic range, has excellent frequency response, operates on a single 4.9 to 5.5 VDC power supply, and is easy to interface to standard data acquisition systems. The 3-axis version (GP3) can be specified with an internal regulator (-R option) for use with a 5.5 to 36 V unregulated power supply.

The GP Series sensors provide a direct high-level analog voltage output. The output requires no external signal conditioning electronics and may be directly interfaced to an A/D or other data acquisition hardware.

Compared to traditional piezoelectric and piezoresistive accelerometer technologies, the silicon micromachined sensors offer equivalent performance at a significantly lower cost.

The GP Series is offered with a standard 5-pin female connector. The highly flexible, low-mass cable prevents disruption of the measurement.

Document Part Number: 6020-0114-01 Rev B

Specifications	CXL04GP1 CXL04GP1Z CXL04GP3	CXL10GP1 CXL10GP1Z CXL10GP3	CXL25GP1 CXL25GP1Z CXL25GP3	Remarks
Performance				
Input Range (g)	± 4	± 10	± 25	± 5%
Zero g Drift (g)	± 0.1	± 0.3	± 0.5	0°C to 70°C
Sensitivity (mV/g)	500 ± 15	200 ± 5	80 ± 2	
Transverse Sensitivity (% Span)	± 5	± 5	± 5	
Non-Linearity (% FS)	± 0.2	± 0.2	± 0.2	typical
Alignment Error (deg)	± 2	± 2	± 2	typical
Noise (mg rms)	10	25	25	typical
Bandwidth (Hz) [1]	DC -100	DC -100	DC -100	
Environment				
Operating Temp. Range (°C)	-40 to +85	-40 to +85	-40 to +85	
Operating Temp. Range - AL (°C)	-40 to +105	-40 to +105	-40 to +105	
Shock (g)	2000	2000	2000	
Electrical				
Supply Voltage (Volts)	+ 4.9 to 5.5	+ 4.9 to 5.5	+ 4.9 to 5.5	
Supply Voltage -R option (Volts)	+ 5.5 to 36	+ 5.5 to 36	+ 5.5 to 36	
Supply Current (mA)	1/axis	3/axis	3/axis	typical
Zero g Output (Volts)	+ 2.375 ± 0.1	+ 2.375 ± 0.1	+ 2.375 ± 0.1	@25°C
Span Output (Volts)	± 2.0 ± 0.1	± 2.0 ± 0.1	± 2.0 ± 0.1	
Output Loading	> 2.0 Ω, < 2 nF	> 2.0 Ω, < 2 nF	> 2.0 Ω, < 2 nF	
Physical				
Standard package				
Size (in)	0.78 x 1.75 x 1.07	0.78 x 1.75 x 1.07	0.78 x 1.75 x 1.07	
(cm)	1.98 x 4.45 x 2.72	1.98 x 4.45 x 2.72	1.98 x 4.45 x 2.72	
Weight	1.62 oz (46 gm)	1.62 oz (46 gm)	1.62 oz (46 gm)	
Aluminum package (-AL option)				
Size (in)	0.95 x 2.00 x 1.20	0.95 x 2.00 x 1.20	0.95 x 2.00 x 1.20	
(cm)	2.41 x 5.08 x 3.05	2.41 x 5.08 x 3.05	2.41 x 5.08 x 3.05	
Weight	2.40 oz (68 gm)	2.40 oz (68 gm)	2.40 oz (68 gm)	

Notes

[1] -3dB, DC coupled sensor

Non-linearity is the deviation from a best fit straight line at full scale. Transverse sensitivity is error measured in the primary axis output created by forces induced in the orthogonal axis. Transverse sensitivity error is primarily due to the effects of misalignment. Zero g drift is specified as the typical change in 0 g level from its initial value at +25°C to its worst case value at Tmin or Tmax. Specifications subject to change without notice.

Pin	Color	Function
1	Red	Power In
2	Black	Ground
3	White	X-axis Out
4	Yellow	Y-axis Out
5	Green	Z-axis Out

Pin Diagram

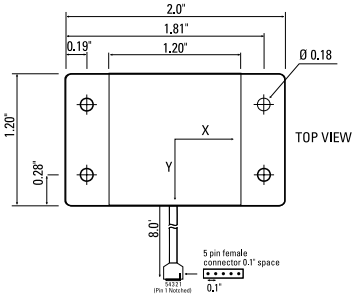

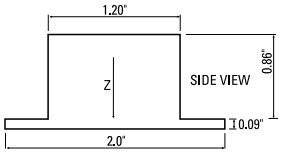

High Temperature Package Dimensions

Ordering Information

Model	Axes	Span (g)	Sensitivity (m V/g)	Noise (mg rms)	Bandwidth (Hz)
CXL04GP1	X	± 4	500	10	DC-100
CXL04GP1Z	Z	± 4	500	10	DC-100
CXL04GP3	TRI	± 4	500	10	DC-100
CXL10GP1	X	± 10	200	25	DC-100
CXL10GP1Z	Z	± 10	200	25	DC-100
CXL10GP3	TRI	± 10	200	25	DC-100
CXL25GP1	X	± 25	80	25	DC-100
CXL25GP1Z	Z	± 25	80	25	DC-100
CXL25GP3	TRI	± 25	80	25	DC-100
OPTIONS					
-R	Voltage Regulator, 5.5 – 36 VDC input. (Available in GP3 models only.)				
-AL	High Temperature Package. Operating Temperature Range (°C): -40 to +105. (Available in GP3 models only.)				

High Temperature Package

Document Part Number: 6020-0114-01 Rev B

Appendix D

A list of all the measured variables

The scope of the measurement project was much wider than what is presented in this thesis. This appendix will present all the variables that were measured. It will also give a brief overview of each and why they were included in the measurement.

D.1 Strain gauges

In total twenty-two strain gauges were applied and used to measure the effects of various load cases. These gauges and their positions are presented in Table D.1. Figure D.1 and D.2 illustrates the general position of each gauge.

Table D.1: A list of all the strain gauges applied to the structure

Gauge #	**Gauge type**	**Position**	**Purpose**
1	Uniaxial	Right side, rear cradle (0°)	To measure strain at the angle to foot intersection for comparative purposes
2	Rosette	Right side, angle between second and third cradle (45°)	FE model correlation. Area with a low stress gradient
3	Rosette	Right side, angle between second and third cradle (0°)	FE model correlation. Area with a low stress gradient
4	Rosette	Right side, angle between second and third cradle (-45°)	FE model correlation. Area with a low stress gradient

continued on next page

continued from previous page

5	Rosette	Right side, front cradle (90°)	To measure strain at the angle to foot intersection for comparative purposes
6	Rosette	Right side, front cradle (135°)	To measure strain at the angle to foot intersection for comparative purposes
7	Rosette	Right side, front cradle (180°)	To measure strain at the angle to foot intersection for comparative purposes
8	Uniaxial	Right side, centre of front outrigger (90°)	To measure strain in the outrigger for comparative purposes
9	Rosette	Right side, corner of front outrigger (135°)	To measure strain at a known crack area for use in fatigue calculations
10	Rosette	Right side, corner of front outrigger (90°)	To measure strain at a known crack area for use in fatigue calculations
11	Rosette	Right side, corner of front outrigger (45°)	To measure strain at a known crack area for use in fatigue calculations
12	Uniaxial	Right side, centre cradle	To measure strain at a known crack for use in fatigue calculations
13	Uniaxial	Right side, centre of middle outrigger (90°)	To measure strain in the outrigger for comparative purposes
14	Rosette	Right side, corner of middle outrigger (135°)	To measure strain at a known crack area for use in fatigue calculations
15	Rosette	Right side, corner of middle outrigger (90°)	To measure strain at a known crack area for use in fatigue calculations
16	Rosette	Right side, corner of middle outrigger (45°)	To measure strain at a known crack area for use in fatigue calculations
17	Rosette	Right side, middle cradle (90°)	To measure strain at a known crack area for use in fatigue calculations

continued on next page

continued from previous page			
18	Rosette	Right side, middle cradle (45°)	To measure strain at a known crack area for use in fatigue calculations
19	Rosette	Right side, middle cradle (0°)	To measure strain at a known crack area for use in fatigue calculations
20	Uniaxial	Centre mild steel insert (viewed from the rear). Lower left corner. (180°)	To provide clarity to the dynamics and loading mechanisms of the system
21	Uniaxial	Centre mild steel insert (viewed from the rear). Centre, top. (180°)	To provide clarity to the dynamics and loading mechanisms of the system
22	Uniaxial	Left side, centre of middle outrigger (90°)	To measure strain in the outrigger for comparative purposes

D.2 Accelerations

Acceleration measurements were recorded as described in Section 4.1. The various positions and directions are listed in Table D.2.

Table D.2: Accelerometer directions recorded during the vehicle tests

Direction	**Position**
Z-axis	Left side above the truck tractor bogie
X-axis	Right side above the truck tractor bogie
Y-axis	Right side above the truck tractor bogie
Z-axis	Right side above the truck tractor bogie

D.3 GPS data

GPS data was recorded to assist in determining the exact position and thus the cause of an event. Table D.3 lists all the GPS data that was recorded.

D.4 CAN bus data

Vehicle data was collected from the truck via a CAN bus interface as explained in Section 4.5. All the data that was collected is listed in MAN's guide to the KSM module (MAN's KSM module). The variables listed in Table D.4 were

Table D.3: GPS data recorded during the vehicle tests

Description	**Purpose**
Longitude	To determine the position of the truck
Latitude	To determine the position of the truck
Altitude	To determine the altitude of the truck
Number of satellites	To check if enough satellites are detected to ensure accurate data

of interest in the investigation. The rest of the data was also recorded since it does not require a large amount of memory (it has a sample rate of 1 Hz) and is 'cheap' since it does not require any additional transducers and is readily available.

Table D.4: CAN bus data collected from the truck interface

Variable #	**Variable name**	**Description**	**Purpose**
1	veh_speed_MTCO	Vehicle speed [km/h]	To record the actual vehicle speed vs time
2	amb_air_temp	Ambient air temperature [°C]	Records the operational air temperature
3	tot_veh_dist	Total vehicle distance [km]	Records the current odometer value of the vehicle

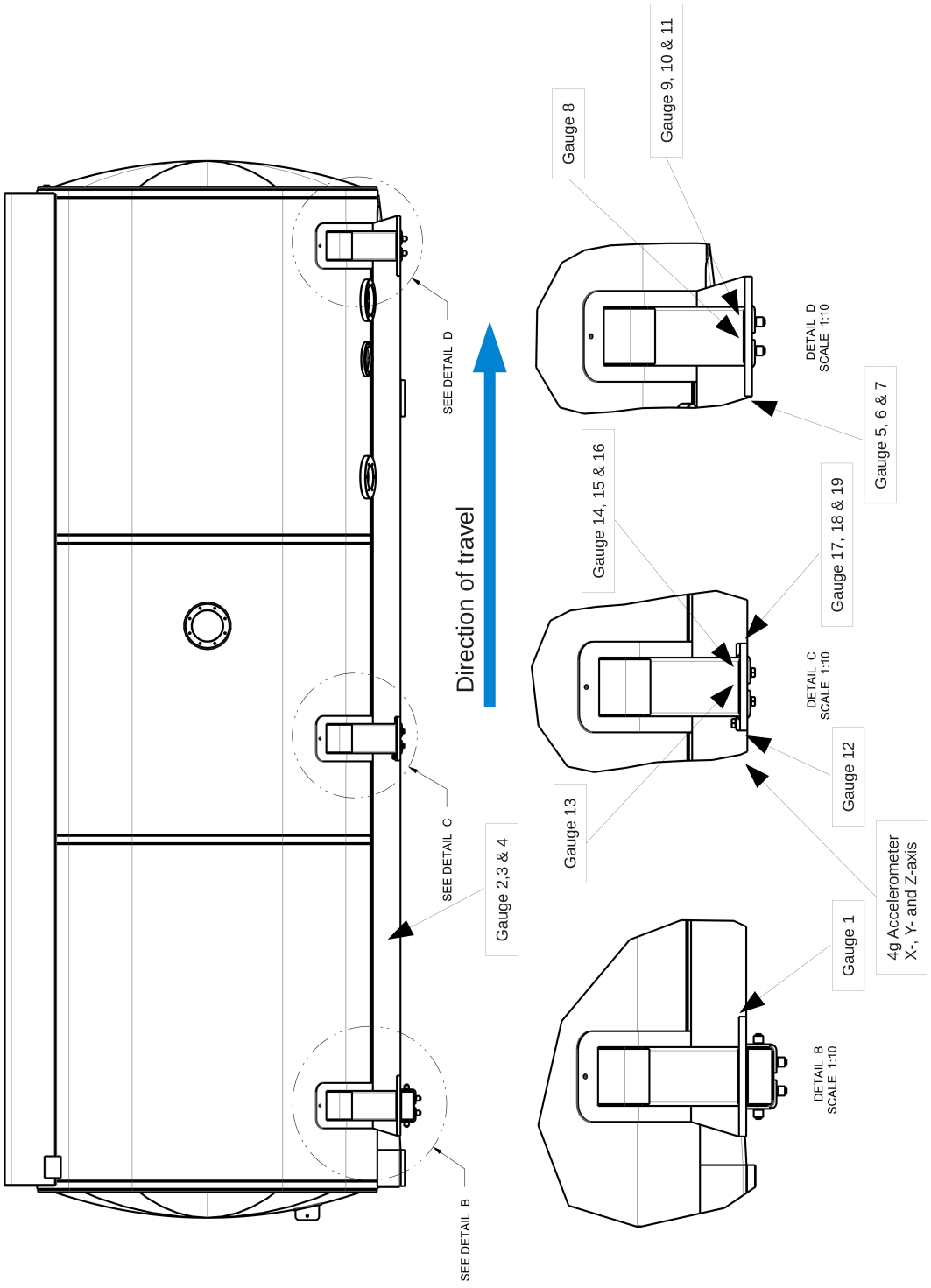

Figure D.1: A right side view of the tank showing the positions of gauge one to nineteen.

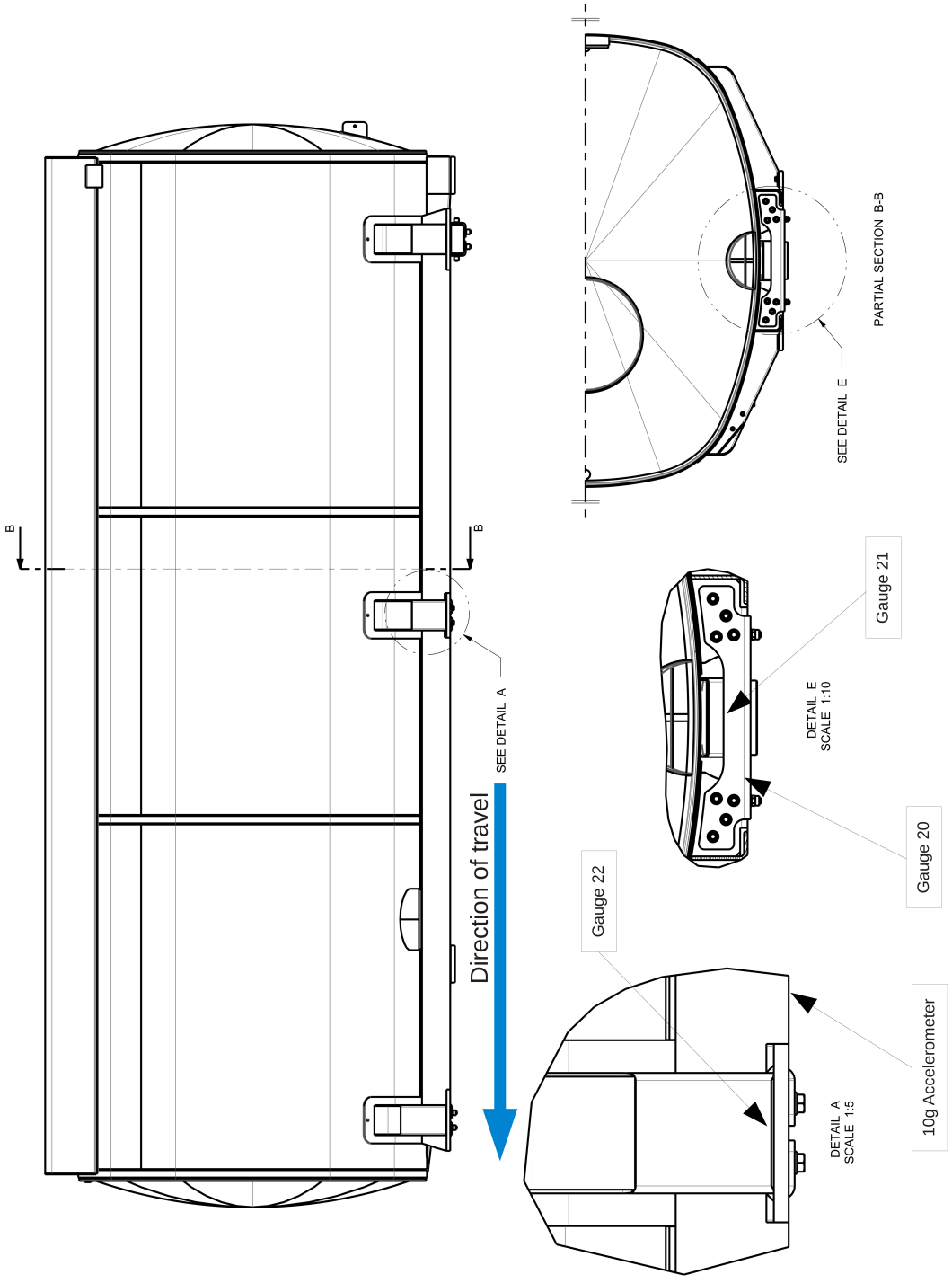

Figure D.2: A left side view of the tank showing the positions of gauge twenty to twenty-two.

Appendix E

Mohr circle calculations

This section provides the equations to calculate the principal strains from strains obtained by a three element rosette as shown in Figure E.1. The calculations provided here are derived from those given by Lee *et al.* (2005)

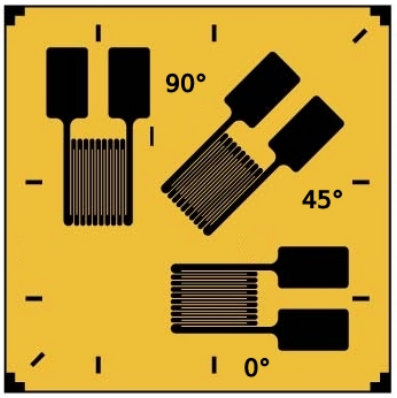

Figure E.1: A rectangular triaxial strain gauge

Calculating the maximum principal strain:

$$\varepsilon_1 = \frac{\varepsilon_0 + \varepsilon_{90}}{2} + \frac{\sqrt{(\varepsilon_0 - \varepsilon_{90})^2 + (2\varepsilon_{45} - \varepsilon_0 - \varepsilon_{90})^2}}{2} \tag{E.1}$$

Calculating the minimum principal strain:

$$\varepsilon_2 = \frac{\varepsilon_0 + \varepsilon_{90}}{2} - \frac{\sqrt{(\varepsilon_0 - \varepsilon_{90})^2 + (2\varepsilon_{45} - \varepsilon_0 - \varepsilon_{90})^2}}{2} \tag{E.2}$$

Calculating the angle to the maximum principal strain:

$$\tan 2\phi = \frac{2\varepsilon_{45} - \varepsilon_0 - \varepsilon_{90}}{\varepsilon_0 - \varepsilon_{90}} \tag{E.3}$$

Where:

ε_1	=	Maximum principal strain	[m/m]
ε_2	=	Minimum principal strain	[m/m]
ε_0	=	Strain at 0°	[m/m]
ε_{45}	=	Strain at 45°	[m/m]
ε_{90}	=	Strain at 90°	[m/m]
ϕ	=	The angle to the maximum principal strain	[°]

Appendix F

Unidirectional strain proof

The Mohr circle calculations presented in Appendix E always calculates a minimum and a maximum principal stress. When the governing stress oscillates about zero it produces a continuously varying principal stress angle. This gives the impression that the governing stress keeps changing direction which implies that multi-axial fatigue calculations are required. However, this is not the case since the governing stress does not change direction. Figure F.1 shows a sample of the calculated principal strains (for crack two) versus the strain measured by gauge fifteen. It is clear that the governing strain is continually measured by gauge fifteen and thus does not change direction.

In this case it would be a mistake to use the calculated principal strains for the fatigue calculations without mathematically combining them. Doing so will produce non-conservative stress ranges.

A similar example for crack 3 is presented in Figure F.2. In this case gauge 19 measures the governing strain.

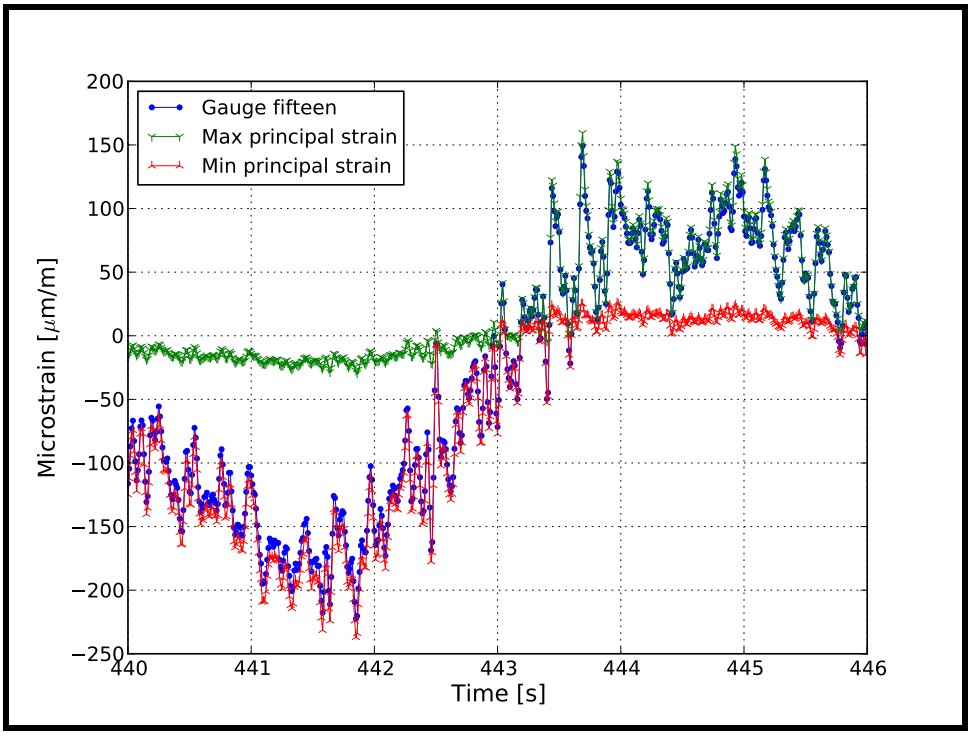

Figure F.1: A plot of the minimum and maximum principal strain versus the strains measured by gauge fifteen

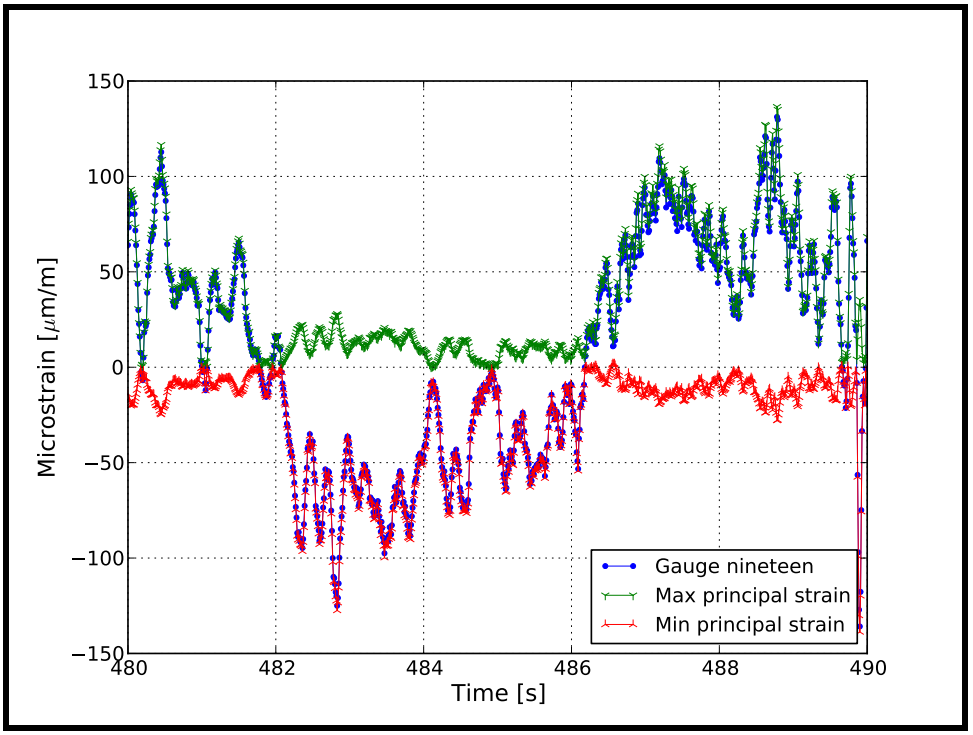

Figure F.2: A plot of the minimum and maximum principal strain versus the strains measured by gauge nineteen

Appendix G

Suspension characteristics

Figures G.1 and G.2, provided by MAN, is the graphical representation of the spring stiffness of the front and rear suspension respectively.

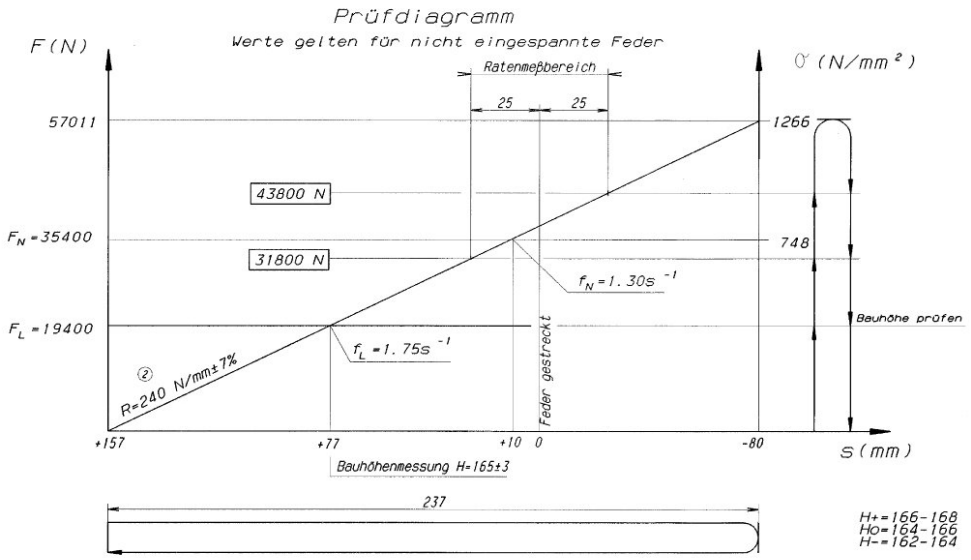

Figure G.1: The spring stiffness characteristics of the front axle suspension

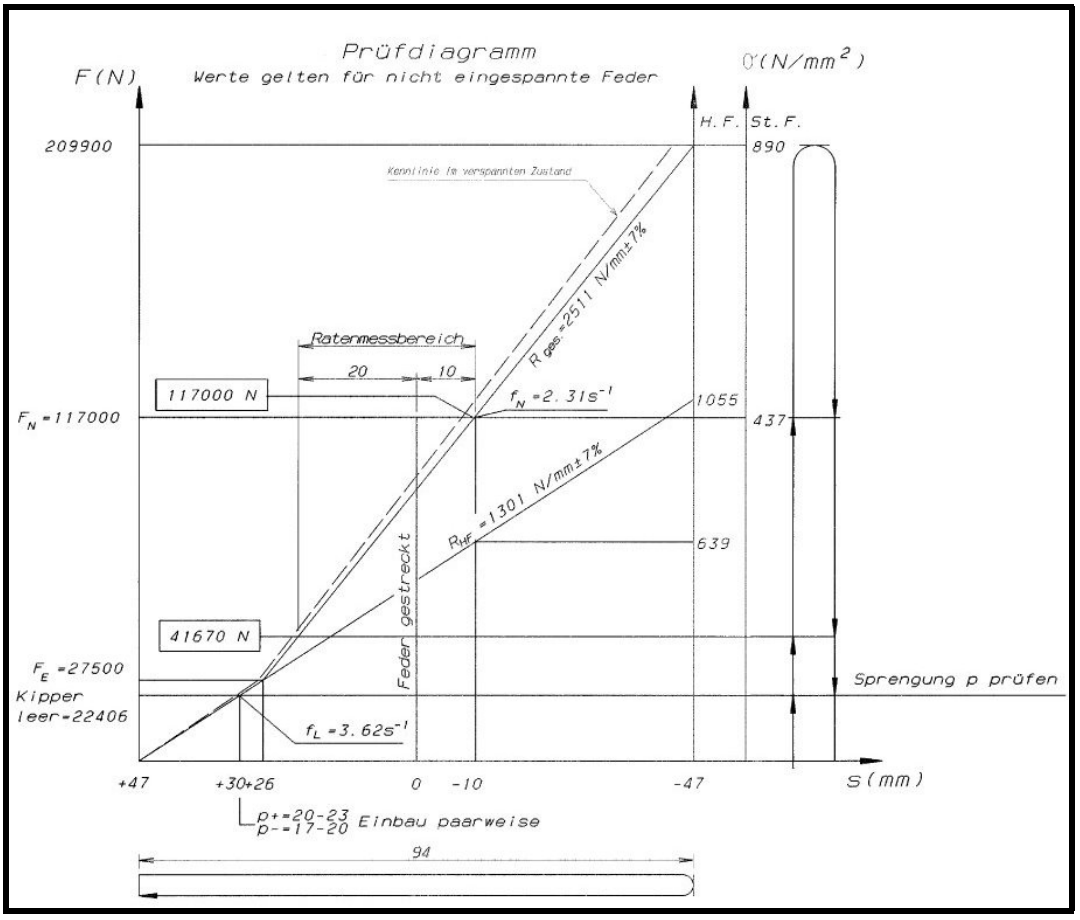

Figure G.2: The spring stiffness characteristics of the rear axle suspension

List of References

Abaqus Analysis user Manual (2010 January). *Abaqus Analysis user Manual*. Dassault Systèmes Simulia Corp.

Bannantine, J.A., Comer, J.J. and Handrock, J.L. (1990). *Fundamentals of Metal Fatigue Analysis*. Prentice Hall.

BS7910:2005 (2005). *Guidance on methods for assessing the acceptability of flaws in metallic structures*. British Standards Institution, London.

CEN/TC250 (ed.) (2005). *Eurocode 3: Design of Steel Structures - Part 1-9: Fatigue*, vol. EN 1993-1-9 : 2005. CEN.

CEN/TC250 (ed.) (2007). *Eurocode 9: Design of Aluminium Structures - Part 1-3: Structures susceptible to fatigue*, vol. EN 1999-1-3 : 2007. CEN.

CSIR (2011). 7th Annual State of Logistics Survey For South Africa. Tech. Rep., CSIR.

Downing, S.D. and Socie, D.F. (1982). Simple rainflow counting algorithms. *International Journal of Fatigue*, vol. 4, no. 1, pp. 31 – 40. ISSN 0142-1123.

Franken, C.M. (2010 December). DR101103, Large capacity aircraft refueller system (LCARS) fatigue life investigation. In-house technical report.

Fricke, W. (2003). Fatigue analysis of welded joints: state of development. *Marine Structures*, vol. 16, no. 3, pp. 185–200.

GRW (2011). History. See `http://www.grw.co.za`. [2011, Nov 1].

Hansen, P. (2010 July). Compression testing of rubber pads for road tankers. Report on testing done by MERL laboratories.

Hashin, Z.A. (1980). A reinterpretation of the Palmgren-Miner rule for fatigue life prediction. *Journal of Applied Mechanics*, vol. 47, pp. 324–328.

Hobbacher, A. (1996). *Recommendations for Fatigue Design of Welded Joints and Components*, vol. IIW Doc. XIII-2151-07/XV-1254-07 (2008). Abington Publishing, Cambridge, UK.

Hoffman, K. (1989). *An Introduction to Measurements using Strain Gauges*. HBM.

Hoffman, K. (2001). *Applying the Wheatstone bridge circuit*. HBM.

Issler, L. (2011). Design concepts for engineering structures. Lecture notes.

Lee, Y., Pan, J., Hathaway, R. and Barkey, M. (2005). *Fatigue Testing and Analysis*. Elsevier.

MacDonald, K. (ed.) (2011*a*). *Fracture and Fatigue of Welded Joints and Structures*. Woodhead Publishing in Materials. Woodhead Publishing. ISBN 9781845695132.

MacDonald, K. (ed.) (2011*b*). *Fracture and Fatigue of Welded Joints and Structures*, chap. Four. Woodhead Publishing in Materials. Woodhead Publishing. ISBN 9781845695132.

MacDonald, K. (ed.) (2011*c*). *Fracture and Fatigue of Welded Joints and Structures*, chap. Five. Woodhead Publishing in Materials. Woodhead Publishing. ISBN 9781845695132.

MacDonald, K. (ed.) (2011*d*). *Fracture and Fatigue of Welded Joints and Structures*, chap. Eleven. Woodhead Publishing in Materials. Woodhead Publishing. ISBN 9781845695132.

Maddox, S.J. (2000). Fatigue design rules for welded structures. *Progress in Structural Engineering and Materials*, vol. 2, no. 1, pp. 102–109. ISSN 1528-2716.

Maddox, S.J. (2011). *Fatigue design for welded structures*, chap. 7. Woodhead Publishing Limited.

MAN's bodybuilder bulletin 100 (2008 February). *BB100: Connections to the Bodybuilder Interface Module (KSM)*. MAN.
Available at: `http://www.man-bodybuilder.co.uk/bulletins/pdf/BB100.pdf`

MAN's bodybuilder bulletin 103 (2008 June). *BB103: Power Supply and Ground Connections for Auxiliary Consumers*. MAN.
Available at: `http://www.man-bodybuilder.co.uk/bulletins/pdf/BB103.pdf`

MAN's KSM module (2005 January). *ZDR interface with customer-specific control module (KSM) for external speed control in TG-A*. MAN.
Available at: `http://www.manted.de/manted/aufbaurichtlinien/_pdf/zdr/zdr_ksm_gb.pdf`

Marquis, G.B. (2011). *Fatigue assessment methods for variable amplitude loading of welded structures*, chap. 8. Woodhead Publishing Limited.

Matsuishi, M. and Endo, T. (1968). Fatigue of metals subjected to varying stress. *Japan Society of Mechanical Engineers, Fukuoka, Japan*, pp. 37–40.

MSC Software Corporation (2012). Introduction to Fatigue theory. See `http://www.mscsoftware.com/training_videos/patran/reverb3/index.html#page/Fatigue%20Users%20Guide/fat_theory.15.2.html`. [2012, Nov 16].

Niemi, E., Fricke, W. and Maddow, S. (2006). *Fatigue Analysis of Welded Components - Designer's guide to the structural hot-spot stress approach*. Woodhead Publishing Limited.

PVE/1 (ed.) (2009). *Specification for unfired fusion welded pressure vessels*, vol. PD5500:2009. BSI.

Rooke, D.P., Cartwright, D.J. and Great Britain, Ministry of Defence, Procurement Executive (1976). *Compendium of stress intensity factors*. H.M.S.O. ISBN 9780117713369.

Sih, G.C. (1973). *Handbook of stress-intensity factors: stress-intensity factor solutions and formulas for reference*. No. v. 1 in Handbook of Stress-intensity Factors: Stress-intensity Factor Solutions and Formulas for Reference. Lehigh University, Institute of Fracture and Solid Mechanics.

Subramanyan, S. (1976). "a cumulative damage rule based on the knee point of the s-n curve". *Journal of Engineering Materials and Technology*, vol. 98, no. 4, pp. 316–321.

UL FGG (2011*a*). Lecture 12.13: Fracture Mechanics Applied to Fatigue. See `http://www.fgg.uni-lj.si/kmk/esdep/master/wg12/l1300.htm`. [2011, October].

UL FGG (2011*b*). Lecture 2.5: Selection of Steel Quality. See `http://www.fgg.uni-lj.si/kmk/esdep/master/wg02/l0500.htm`. [2011, October].

WP.15 (ed.) (2008). *European Agreement concerning the International Carriage of Dangerous Goods by Road*, vol. ADR 2009. United Nations.